November 2015

Multi-scale characterization and engineering of Taxus suspension cultures

Sarah A. Wilson
University of Massachusetts - Amherst

Multi-scale characterization and engineering of *Taxus* suspension cultures

A Dissertation Presented

by

Sarah A. Wilson

Submitted to the Graduate School of the

University of Massachusetts Amherst in partial fulfillment

of the requirements for the degree of

DOCTOR OF PHILOSOPHY

September 2015

Department of Chemical Engineering

Multi-scale characterization and engineering of *Taxus* suspension culture

A Dissertation Prospectus Presented

by

Sarah A. Wilson

Approved as to style and content by:

_____
Susan C. Roberts, Chair

_____
Neil S. Forbes, Member

_____
Jennifer Normanly, Outside Member

_____
John Collura, Department Head
Department of Chemical Engineering

DEDICATION

To my mom and dad

for their unwavering love and support

through the good and the bad.

And to my family,

those who have become family,

and my Poppop

for being a constant source of motivation.

ACKNOWLEDGEMENTS

There are very few opportunities that you have in life to truly thank the people that you appreciate. For the past six year of my life, I have taken many opportunities to think about this moment and reflect on those who have been the biggest influences on my life. Although I have had many years to prepare, I know that my words will not do me justice and my gratitude will go far beyond these pages.

First, I would like to express my sincere gratitude to my advisor, Susan Roberts, for her constant support and guidance over the last six years. Through her, I have learned the importance of creativity in science, enthusiasm in teaching and compassion in mentorship, all skills which I aim to develop throughout my own career. Sue has continued to challenge me throughout my Ph.D. and her extreme faith in me has helped me to develop confidence in my own abilities. She has truly helped to shape my research, career and life in ways that I could never imagine, and for that I will be forever grateful.

I would like to thank my committee members, Neil Forbes and Jennifer Normanly, for their mentorship and support. Neil's passion for science is truly infectious and inspiring. As a future teacher and mentor, I hope that I can motivate my students with the same level of excitement for my work. Jennifer has continuously helped to guide my research and supported my professional development. I thank them both for the time, insight and advise that they have offered me as members of my thesis committee.

Throughout my time at UMass, I have had the opportunity to work under amazing professors (Scott Auerbach, Alice Cheung, Shannon Compton and Bob Zimmerman) that have allowed me to develop my own skills as a teacher, and taught me how to engage students and push them further than I thought possible. The time that I have spent

teaching for the Integrated Concentration in Science (iCONS) courses has been invaluable, and I am forever thankful to Scott Auerbach and Bob Zimmerman for providing me with the initial opportunity to participate in their courses. The iCONS program at UMass is truly unique and produces students who are creative and motivated problem solvers. Working with the iCONS program has been instrumental in driving my career path and I look forward to applying the skills that I have learned from the program throughout my career.

Through my collaboration with Weyerhaeuser both at UMass and at Weyerhaeuser, I was able to work with an amazing group of scientists (Tony Swanda, Pat Brownell, Jim Grob and Pramod Gupta) that helped me to develop during the early years of graduate school. I would especially like to thank Tony for the passion and enthusiasm that he has for his work and for putting a large amount of faith in me as a researcher. I would also like to thank Pat for being a great colleague and scientist. Pat pushed me to truly understand my data, which is a skill that I have brought with me through my Ph.D. My experience at Weyerhaeuser is one that I will never forget and I am grateful for the people that I have met through the collaboration.

I cannot begin to express my gratitude towards my lab mates (Marty Kolewe, Rohan Patil, Whitney Stoppel, Lisa Leone, Liz Cummings, Michelle McKee, Greg Andrews, James Fargnoli and Vanessa Bartolo). They have not only helped me to develop as a researcher, but have also helped to keep me sane. Most importantly, I would like to thank Marty, Rohan and Whitney who took me into the lab and patiently trained me to become independent. Additionally, Rohan and Whitney were huge sources of support throughout my entire Ph.D. and I truly don’t think I could have survived without

them in the lab. I thank Lisa, Liz, Michelle and Greg who quickly adapted to our lab and helped to not only make our lab more productive, but also a fun work environment. And finally, I would like to thank James and Vanessa for helping our lab in the huge undertaking of the UMass BioFoundry. I cannot imagine going through the past year with anyone else on my team. Their patience with me and devotion to the project has been truly appreciated and I was thankful to be able to trust our cells in their hands.

I would also like to thank the many undergraduate students (Steve Ayotte, Alpha Abdoul Bamba, Steven Bevacqua, Michaela Brown, Nick Cadirov, Angela Chen, Meghan Combs, Bronwyn Finney. Kristen Garcia, Matt Long, Julia Petrullo, Nicole Raia, John Vetrano and Mike Vilkhovoy) that I have worked with in the lab. I have been lucky to work with trust-worthy, hard working students that have made my job as a mentor easy. I especially want to thank my honors thesis students (Nick, Nicole, Mike, Bronwyn, John and Steve) for your devotion to the lab. I look forward to watching all of your successes as you continue your own careers.

In my six years at UMass, I have been lucky to build friendships with more people than I could possibly list. I would especially like to thank my incoming first year class for helping me to adapt to UMass and becoming a huge support group throughout my entire Ph.D. I could not imagine making it through a stressful first year of courses with a better group of people. I would like to thank all of my roommates (Whitney Stoppel, Tim Hanley, Charley Swofford, Erika Saffer, Andrew Teixeira, Alex Paulsen, Christoph Krumm, Ray Gasper, Greg Andrews, Brandon Dunham and Bryan Sharkey) for being a source of support, entertainment and distraction over the years. Without Andrew, Erika, Whitney and Emily Pentzer, I truly don’t know that I would have been

able to survive graduate school with my sanity intact. I am extremely grateful for the wonderful community of graduate students at UMass and could not have asked for a better experience.

In addition to the wonderful support group that I have gained at UMass, I must also thank the support of the friends who have been with me the longest. First, I would like to thank Stephanie Seng and Ryan Burch, who have been with me since high school and provided me with unlimited support throughout both college and graduate school. Steph, I cannot begin to thank you for all that you have done for me in my life. You have been my go-to person for many years and I don't think I would have made it this far without your advice and encouragement. You have also blessed me with two of my favorite people in the entire world, Juliana and Joe-Joe. They have clearly inherited your heart and never fail to bring a smile to my face. Ryan, you have never failed to make me laugh when I needed it the most, and I can't thank you enough for that. Thank you for being the one that I can always go to when I need to get pulled out of a funk. And finally, I would like to thank Sarah Jane Cummings and the geniuses at Rowan University who decided that we would be the perfect roommates. I cannot thank you enough for your love and support both through college and in the many years since then. You truly have been my rock and I can't imagine where either of us would have ended up if we hadn't been thrown in a dorm room together during our freshmen year.

Finally, and most importantly, I would like to thank my amazing family for their continual faith in me. First, I would like to thank my sister Kristen for putting up with her brat of a little sister over the years and for always being there for me to vent. To my wonderful Mommom, I would like to thank you for always being a source of support and

for loving me unconditionally. To my amazing Poppop, I cannot begin to explain the effect that you have had on my life in graduate school. Losing you was one of the hardest things that I have endured and I will continue to use you as a source of motivation as I move beyond graduate school. And finally, to my mom and dad. You have continually supported me through all of my life decisions (as crazy as they may have seemed at the time) and I cannot begin to express how grateful I am because of that. Thank you for always answering the phone, for putting up with me when I am home and for always treating me like your little girl, no matter how old I may be.

ABSTRACT

MULTI-SCALE CHARACTERIZATION AND ENGINEERING OF *TAXUS* SUSPENSION CULTURES

September 2015

SARAH AMY WILSON, B.S., ROWAN UNIVERSITY

Ph.D., UNIVERSITY OF MASSACHUSETTS AMHERST

Directed by: Professor Susan C. Roberts

Plants produce a diversity of natural products that have commercial applications as flavorings, fragrances, pesticides and pharmaceuticals. These compounds are often the result of specialized metabolic pathways that are unique to plant systems, and have complex structures that make chemical synthesis routes infeasible. This necessitates exploitation of biological production routes. This thesis work presents a multi-scale characterization and engineering approach to understand and manipulate plant cell cultures on the extracellular (culture) and intracellular (metabolic pathway) levels. Studies focus on the commercially relevant suspension culture system *Taxus*, a medicinal plant species used for production of the FDA-approved anticancer drug paclitaxel.

Extracellular engineering: One of the unique characteristics of plant cell cultures is the tendency to grow in aggregates, which range in size from 50 to 2,000 μm in diameter. In *Taxus*, smaller aggregates accumulate higher levels of paclitaxel. Studies have looked at the effect of aggregation on product accumulation, but no methods have been developed to control aggregation properties in culture. In this study, a method was developed to decrease the mean aggregate size of *Taxus* suspension cultures through applied mechanical shear. Long-term application of shear did not affect culture growth

and the mean aggregate size of the sheared population was reduced when compared to an unsheared control. Despite these promising results, the mean aggregate size of the sheared population fluctuated by over two-fold throughout the course of the experiment, indicating a lack of control over the aggregation dynamics. As a result, a population balance equation model was developed, which was used to determine the amount of mechanical shear necessary to reach a target aggregate size distribution, providing a new approach for controlling culture-level properties.

Intracellular engineering: In addition to conserved metabolic pathways, which are pathways involved in growth and development, plants have specialized metabolic pathways that allow them to adapt to their environment. These specialized pathways are often species specific and, as a result, are poorly defined. Additionally, the interactions between conserved and specialized metabolism are poorly understood, limiting the application of metabolic engineering strategies. To better understand global specialized metabolism, methods were developed to characterize active pathways in *Taxus*. It was found that all *Taxus* cultures divert carbon flux towards the production of phenolics, flavonoids and lignin, along with paclitaxel and related taxanes. Additionally, production of these compounds varies significantly over time and is directly related to culture aggregate size. These studies are amongst the first to address global specialized metabolism (consisting of both cooperative and competing pathways) in a non-model plant species and provide valuable insights into the design of effective metabolic engineering strategies to promote production of a particular class of products.

Due to the high level of interaction amongst cells in these complex cellular systems, successful engineering efforts must look beyond the level of the metabolic

pathway. This thesis characterized and manipulated *Taxus* cultures on multiple scales to allow for the effective engineering of cultures for increased paclitaxel production.

TABLE OF CONTENTS

Page

LIST OF TABLES

Page

LIST OF FIGURES

Page

CHAPTER 1.

INTRODUCTION AND BACKGROUND[1]

1.1. Plant specialized metabolites

For centuries, plants have traditionally been used as both a food source and a source of active pharmaceutical agents. As of 2010, 75% of anti-bacterial compounds and 48.6% of anti-cancer compounds were either a natural product or natural product analog (Newman and Cragg, 2012). To aid in development and defense against stress, plants synthesize hundreds of thousands of compounds, many of which are produced through species-specific and complex biosynthetic pathways (DellaPenna and O'Connor, 2012). For instance, the shikimic acid, non-mevalonate (MEP) and mevalonate (MVA) pathways lead to diverse classes of compounds, which include the terpenoids, monoterpene indole alkaloids, isoquinoline alkaloids, flavonoids and anthocyanins (Figure 1.1).

[1] Portions of this introduction were taken from 1) Recent advances towards development and commercialization of plant cell culture processes for the synthesis of biomolecules. Plant Biotechnology Journal 10(3):249-268, 2) Wilson, S. A., Roberts, S. C., 2014. Metabolic engineering approaches for production of biochemicals in food and medicinal plants. Current Opinion in Biotechnology. 26**,** 174-182, and 3) Wilson SA, Cummings EM, Roberts SC. 2014. Multi-scale engineering of plant cell cultures for promotion of specialized metabolism. Current Opinion in Biotechnology 29(0):163-170 and Wilson SA, Roberts SC. 2012.

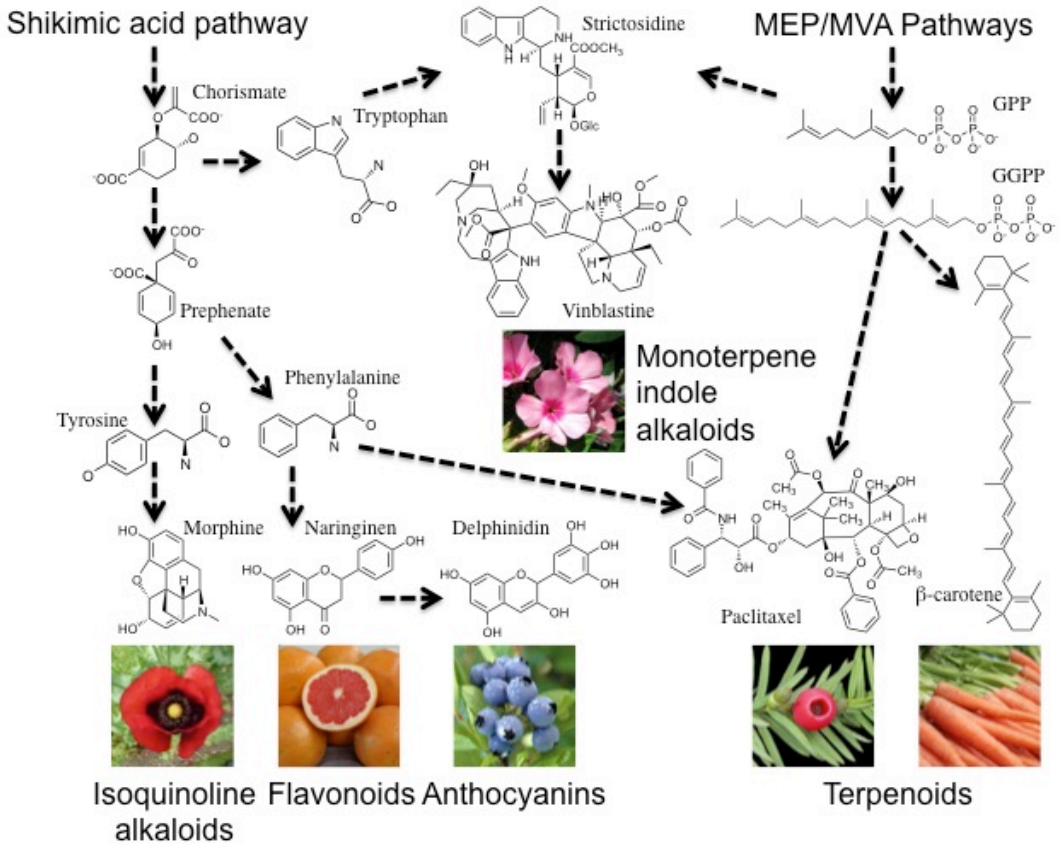

Figure 1.1 Examples of biosynthetic pathways leading to large classes of pharmaceutical or nutraceutical plant natural compounds. Arrows represent carbon flux through a pathway starting from primary metabolism (shikimic acid and MEP/MVA pathways) and leading to classes of specialized metabolites. Vinblastine and paclitaxel require precursors from both primary metabolic pathways as indicated by the arrows.

Due to the high degree of structural diversity of specialized metabolites, these compounds have significant commercial value as pharmaceuticals, nutraceuticals, dyes, fragrances, flavors and pesticides. In addition to their commercial applications, many dietary health benefits can be attributed to specific plant natural products in popular food crops. For instance, the compounds seen in Figure 1.1 are anti-cancer compounds (vinblastine and paclitaxel), analgesics (morphine), antioxidants (naringenin and delphinidin) and provitamins (β-carotene). Although some valuable plant natural products

with simple structures are easily chemically synthesized (e.g., aspirin and ephedrine), many have complex structures with multiple chiral centers, making chemical synthesis both difficult and commercially infeasible (De Luca et al., 2012). As a result, these compounds are often produced through the exploitation of native biological pathways using natural harvest (e.g., codeine, morphine and dietary food compounds), semi-synthesis (e.g., paclitaxel), heterologous production (e.g., vanilla) or plant cell culture techniques (e.g., paclitaxel, ginseng and anthocyanins) (Wilson and Roberts, 2012).

In addition to their application as commercial products, plant specialized metabolites are also involved in complex stress processes such as root elongation, shoot formation, redirection of cell differentiation and somatic embryogenesis (Ikeda-Iwai et al., 2003; Patakas, 2012). Somatic embryogenesis is a process through which somatic cells dedifferentiate and undergo a reprogramming of physiology, metabolism and gene expression to form a somatic or zygotic embryo capable of regenerating a plant (Yang and Zhang, 2010). This process is heavily reliant on the plant stress response and elicitors of the stress response such as abscicic acid, 2,4- dichlorophenoxyacetic acid, wounding and osmotic stressors are often used to initiate somatic embryogenesis (Feher, 2015). After the generation of somatic embryogenic cultures, the presence of specialized metabolites such as phenolics can inhibit embryogenesis (Abohatem et al., 2011; Nic-Can et al., 2015), making control of specialized metabolism in these cultures especially important. *In vitro* somatic embryogenesis for production of synthetic seeds is a process being developed for the clonal propagation of high value plant species (e.g., lumber crops, medicinal plants, biofuels crops) and conservation of rare or endangered plant species (Sharma et al., 2013).

Therefore, developing an understanding of plant specialized metabolism and regulation as well as identifying strategies for manipulating specialized product formation is important for a variety of applications including the production of high-value specialized metabolites, manipulation of nutrient or nutraceutical content in food products and control of somatic embryogenesis for clonal propagation.

1.2. Plant cell culture

The use of *in vitro* plant systems allows for the study of plant metabolism without the limitations associated with full plants such as a lack of a controlled growth environment and slow growth rate. The initiation of plant cell cultures is possible due to the exploitation of the inherent plant stress response. Typically, plant cells respond to high stress levels through cell death, but application of low levels of stress can activate adaptation mechanisms, which can lead to cellular dedifferentiation or inducting of somatic embryo (Feher et al., 2003). Through the exploitation of this defense mechanism, plant cell cultures can now be created from virtually any plant through the isolation of plant tissue (Figure 1.2).

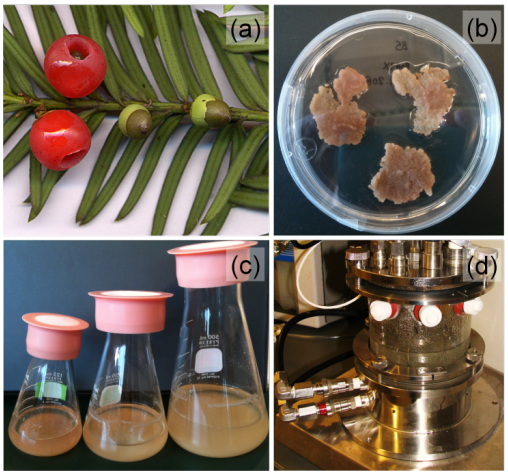

Figure 1.2. Development of a plant cell suspension culture. Explants from the whole plant (a) are plated on solid culture medium. With the correct nutrients and hormones combination, explants grow into a callus of undifferentiated cells (b). Callus cells are transplanted into liquid media, creating a suspension culture (c), which can be scaled-up for growth and production in a controlled bioreactor (d).

Low stress levels are generated through isolation of an explant (i.e., isolated plant tissue), which activates the plant wound-response (Grosset et al., 1990). These explants are then plated on solid growth media that is formulated to contain the growth hormones and nutrients necessary for each species, as well as compounds that can initiate additional stress responses (e.g., oxidative stress) (Pasternak et al., 2002). With correct media composition, explants proliferate into a callus of dedifferentiated cells, which can be screened for product(s) of interest, and then isolated and transferred to liquid medium to create suspension cultures. With the application of appropriate growth hormones (e.g., 2,4-Dichlorophenoxyacetic acid, 6-Benzylaminopurine, etc.) and media conditions (e.g., salt concentration, osmolality, etc.), dedifferentiated tissue can be directed towards embryogenesis (Feher et al., 2003).

1.3. Engineering of plant cell cultures for specialized metabolite production

The production of specialized metabolites via plant cell culture is limited by low product yields and unpredictable scale-up. Additionally, specialized metabolite accumulation over time within a single cell line and amongst cultures of the same cell line is often variable, which is likely related to cellular heterogeneity (Kolewe et al., 2008). Despite these limitations, several specialized metabolites have been successfully produced on a commercial scale using plant cell culture (Table 1.1).

Table 1.1. Products produced commercially via plant cell culture (updated from (Wilson and Roberts, 2012))

Product	Species	Manufacturer	Use/Application	Ref.
Specialized Metabolites				
Alpine rose derived compounds*	*Rhododendron ferrugineum*	PhytoCellTec, Buchs, Switzerland	• Cosmetic ingredient	(Lehmann et al., 2014)
Anthocyanins	*Euphorbia milli* *Aralia cordata*	Nippon Paint Co., Ltd., Osaka, Japan	• Textile dye • Coloring agents for fruit juices, wine and other beverages	(Meyer and Schmidhalter, 2014)
Apple derived compounds*	*Malus domestica*	PhytoCellTec, Buchs, Switzerland	• Cosmetic ingredients	(Lehmann et al., 2014)
Arbutin	*Catharanthus roseus*	Mitsui Chemicals, Inc., Tokyo, Japan	• Whitening agent for cosmetics • Pigment • Antiseptic	(Meyer and Schmidhalter, 2014)
Arctic cloudberries-derived bioactive compounds	*Rubus chamaemorus*	Lumene Cosmetics, Espoo, Finland	• Cosmetic ingredient	(Meyer and Schmidhalter, 2014)

Argan derived compounds*	*Argania spinosa*	PhytoCellTec, Buchs, Switzerland	• Cosmetic ingredient	(Lehmann et al., 2014)
Berberines	*Coptis japonica* *Thalictrum minus*	Mitsui Chemicals, Inc.	• Pharmaceutical ingredient • Anticancer • Antibiotic • Anti-inflammatory • Most commonly used for bacterial diarrhea and intestinal parasite and eye infections	(Meyer and Schmidhalter, 2014)
Betacyanins	*Beta vulgaris*	Nippon Shinyaku Co., Ltd., Kyoto, Japan	• Food dye • Red to red-violet pigment	(Meyer and Schmidhalter, 2014)
Carthamin	*Carthamus tinctorius*	Kibun Foods, Inc., Tokyo, Japan	• Cosmetic pigment • Food colourant and dye	(Meyer and Schmidhalter, 2014)
Date palm-derived compounds	*Phoenix dactylifera* L.	XTEM cell, St. Malo, France	• Cosmetic ingredients	(Meyer and Schmidhalter, 2014)
Docetaxel*	*Taxus* spp.	Phyton Biotech GmbH, Ahrensburg, Germany Samyang Biopharmaceuticals Corporation, Seoul, South Korea	• Anticancer • FDA approved for the treatment of head and neck, gastric, breast, prostate and non-small cell lung cancers	http://www.phytonbiotech.com/, https://www.samyangbiopharm.com/
Echinaceae polysaccharides*	*Echinacea purpurea* *Echinacea*	Diversa, Ahrensburg, Germany	• Pharmaceutical ingredient • Immunostimulent • Anti-inflammatory	(Meyer and Schmidhalter, 2014)

	augustifolia			
Geraniol	*Gramineae spp.*	Mitsui Chemicals, Inc.	• Essential oil • Primary component of rose, palmarosa and citronella oils	
Ginseng saponins	*Panax ginseng* CA Meyer	CBN Biotech, Korea	• Dietary supplement • Cosmetic ingredient • Food additive	(Meyer and Schmidhalter, 2014)
	Panax ginseng	Nitto Denko Corporation, Osaka, Japan		
	Wild *ginseng* stem cells	Unhwa Biotech Corp., Jeonbuk, Korea		
Grape derived compounds*	*Vitis vinifera*	PhytoCellTec, Buchs, Switzerland	• UV protection for skin	(Lehmann et al., 2014)
Leontopodic acids A and B	*Leontopodium alpinum*	Instituto di Ricerche Biotechnologiche (IRB), Italy	• Cosmetic ingredient	
Paclitaxel*	*Taxus* spp.	Phyton Biotech GmbH	• Anticancer • FDA approved for the treatment of ovarian, breast and lung cancers • Largest application of commercial plant cell culture	http://www.phytonbiotech.com/, https://www.samyangbiopharm.com/
		Samyang Biopharmaceuticals Corporation		
Podophyllotoxin	*Podophyllum* spp.	Nippon Oil, Tokyo, Japan	• Anticancer • Starting compound for the anticancer agents etoposide and teniposide (Chattopadhyay et al.,	(Lehmann et al., 2014)

			2002)	
Resistem	*Albizia julibrissin*	Sederma, Le Perray En Yvelines, FR	• Anti-ageing cosmetic ingredient	http://www.sederma.com/
Rosmarinic acid	*Coleus blumei*	A. Nattermann & Cie. GmbH , Cologn, Germany	• Anti-inflammatory	(Lehmann et al., 2014)
Scopolamine	*Duboisia* spp.	Sumitomo Chemical Co., Ltd., Tokyo, Japan	• Anticholinergicum • Antimuscarinic • Used in the treatment of motion sickness, nausea and intestinal cramping	(Lehmann et al., 2014)
Shikonin	*Lithosperum erythrorhizon*	Mitsui Chemicals, Inc.	• Red pigment/dye • Antibiotic	(Meyer and Schmidhalter, 2014)
Symphytum*	*Symphytum officinale*	PhytoCellTec, Buchs, Switzerland	• Cosmetic ingredient	http://www.phytocelltec.ch/
Heterologous Proteins				
Vaccines				
HN protein of Newcastle disease virus	*Nicotiani* spp.	Dow AgroSciences LLC, Indianapolis, IN	• Vaccine for Newcastle disease in poultry • First FDA approved plant-derived vaccine • Currently not on market	(Meyer and Schmidhalter, 2014)
Proteins				
α-galactosidase-A (PRX-102)*	*Daucus carota*	Protalix Biotherapeutics, Carmiel, Israel	• Potential Fabry Disease treatment • In phase I/II clinical trials	http://www.protalix.com/
AIR DNase (deoxyribonuclease I) (PRX-110)*	*Daucus carota*	Protalix Biotherapeutics	• Potential inhalable treatment for Cystic Fybrosis • In preclinical development	http://www.protalix.com/

Albumin*	*Oryza sativa*	InVitria, Junction City, KS	• Cell culture additive	https://www.invitria.com/
Anti-tumour necrosis factor (PRX-106)*	*Daucus carota*	Protalix Biotherapeutics	• Potential therapeutic for autoimmune diseases, such as rheumatoid arthritis • In preclinical development	http://www.protalix.com/
Human glucocerebrosidase (ELELYSO/ UPLYSO)*	*Daucus carota*	Protalix Biotherapeutics	• Enzyme replacement therapy for Gaucher's disease • Licensed by Pfizer, Inc. • Completed Phase III trial in Sept., 2009 • Received FDA approval in May, 2012	http://www.protalix.com/
Human lysozyme*	*Oryza sativa*	InVitria	• Bacterial cell lysis agent • Food and beverage preservative	https://www.invitria.com/
Lactoferrin*	*Oryza sativa*	InVitria	• Animal-free mammalian cell culture additive	https://www.invitria.com/
Moss-aGal (agalsidase)	*Physcomitrella patens*	Greenovation Biopharmaceuticals, Heilbronn, Germany	• Potential therapeutic for the treatment of Fabry Disease • In preclinical development	http://www.greenovation.com/
Moss-GBA (glucerase)	*Physcomitrella patens*	Greenovation Biopharmaceuticals	• Potential therapeutic for Gaucher's disease • In preclinical development	http://www.greenovation.com/
Oral human glucocerebrosidase (PRX-112)*	*Daucus carota*	Protalix Biotherapeutics	• Oral delivery of enzyme replacement therapy for Gaucher's disease • Carrot plant cells used as	http://www.protalix.com/

			delivery vehicle for the therapeutic protein • In phase II clinical trails	
Transferrin*	*Oryza sativa*	InVitria	• Cell culture additive	https://www.invitria.com/

*Verified to be commercially produced via plant cell culture as of 2015

To further optimize and engineer plant cell culture production platforms, strategies must be combined to address the three functional scales of cellular engineering, defined here as intracellular (pathway), intercellular (cell aggregation), and extracellular (external environment).

1.3.1. Extracellular engineering

Extracellular engineering can be defined as manipulation of a culture at the flask or process level. Traditionally, cultures are manipulated at this level through optimization of media components, application of elicitor treatments or changing of culturing parameters (temperature, light exposure, mixing rate, etc.). Due to the presence of aggregates in plant cell cultures (typically 50-2,000 μm in diameter) (Kolewe et al., 2008), manipulation at the process level can also be used to alter aggregation profiles. These extracellular treatments can significantly affect product accumulation in plant cell culture systems.

Elicitation is a traditional method used to increase specialized metabolite accumulation in plant cell cultures (Bourgaud et al., 2001). Many plant specialized metabolites are linked to plant defense against pathogens and herbivores, so cellular metabolism can be shifted to favor specialized metabolism through the introduction of chemical or physical stresses (Pauwels et al., 2009). Common elicitors can be

characterized as biotic (e.g., microbial extracts, proteins, etc.) and abiotic elicitors (e.g., hormones, heavy metals, osmotic or thermal stress, etc.), as recently reviewed (Gorelick and Bernstein, 2014).

Jasmonic acid and its conjugates and precursors, collectively known as jasmonates, are lipid-derived compounds involved in plant growth and development (Wasternack, 2007). They are able to induce a metabolic shift from growth to defense in many species, allowing a plant to defend itself from a hostile environment (Pauwels et al., 2009). Jasmonic acid and its methyl ester, methyl jasmonate, were first shown to increase the accumulation of specialized metabolites in suspension cultures of 36 distinct plant species (Gundlach et al., 1992), and exogenous methyl jasmonate addition increased paclitaxel production up to 46-fold over unelicited cells (Mirjalili and Linden, 1996; Yukimune et al., 1996; Ketchum et al., 1999). In *Arabidopsis thaliana* suspension cultures, methyl jasmonate was found to first induce genes involved in transcriptional regulation and jasmonic acid biosynthesis, followed by repression of cell cycle genes and induction of genes leading to phenylpropanoid production (Pauwels et al., 2008). Elicitation can also be used to understand the regulation of specialized metabolic pathways through differential gene expression studies of cultures that accumulate low/no versus high levels of specialized metabolites.

The presence of aggregates in plant cell culture can lead to the development of subpopulations due to diffusion limitations, differences in cell to cell signaling and shear exposure (Figure 1.3).

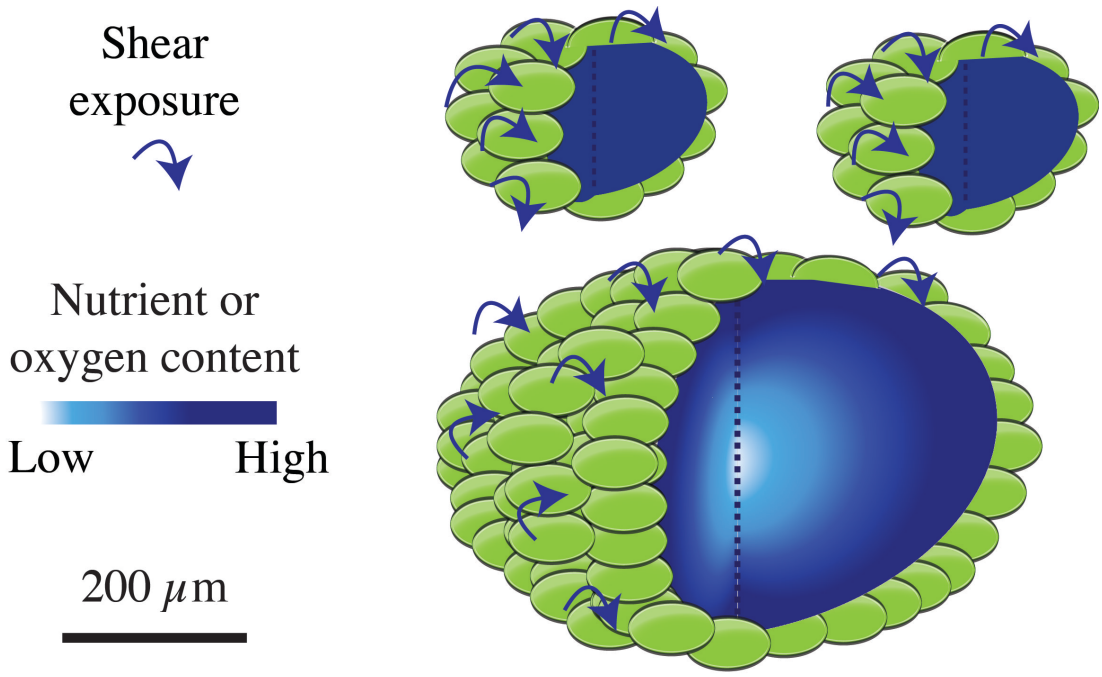

Figure 1.3 In suspension culture, plant cells grow as aggregates that can range in size from 50-2,000 µm in diameter. These aggregates lead to culture heterogeneity due to the presence of subpopulations, which result from differences in metabolic capacities due to cell signaling, varying exposure to shear or differing microenvironmental concentrations of nutrients and oxygen.

The production of specialized metabolites has been shown to depend upon the aggregation characteristics of a culture. For instance, small aggregates within *Taxus* suspension cultures have been shown to have up to a 40-fold increase in paclitaxel production (Kolewe et al., 2011a; Patil et al., 2012; Patil et al., 2013). Similarly, a study of *Vaccinium pahalae* culture with aggregates as large as 2 mm in diameter, showed that over 70% of anthocyanin production was in aggregates less than 240 µm in diameter (Pepin et al., 1999). In contrast, in the cultured strawberry line *Fragaria ananassa* R, aggregates with a mean diameter of 390 µm accumulated higher amounts of anthocyanins than those with a mean diameter of 200 µm (Edahiro and Seki, 2006). Although studies

have shown a link between aggregation and product yield, few studies have developed process level strategies to control aggregation in culture (Edahiro and Seki, 2006).

1.3.2. Intercellular engineering

Intercellular engineering can be defined as manipulation of a culture on a single cell level to improve product accumulation. The presence of aggregates in plant cell culture systems results in heterogeneity on a single cell level. As previously mentioned, this has direct effects on culture specialized metabolism. Therefore, it is important to examine culture heterogeneity on a single cell level to identify and characterize subpopulations. Additionally, when considering culture average data sets, key metabolic information is often diluted by non-producing cells, which can negatively influence the choice of metabolic engineering targets and strategies. The development of methods to characterize heterogeneity on a single cell level and to select for high producing subpopulations could allow for the development of superior cell lines.

Many techniques have been developed to study plant cell cultures on a single cell level (Figure 1.4).

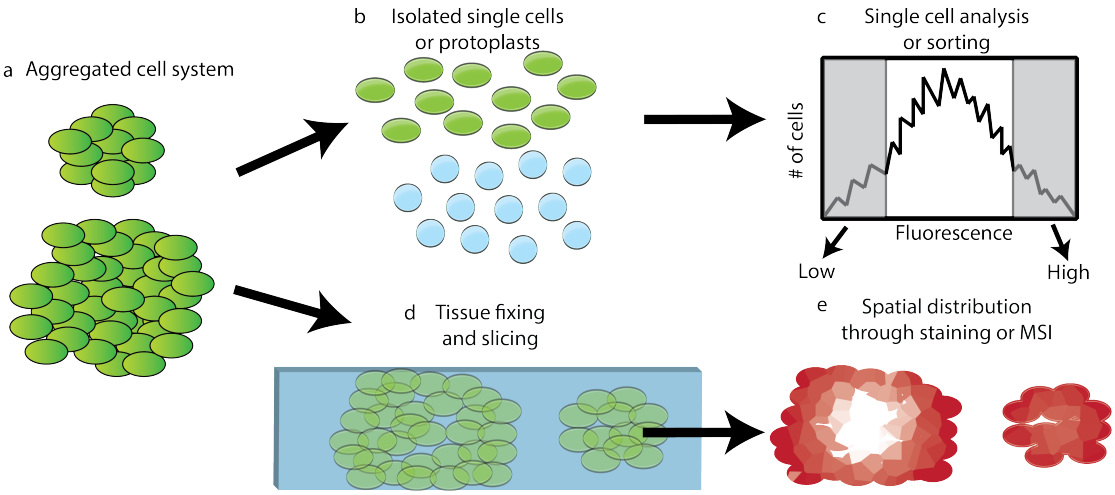

Figure 1.4. Methods used to study aggregated plant cell cultures on a single cell level. Aggregated cultures (a) can be digested into single cells using enzymes (b), allowing for study or sorting of cells on a single cell level (c). Additionally, tissue can be fixed and sliced (d) to allow for the visualization of the spatial distribution metabolites, proteins or mRNA within single cells of an aggregate (e).

For instance, organelles (nuclei, plastids, chromosomes or mitochondria), protoplasts and single cells can be isolated from cellular aggregates, allowing for the study of single particles using flow cytometry, as recently reviewed (Vrána et al., 2014). This technique has traditionally been used to characterize nuclear DNA content, ploidy levels and cell cycle participation in many cell systems, such as *Taxus* (Naill and Roberts, 2005a; Naill and Roberts, 2005c; Patil et al., 2014a) or *Harpagophytum procumbens* (Stancheva et al., 2011).

Through the use of fluorescence activated cell sorting (FACS), single cells producing high levels of specialized metabolites or proteins can be selected. By co-expressing a fluorescent reporter with a pharmaceutical protein in tobacco BY-2 cells, protoplasts with high-protein levels were successfully sorted (Kirchhoff et al., 2012). This strategy resulted in up to a 13-fold increase in the sorted cell protein productivity,

which remained stable for 12 months in culture. For metabolic analysis of specific cell types found within the roots of *Arabidopsis thaliana*, FACS was used to isolate cells that had been specifically tagged with GFP (Moussaieff et al., 2013). LC-MS was then used to create a metabolic map of the root through the identification of 50 metabolites within the individual cell types. Similarly, GFP tagged with a nuclear membrane target sequence and a biotin recognition peptide was expressed in *Arabidopsis* roots using a cell-type specific promoter (Deal and Henikoff, 2011). Labeled nuclei were isolated using biotin affinity purification, allowing for global gene expression and chromatin level studies in the specific cell types. Through the use of fluorescently tagged or biotinylated proteins and antibodies, these techniques could be applied to cell culture systems to investigate differences in metabolite levels and gene expression in differing aggregate subpopulations.

Single cells or specific cell types can be isolated through laser microdissection, mechanical isolation, protoplasting or cell sorting, allowing for metabolomic level analyses, as recently reviewed (Misra et al., 2014). Although these studies provide insight at the single cell level, the spatial distribution of metabolites within the cell aggregate/tissue is typically lost. Recently, mass spectrometry imaging methods have been developed to study metabolites on a single cell level in intact plant tissue or tissue slices (Bjarnholt et al., 2014). By imprinting of leaf or petal tissue onto the surface of a polytetrafluoroethylene or thin-layer chromatography plate, desorption electrospray ionization can be used study metabolite distributions with up to 100 μm resolution (Hemalatha and Pradeep, 2013; Li et al., 2013a). Using a matrix to aid in the ionization of metabolites can increase resolution up to 20 μm (Bjarnholt et al., 2014; Ye et al., 2013).

MSI has yet to be applied to cell culture systems, but could provide substantial insight into the spatial distribution of metabolites within cellular aggregates, leading to improved understanding of culture heterogeneity and allowing for the development of superior culture engineering strategies.

1.3.3. Intracellular engineering

Finally, intracellular engineering can be defined as the manipulation of a cell on the level of the metabolic pathway. Plant metabolic engineering on an intracellular level is a challenge due to the extensive number and diversity of metabolites produced in plant systems, as well as the complex interactions between plant primary and specialized metabolic pathways (Figure 1.1, Figure 1.5).

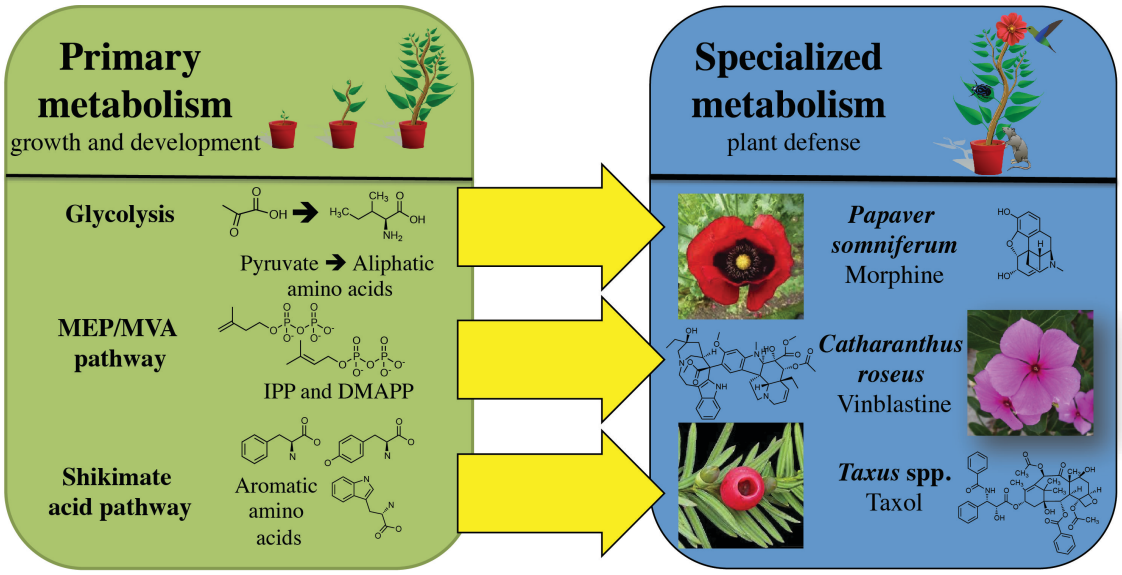

Figure 1.5 Whereas plant primary metabolism is conserved across plant species, plant specialized metabolism is species-specific. As a result, the pathways involved in plant primary metabolism (glycolysis, MEP/MVA pathways, shikimate acid pathway) are well characterized, whereas those involved in specialized metabolism are largely undefined. Additionally, the regulation of carbon flux through primary metabolism and into specialized metabolism is poorly understood.

Although plant primary metabolism is well characterized and well conserved across species, specialized metabolism is species-specific and metabolic pathways are sparsely defined (Aharoni and Galili, 2011; Chae et al., 2014).

It has been estimated that there are between 200,000 and 1,000,000 plant metabolites, making identification and characterization of specific metabolites an enormous bottleneck to plant metabolomics (Afendi et al., 2012; Dixon and Strack, 2003; Yang et al., 2013). In addition, regulation of carbon flux between central and specialized metabolism is poorly understood. There has been an influx of 'omics' information for many model and non-model plant species, necessitating the development of methods to begin to elucidate these complex pathways and interactions. Characterization of flux through key primary and specialized metabolic pathways is especially important in the design of metabolic engineering strategies.

Once metabolic engineering strategies have been identified, stable transformation methods must be available for implementation. Traditional gene transfer approaches (most commonly *Agrobacterium* transformation and particle bombardment) have advanced greatly over the last decade, allowing for development of reliable stable transformation methods for many non-model plant species that were previously recalcitrant (Barampuram and Zhang, 2011). That being said, transformation efficiencies for non-model plant species are often low and the time required for isolation of stably transgenic lines can be on the order of months, hindering metabolic engineering efforts.

1.4. Engineering a non-model plant species – The story of paclitaxel

1.4.1. Paclitaxel production routes

Paclitaxel was first discovered during a U.S. Department of Agriculture screen for plant derived anti-cancer between 1960 and 1982 (Cragg et al., 1996) and was approved for marketing as an anti-cancer agent in 1992 (Bristol-Myers Squibb). Used in the treatment of ovarian, breast and lung cancers as well as AIDS-related Kaposi's sarcoma, paclitaxel usage continues to increase dramatically from the initial 25 kg per year required to treat ovarian cancer in the U.S. (Cragg et al., 1993; Vongpaseuth and Roberts, 2007). Therefore, sustainable and reliable paclitaxel production routes are crucial for the continued success of the drug.

Initially, paclitaxel demand was met by harvesting bark of *T. brevifolia*. Because of the low paclitaxel content in the bark, 340,000 kg of *Taxus* bark, or 38,000 trees, were required to extract the desired 25 kg of drug per year (Cragg et al., 1993). Paclitaxel total synthesis has been accomplished, but reaction schemes are complex with low yields (Holton et al., 1994a; Holton et al., 1994b; Nicolaou et al., 1994; Wender et al., 1997a; Wender et al., 1997b). As a result, total synthesis is economically and environmentally unfavorable. The European yew tree, *T. baccata*, contains about 0.1% of two precursors (baccatin III and 10-deacetylbaccatin III), which can be synthetically converted into paclitaxel (Denis et al., 1988; P.G.M., 1998; Patel, 1998). Initially, semi-synthesis yields were approximately 50%, but a commercially viable semi-synthesis route was patented in 1992 (Holton, 1991). With this process, paclitaxel synthesis became commercially viable and Taxol® went on the market in 1993 (Mountford, 2010).

Semi-synthesis required 11 chemical transformations using 13 solvents and 13 organic reagents, making it costly and harmful to the environment (Vongpaseuth and Roberts, 2007). In 2002, Bristol-Myers Squibb discontinued the use of the semi-synthetic production route, switching entirely to a plant cell culture fermentation process for both environmental health and safety reasons and a financial incentive for a green pharmaceutical process (Mountford, 2010). This production system, developed by Phyton Biotech, Inc. is the largest commercial application of plant cell culture, utilizing the Chinese yew (*T. chinensis*) cultivated in 75,000 L bioreactors (Huang and McDonald, 2009) and has recently been described in detail by (Mountford, 2010). Whereas the semi-synthetic production route decreased costs to 25% of that for natural harvest, the plant cell fermentation process reduced costs to just 20% of that for natural harvest (Mountford, 2010).

Production of paclitaxel through this plant cell culture platform is currently sustainable, but demand could potentially exceed 200-300 kg per year as applications are being developed for paclitaxel in the treatment of Alzheimer's and post-heart surgery patients (Cragg et al., 1993; Nims et al., 2006). For these reasons, research efforts need to be directed towards development of superior plant cell culture processes to increase culture yields and decrease production costs, making *Taxus* plant culture an ideal non-model plant system to study.

1.4.2. Paclitaxel biosynthetic pathway

The paclitaxel biosynthetic pathway is believed to involve approximately 19 enzymatic steps after geranylgeranyl pyrophosphate (GGPP) (Chang and Keasling, 2006). Through precursor feeding, hybridization probes and differential gene expression

studies, many of the 19 putative steps within the paclitaxel biosynthetic pathway have been fully characterized [34,35], although some key steps remain elusive (e.g., oxetane ring formation) (Figure 1.6).

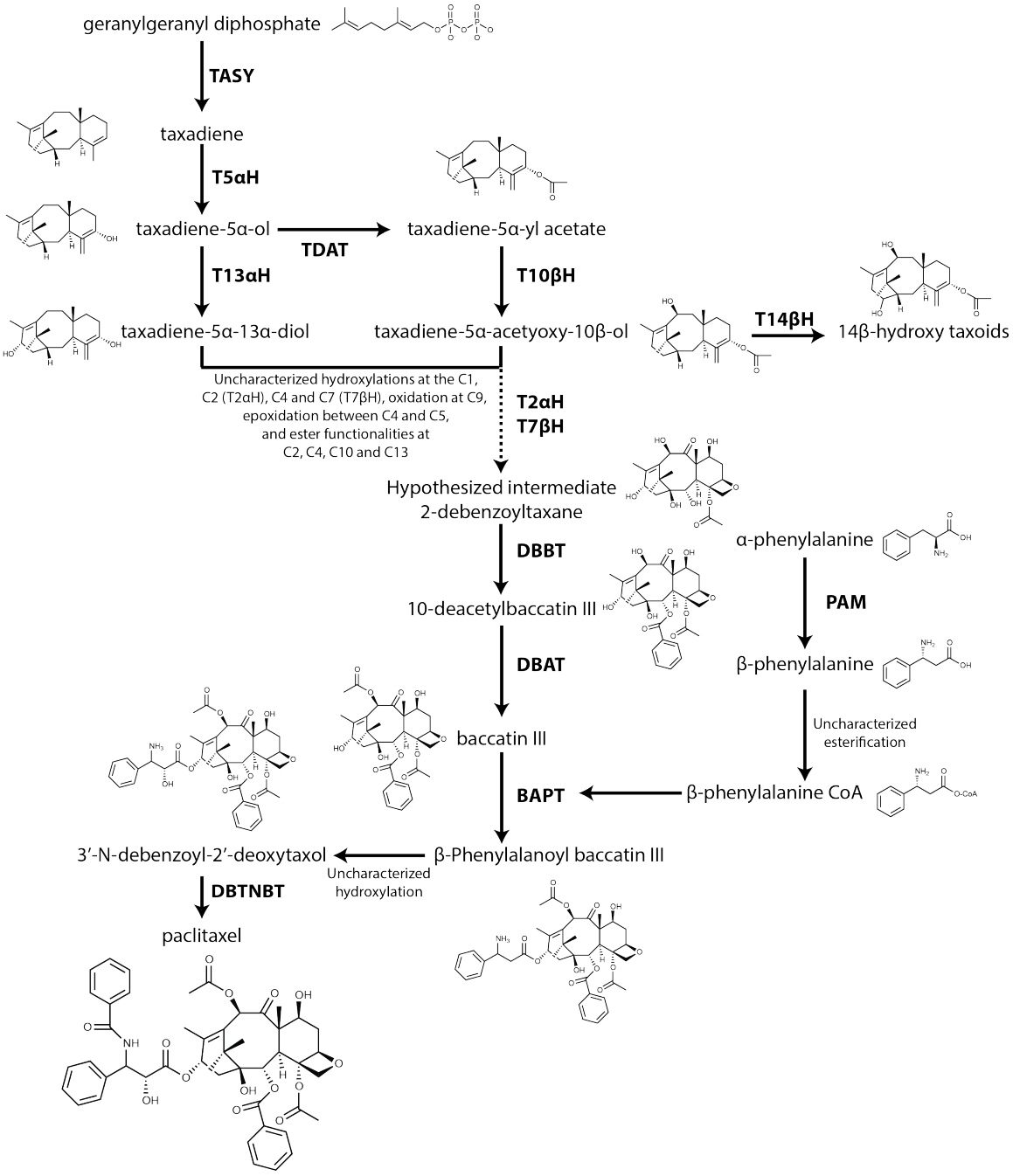

Figure 1.6. Paclitaxel biosynthetic pathway (Abbreviations of enzymes: TASY – taxadiene synthase; T5αH – taxadiene-5α-hydroxylase; T13αH – taxadiene-13α-hydroxylase; TDAT – taxadiene-5α-ol-O-

acetyl transferase; T10βH – taxadiene-10β-hydroxylase; T14βH – taxadiene-14β-hydroxylase T2αH – taxoid-2α-hydroxylase; T7βH – taxoid-7β-hydroxylase; DBBT - 2α-O-benzoyl transferase; DBAT – 10-deacetylbaccatin-III-10-O-acetyl transferase; BAPT – C-13-O-phenylpropanoyl-CoA transferase; DBTNBT – 3'-N-debenzoyl-2'-deoxytaxol N-benzoyl transferase; PAM - phenylalanine aminomutase)

Geranylgeranyl pyrophosphate (GGPP) is synthesized by three molecules of isopentenyl diphosphate (IPP) and one molecule dimethylallyl diphosphate (DMAPP) (products of the 2-C-methyl-D-erythritol 4-phosphate (MEP) and mevalonate (MVA) pathways) with geranylgeranyl pyrophosphate synthase (GGPPS) prior to the first committed step in the biosynthetic pathway (Cusido et al., 2007; Vongpaseuth and Roberts, 2007). Taxadiene synthase then converts GGPP to taxa-4(5),11(12)-diene (Koepp et al., 1995; Wildung and Croteau, 1996), which is then converted by taxadiene 5α-hydroxylase (T5αH), a cytochrome P450, to taxa-4(5),11(12)-dien-5α-ol (Hefner et al., 1996). With the identification of the enzymes taxadiene 13α-hydroxylase (T13αH) and taxadiene-5α-ol-O-acetyl transferase (TDAT) and the known intermediates, it was determined that a branch point exists, where at least two pathways use the substrate taxa-4(5),11(12)-dien-5α-ol. This intermediate can be diverted to either taxadiene 5α-yl-acetate by taxadiene-5α-ol-O-acetyl transferase (T5αH) (Walker et al., 1999) or taxadien-5α-13α-diol by the enzyme taxadiene 13α-hydroxylase (T13αH) (Jennewein et al., 2001). Taxadiene 5α-yl-acetate is then converted to taxadiene 5α-yl-acetyoxy-10β-ol by taxadiene-10β-hydroxylase (T10βH) (Schoendorf et al., 2001). This intermediate can be converted to a class of competing compounds called 14β-hydroxy toxoids by taxadiene-14β-hydroxylase (T14βH) (Jennewein et al., 2003).

After the formation of taxadien-5α-13α-diol or taxadiene 5α-yl-acetyoxy-10β-ol at the branchpoint, there are a series of uncharacterized hydroxylations at the C1, C2 (T2αH (Chau and Croteau, 2004)), C4 and C7 (T7βH (Chau et al., 2004)), oxidation at C9, epoxidation between C4 and C5, and ester functionalities at C2, C4, C10 and C13 where the order of reactions, as well as many of the enzymes are uncharacterized (Howat et al., 2014). This series of reactions leads to a hypothesized intermediate, 2-debenzoyltaxane. This hypothesized intermediate is then converted by 2α-O-benzoyl transferase (DBBT) to 10-deacetyl baccatin III (10-DAB) (Walker and Croteau, 2000b).

10-DAB is converted to the last non-side chain containing taxoid, Baccatin III, through the acylation of a hydroxyl group at the C10 position by 10-deacetylbaccatin-III-10-O-acetyl transferase (DBAT) (Walker and Croteau, 2000a). Baccatin III is conjugated to the β-phenylalanoyl-CoA side chain to form 3'-N-debenzoyl-2'-deoxytaxol by C-13-O-phenylpropanoyl-CoA transferase (BAPT) (Walker et al., 2002a). The β-phenylalanoyl-CoA side chain is derived from α-phenylalanine through phenylalanine aminomutase (PAM) (Walker et al., 2004). Finally, 3'-N-debenzoyl-2'-deoxytaxol N-benzoyl transferase (DBTNBT) catalyzes the benzamidation of 3'-N-debenzoyl-2'-deoxytaxol with benzoyl-CoA to form paclitaxel (Walker et al., 2002b).

1.4.3. Metabolic engineering of *Taxus* cell cultures

Taxadiene synthase (TASY), the first committed step in paclitaxel biosynthesis, was upregulated in hairy roots of *Taxus x media*, resulting in a 265% increase in paclitaxel production over untransformed cultures (Exposito et al., 2010). In *T. chinensis* suspension cultures, upregulation of 10-deacetylbaccatin III-10 β-*O*-acetyltransferase (DBAT), a key enzyme in paclitaxel biosynthesis, resulted in a 1.7 fold increase in

paclitaxel production (Zhang et al., 2011). Additionally, taxoid-14β-hydroxylase was down-regulated, with no effect on paclitaxel production . Although upregulation of key pathway genes has led to an increase in paclitaxel production (Li et al., 2011), studies have shown that paclitaxel accumulation is not entirely dependent upon biosynthetic pathway transcript levels within a culture (Onrubia et al., 2013; Patil et al., 2012). In *Taxus* suspension cultures, differences in the expression level of known paclitaxel biosynthetic pathway genes were negligible or minor for cell populations that accumulated up to a 15-fold difference in paclitaxel (Patil et al., 2012). These results suggest the need for studies on regulatory mechanisms outside of the biosynthetic pathway. Using particle bombardment, 9-cis-epoxycarotenoid dioxygenase, a key gene involved in abscisic acid (ABA) biosynthesis (a regulator of the plant stress response) was upregulated resulting in a 48% increase in ABA accumulation and a 2.7 fold increase in paclitaxel accumulation (Li et al., 2012a). Finally, a neutral/alkaline invertase (involved in sucrose hydrolysis) was upregulated in *Taxus* cultures, resulting in an increasing in taxane production and up to a two-fold increase in paclitaxel accumulation (Dong et al., 2015).

To improve metabolic engineering strategies, transcriptomic analyses have been used to identify putative pathway genes, transcription factors and other genes involved in the regulation of paclitaxel biosynthesis (Hao et al., 2011; Lenka et al., 2012; Li et al., 2012b; Wu et al., 2011). Recently, a transcriptome was generated for *Taxus x media* cells during steady state paclitaxel production (7 days after elicitation with 200 μM methyl jasmonate) (Sun et al., 2013). Although gene expression changes have been shown to return to basal levels within four days after elicitation with methyl jasmonate (Nims et al.,

2006; Onrubia et al., 2013), the sequencing project was able to identify putative genes within the paclitaxel biosynthetic pathway, as well as proposed genes involved in paclitaxel transport and degradation

1.5. Expanding beyond traditional pathway engineering approaches

The complexity of the paclitaxel biosynthetic pathway and the lack of knowledge regarding the balance of flux between conserved and specialized metabolism complicates traditional engineering strategies for *Taxus* cell cultures. This thesis applied a multi-scale approach to successfully engineer *Taxus* plant cell culture for enhanced synthesis of paclitaxel and to further characterize the balance between plant conserved and specialized metabolism. My thesis research can be organized according to the three functional scales previously introduced:

- Extracellular engineering: Application of mechanical shear and population balance modeling to control and manipulate aggregate size distributions in *Taxus* suspension cultures (Chapter 2)
- Intercellular engineering: Examining the distribution of paclitaxel in individual cells within *Taxus* aggregates (Chapter 3) and isolation of paclitaxel-producing subpopulations using a paclitaxel binding caspase system (Chapter 4)
- Intracellular engineering: Characterization of active specialized metabolic pathways (Chapter 5) and optimization of an *Agrobacterium*-mediated transformation method to enable metabolic engineering (Chapter 6)

It is important to note that these methods can be applied beyond the *Taxus* cell culture system through the multi-scale characterization and engineering of other non-model plant cell culture systems. Here, techniques were developed to characterize loblolly pine

somatic embryogenesis cultures, with the aim of developing culture-engineering strategies for improved embryo yield (Chapter 7). Methods developed to target each functional scale can then be applied to synergistically affect culture metabolism, allowing for optimization of culture performance.

CHAPTER 2.

EXTRACELLULAR ENGINEERING

2.1. Collaborators

Shashank Maindarkar, Chemical Engineering Graduate Student

Michael Vilkhovoy, Chemical Engineering Undergraduate Student

Michael Henson, Chemical Engineering Professor

2.2. Abstract

Plants are a valuable source of natural products with commercial applications as flavorings, insecticides and pharmaceuticals. Aggregation in plant suspension cultures, including *Taxus*, has been shown to directly affect the accumulation of high value products. Through application of mechanical shear by manual pipetting through a 10 mL pipet with a 1.6 mm aperture, the mean aggregate size of a *Taxus* culture can be reduced without affecting culture growth. When a constant level of mechanical shear was applied over eight generations of cell growth (two weeks per generation), the sheared population was maintained at a mean aggregate diameter 194 μm lower than an unsheared control, but the mean aggregate size fluctuated by over 600 μm, indicating unpredictable culture variability. To better understand the dynamics of disaggregation under applied mechanical shear, a population balance equation model was developed. Key culture parameters (age, biomass density and cell line) had a negligible affect on culture disaggregation and operating parameters (flow rate and aperture diameter) could be maintained constant to simplify the model. Four adjustable parameters involved in the breakage frequency function of the population balance equation model were estimated by nonlinear optimization from experimentally measured size distributions. A daughter

aggregate distribution function was selected to mimic a proposed breakage hypothesis, where large aggregates break to form a higher number of small daughter aggregates. The optimized model predictions were in strong agreement with measured size distributions. The model was then used to determine the shear required to successfully reach a target aggregate size distribution. This model will be used in the future to maintain a culture with a constant size distribution, with a goal of decreasing culture variability and increasing paclitaxel yields.

2.3. Introduction

Plants are a valuable source of commercial compounds with applications as pharmaceuticals, nutraceuticals, fragrances, flavors and dyes. Due to the complex structure of many of these natural compounds, chemical synthesis methods are often not feasible for large scale supply. As an alternative to chemical synthesis or natural harvest, plant cell suspension cultures can be used to sustainably produce these commercial compounds (Wilson and Roberts, 2012). One complication in working with plant cell systems is that as the cells divide, the cell wall does not always fully separate, leading to the formation of cellular aggregates that are connected by the middle lamella (Naill and Roberts, 2004). Aggregates that range in size from 100-2,000+ μm lead to the development of subpopulations within a culture due to the varying environmental conditions that result from diffusion limitations, differences in cell to cell signaling and exposure to shear (Kolewe et al., 2008). These subpopulations have been shown to accumulate varying levels of specialized metabolites, making aggregation an important processing parameter. To better understand the effect of aggregation on production of the anticancer compound paclitaxel, several studies have used filtration to segregate specific

subpopulations within a *Taxus* suspension culture based on size. Through these studies, smaller aggregates were found to accumulate higher levels of paclitaxel (Kolewe et al., 2011a; Patil et al., 2012; Patil et al., 2013). Studies in other species have also shown similar effects of aggregation on metabolite accumulation (Edahiro and Seki, 2006; Fu et al., 2005; Hulst et al., 1989; Kessler et al., 1999; Madhusudhan and Ravishankar, 1996; Miao et al., 2013; Pepin et al., 1999; Zhao et al., 2003).

To reduce aggregation in plant suspension cultures, either chemical or physical methods can be used (Wilson et al., 2014a). For example, arabinogalactan proteins play a role in the aggregation of suspension cultures of *Beta vulgaris*, with inhibition of these proteins resulting in a reduction in both aggregation and cell growth (Capataz-Tafur et al., 2011). Additionally, suppression of phenylpropanoid biosynthesis through addition of a metabolic inhibitor of phenylalanine ammonia lyase resulted in smaller aggregates without affecting growth in a strawberry suspension culture (Edahiro and Seki, 2006). Enzymes such as pectolyase and cellulase can be used to dissociate a cell from an aggregate without complete removal of the cell wall. This approach has been used to create single cell populations in *Taxus* suspension cultures, allowing for studies of the culture on a single cell level (Naill and Roberts, 2004). Using flow cytometry to look at the paclitaxel content of individual cells within a *Taxus* suspension culture showed that there was a broad range in the accumulation of the specialized metabolite (Naill and Roberts, 2005d). The main limitation of enzymatic digestion to create single cells is maintaining cell viability. Finally, mechanical shearing can be applied to reduce culture aggregation through aggregate breakage. *Taxus* suspension cultures under laminar flow conditions in a Couette flow bioreactor initiated a stress response, resulting in reduced

growth, cell viability and paclitaxel production (Han et al., 2013; Han and Yuan, 2009). Existing chemical and mechanical methods largely result in decreased cell growth and viability; therefore, alternative methods to generate smaller aggregates must be developed to study and use plant cells in bioprocesses.

We have developed a method to reduce the mean aggregate size of a *Taxus* suspension culture through applied mechanical shear by pipetting cultures through a 10 mL serological pipet; this method had no effect on short-term culture growth (Wilson et al., 2014b). In the work presented here, the long-term effect of a constant level of mechanical shear on the growth and aggregation dynamics of a culture was quantified over eight generations. To predict disaggregation of a culture in response to mechanical shear, a population balance equation (PBE) model was developed. The key culture and operating parameters that affect culture disaggregation were determined and incorporated into the PBE model. Kernel functions were established and the model was fit to experimental data sets by adjusting unknown kernel parameters. This model was then verified against non-fitted experimental datasets representing a variety of culture properties (e.g., cell line, day of culture, density and starting aggregate size distribution). Finally, the model was applied to determine the amount of shear required to reach a target aggregate size distribution and verified for a diversity of starting cultures. The combined use of the model and applied shear represents a new approach to engineeri plant suspension cultures for enhanced performance.

2.4. Materials and Methods

2.4.1. Experimental

2.4.1.1. Maintenance of *Taxus* suspension cultures

The *Taxus cuspidata* (PO93X, PO93XC, P991C, P93AF and P93AFC) and *Taxus canadensis* (CO93D) cell lines were provided by the United States Plant Soil and Nutrition Laboratory (Ithaca, NY). All chemicals were purchased from Sigma-Aldrich Co. (St. Louis, MO) unless otherwise noted. Cells were maintained and subcultured on a bi-weekly basis, as previously described (Kolewe et al., 2011a). Aggregate size distributions and cellular biomass were measured using a Multisizer 3™ Coulter counter equipped with a 2,000 μm aperture (Beckman Coulter, Brea, CA), as previously described (Kolewe et al., 2010). For analysis, replicate two mL samples of well-mixed culture were analyzed from each flask at each time point. Because the Coulter counter is calibrated using latex beads with low conductivity, whereas the cells being analyzed are highly aqueous and therefore have some level of conductivity, a correlation must be used to convert the Coulter counter underestimates the size of particles passing through the aperture. Therefore, data from the Coulter counter was converted to true culture properties using a previously established correlation (Kolewe et al., 2010).

2.4.1.2. Mechanical shearing of suspension cultures

Cultures were sheared by drawing the culture through a 10 mL polystyrene disposable standard serological pipet (Fisher Scientific, Pittsburgh, PA) using a Portable Pipet-Aid® XP (Drummond Scientific Company, Broomall, PA). A single iteration of shear refers to the uptake and release of 10 mL of culture volume. Unless otherwise

noted, cultures were sheared using a 10 mL polystyrene serological pipet tip with an inner diameter of 1.6 mm at a constant flow rate of 7.3 mL/s.

2.4.1.3. Monitoring long-term growth and aggregation of sheared cultures

Eight cultures of P93AF cultures (~ 100 mL volume) were maintained in 250 mL flasks for eight generations (each generation refers to a 14-day growth cycle). Experimental flasks were sheared 25 times on day 0, and 10 times on days 4, 7, 11 and 14 of the culture period, whereas control flasks remained unsheared. Replicate two mL culture samples were taken from each flask on days 0, 4, 7, 11 and 14 of each generation for Coulter counter analysis.

2.4.1.4. Determining factors that affect disaggregation

Taxus cells (cell line and day of culture specified for each experiment) were sheared as described above, and a single two mL sample was taken from each flask at 0, 10, 25, 50 and 75 times sheared for Coulter counter analysis. For each experiment, triplicate flasks (biological replicates) of the same condition were cultured in parallel. To determine the effect of aperture diameter on disaggregation, Day 6 PO93XC cultures were sheared with a 10 mL glass disposable serological pipet (inner diameter of 1.5 mm), 10 mL polystyrene disposable serological pipet (inner diameter of 1.6 mm) and a 10 mL polystyrene disposable serological pipet with a broken tip (inner diameter of 7.3 mm). To investigate the effect of flow rate on disaggregation, Day 7 PO93XC cells were sheared using varying flow rates. The flow rate of a Portable Pipet-Aid was varied by changing the speed on the Pipet-Aid to slow (2.4 mL/sec), medium (4.0 mL/sec) and fast (7.3 mL/sec). The volumetric flow rate was estimated by determining the time required to pipet and dispense 10 mL of water. The biomass density of a culture was varied using a

day 12 culture of P93AFC cells. This culture was diluted to three concentrations using fresh cell culture medium to final cell concentrations of 6.3 g/L, 5.3 g/L and 3.1 g/L. Finally, the effect of culture age on disaggregation was studied using a P93AFC culture that was sheared on day 0 through day 8 of a culture generation.

2.4.2. Model

2.4.2.1. Model formulation

Population balance equation (PBE) models can be used to describe the breakage and coalescence of particles through a number balance on the particles within the system (Ramkrishna and Mahoney, 2002). Since the application of shear occurs on a much shorter time-scale than the growth of the culture, only the breakage of aggregates was considered here. Additionally, cells within an aggregate are connected through physical means due to the presence of the middle lamella of the cell wall rather than attractive forces. Therefore, coalescence within the system was considered negligible. Because the Coulter counter accurately measures aggregate volume (and therefore measurements are unaffected by irregular particle shapes), a volume-based PBE was used in this study. The model was treated as a well-mixed, batch system with conserved volume. Under these assumptions, the PBE can be written as (Maindarkar and Henson, 2013; Raikar et al., 2009),

$$\frac{\partial n(v,t)}{\partial t} = -\Gamma(v)\, n(v,t) + \int_{v}^{\infty} \beta(v,v')\, \Gamma(v')\, n(v',t)\, dv' \tag{1}$$

where v is the volume of the aggregate, $n(v,t)dv$ is the number of aggregates that fall within the volume $[v, v+dv]$ at time t, which is a dimensionless time unit that corresponds to the number of iterations of shear; $\beta(v,v')$ is the daughter aggregate

distribution function that determines the probability of a daughter aggregate of size v to be formed from a mother aggregate of size v'; and $\Gamma(v)$ is the breakage frequency representing the fraction of aggregates of size v breaking per unit time. The PBE requires specification of a breakage function $\Gamma(v)$ and a daughter aggregate distribution function $\beta(v, v')$. The PBE describes the evolution of the number density of aggregates $n(v, t)$, whereas the Coulter counter provides measurements of the volume percent distribution, $n_p(v, t)$. The Coulter counter most accurately measures particle volume, which is not affected by irregularities in particle shape. The data is then converted to a number distribution by calculating an equivalent spherical diameter (Raikar et al., 2009). The measured volume distribution of an unsheared cell culture was used as the initial condition to integrate the PBE. One iteration of shear is defined as the uptake and release of 10 mL of culture through the pipet, which corresponds to one dimensionless time unit. The initial condition for each subsequent pass is the predicted aggregate size distribution of the previous pass.

To select the two PBE functions, it is important to understand the aggregate breakage mechanism under shear. It is hypothesized that larger aggregates break more easily than smaller aggregates due to irregularities in the shape of larger aggregates. Based on this proposed mechanism, two breakage frequencies ($\Gamma_1(v), \Gamma_2(v)$) were formulated to predict the breakage of smaller and larger aggregates, respectively, as follows,

$$\Gamma(v) = \Gamma_1(v) + \Gamma_2(v) = K_1 \exp\left(-K_2 \frac{1}{v}\right) + K_3 \exp\left(-K_4 \frac{1}{v}\right) \quad (2)$$

where K_1, K_2, K_3 and K_4 are adjustable parameters. The shape of the exponential function allows breakage of only aggregates above a certain critical size, which is consistent with experimental observations. The values of parameters K_2 and K_4 determine the critical size above which an aggregate will break. To differentiate equations for $\Gamma_1(v)$ and $\Gamma_2(v)$ where $\Gamma_1(v)$ accounts for the breakage of particles greater than 300 μm, a constraint was applied to K_2 ($K_2 > 10^7$). To model the number and size of daughter aggregates being formed, a power law form of generalized Hill-Ng distribution (Hill and Ng, 1996) was selected as the daughter aggregate distribution function $\beta(v, v')$,

$$\beta(v, v') = \frac{p(v)}{v'} \left(p(v) - 1\right) \left(1 - \frac{v}{v'}\right)^{p(v)-2} \tag{3}$$

where $p(v)$ is the number of daughter aggregates. $\beta(v, v')$ represents the uniform probability of daughter aggregate of any size ($v < v'$) being formed due to breakage of the mother aggregate of size v'. Due to the shape of the aggregates, it was hypothesized that smaller, spherical aggregates tend to undergo binary breakage and larger, non-spherical aggregates tend to break into multiple daughter aggregates, as further explained in the discussion section of this paper. Therefore, p was varied as a function of aggregate size. The number of daughter aggregates p was selected to be 2 for aggregates of size smaller than v_1 and for aggregates above certain size v_2, p was selected to be p_{max}. The number of daughter aggregates was varied linearly for mother aggregates of size between v_1 and v_2.

$$p(v) = \begin{cases} 2 & for\ v < v_1 \\ \dfrac{v - v_1}{v_2 - v_1}(p_{max} - 2) & for\ v_1 < v < v_2 \\ p_{max} & for\ v > v_2 \end{cases} \quad (4)$$

The choice of v_1, v_2, p_{max} is further discussed in the following section on parameter estimation.

2.4.2.2. Parameter estimation

The PBE model was solved numerically by approximating the integral term using the fixed pivot technique (Kumar and Ramkrishna, 1996) with 56 node points collected from Coulter counter analysis. The discretized PBE model consisted of 56 differential equations with the independent variable being the dimensionless time (corresponding to the iteration of shear) and the dependent variable corresponding to the volume distribution at each of the node points (Maindarkar and Henson, 2013). The model was solved using the Matlab code ode45 with an input of the initial aggregate size distribution. The optimization problem was formulated to estimate the model parameters. The model involved four parameters in the breakage functions (K_1, K_2, K_3, K_4) and three parameters in the daughter aggregate distribution function (v_1, v_2, p_{max}). The parameters v_1, v_2, p_{max} were determined based on manual optimization using experimental data sets (as specified in the Results section) and were not estimated by computational optimization to reduce the complexity of the optimization problem. For this manual optimization, the parameters v_1, v_2 were varied between 400 and 2,000 μm along the 56 node points, and the parameter p_{max} was varied between 5 and 18. The parameters that provided the best fit to the experimental data sets were selected and used to obtain all model predictions. Parameters K_1, K_2, K_3 and K_4 were estimated from experimental data

sets (as specified in the Results section) by nonlinear optimization. The PBE model was temporally discretized into 15 finite elements and two internal collocation points per element. Using additional finite elements only increased the computational time with no significant effect on the model results (results not shown). The procedure converted the PBE into a large set of algebraic equations. The finite elements could then be related back to the iterations of shear to match the experimental datasets, which were collected at 10, 25, 50 and 75 iterations, with the second finite element corresponding to the particle size distribution after 10 iterations of shear, the fifth element corresponding to the particle size distribution after 25 iterations of shear, etc. The parameters were optimized using a least-squares objective function with the form,

$$\psi_1 = \sum_{i=1}^{N} \frac{\sum_{j=1}^{n}\left[\hat{n}_p(v_j, i) - n_p(v_j, i)\right]^2}{\sum_{j=1}^{n}\left[n_p(v_j, i)\right]^2} \tag{5}$$

where $n_p()$ is the experimental value of the volume distribution at position v_j after i iterations of shear; $\hat{n}_p()$ is the model predicted value of the volume distribution at position v_j after i iterations of shear; n is the total number of node points; and N is the number of times that the sample is sheared. The optimization problem was formulated in AMPL (Fourer et al., 1993) and minimized using the nonlinear solver CONOPT (Drud, 1994).

2.4.2.3. Design methodology

The PBE model was used to predict the number of times a cell culture must be sheared to achieve a target aggregate size distribution. The optimization problem was formulated with the number of passes through the shearing device as the decision

variable. The optimized parameters K_1, K_2, K_3 and K_4were used in the PBE model and the following least-square objective function ψ_2 was used for optimization,

$$\psi_2 = \frac{\sum_{j=1}^{n}\left[\hat{n}_p(v_j) - n_{tar}(v_j)\right]^2}{\sum_{j=1}^{n}\left[n_{tar}(v_j)\right]^2} \tag{6}$$

where n_{tar} represents a target distribution and $\hat{n}_p$ represents the model predicted distribution. The target distributions were chosen based on experimental datasets to represent typical distributions achieved after 10-20 and 20-30 iterations of shear. Similar to parameter estimation, the model was discretized temporally and spatially to generate a set of nonlinear algebraic equations that were used in the optimization problem as equality constraints. The number of iterations of shear was constrained to be between 0 and 100. The problem was solved in AMPL using solver CONOPT to determine the optimal number of iterations of shear to be performed to minimize the error between target and experimental aggregate size distributions.

2.5. Results

2.5.1. Reducing aggregate size in plant cell culture

The mean aggregate size of a *Taxus* suspension culture was successfully reduced by pipetting the culture through a 10 mL pipet with a 1.6 mm aperture (Figure 2.1).

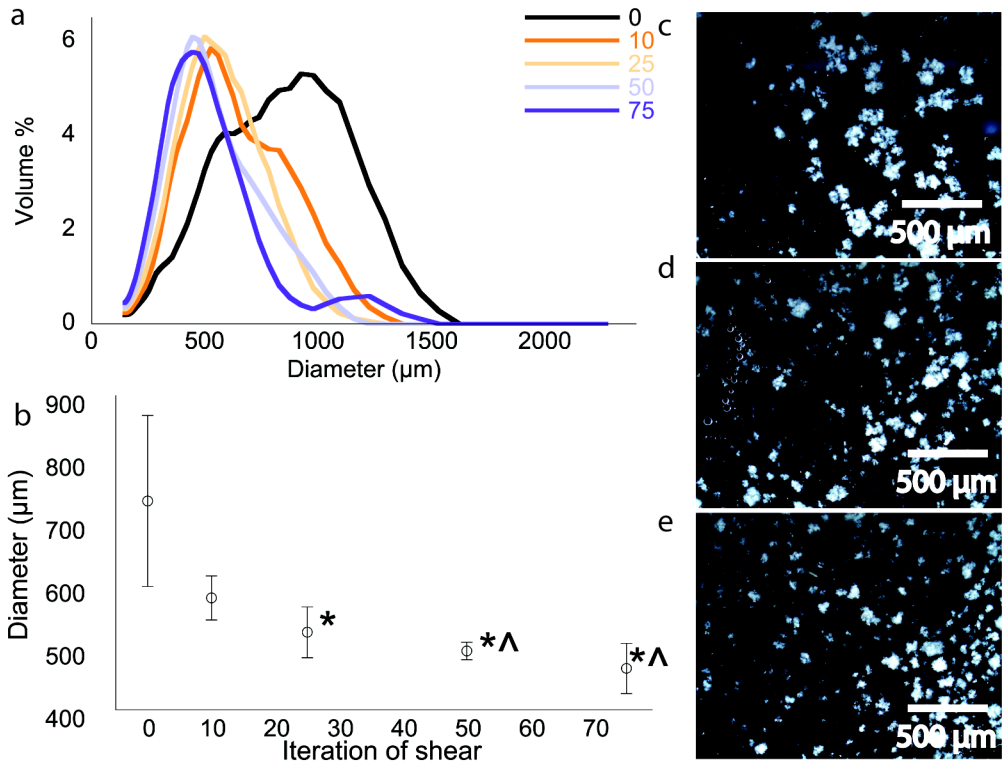

Figure 2.1. Manual pipetting of suspension cultures leads to a successful reduction in mean aggregate size. The volume distribution (a) mean diameter (b) after application of 0, 10, 25, 50 and 75 iterations of shear, as well as microscope images of the cultures after application of (c) 0, (d) 10 and (e) 75 iterations of shear. Data represent the average of three biological replicates. A Student's t-test determined the mean diameter to be statistically different ($p < 0.05$) from the mean diameter after 0 (*) or 10 (^) iterations of shear.

A single iteration of shear refers to the uptake and release of 10 mL of culture. Through mechanical shearing by pipetting, the mean aggregate size of a *Taxus* suspension culture was reduced from 730 µm to 470 µm (Figure 2.1a,b) over 75 iterations of shear. There was no significant change in the mean aggregate size of the culture after application of 50 iterations of shear. Microscopy was used to confirm the reduction in aggregate size, as seen in Figure 2c-e.

2.5.2. Long-term variability in culture aggregation

The growth and aggregation of an unsheared (control) and a sheared *Taxus* suspension culture were monitored over eight generations (Figure 2.2).

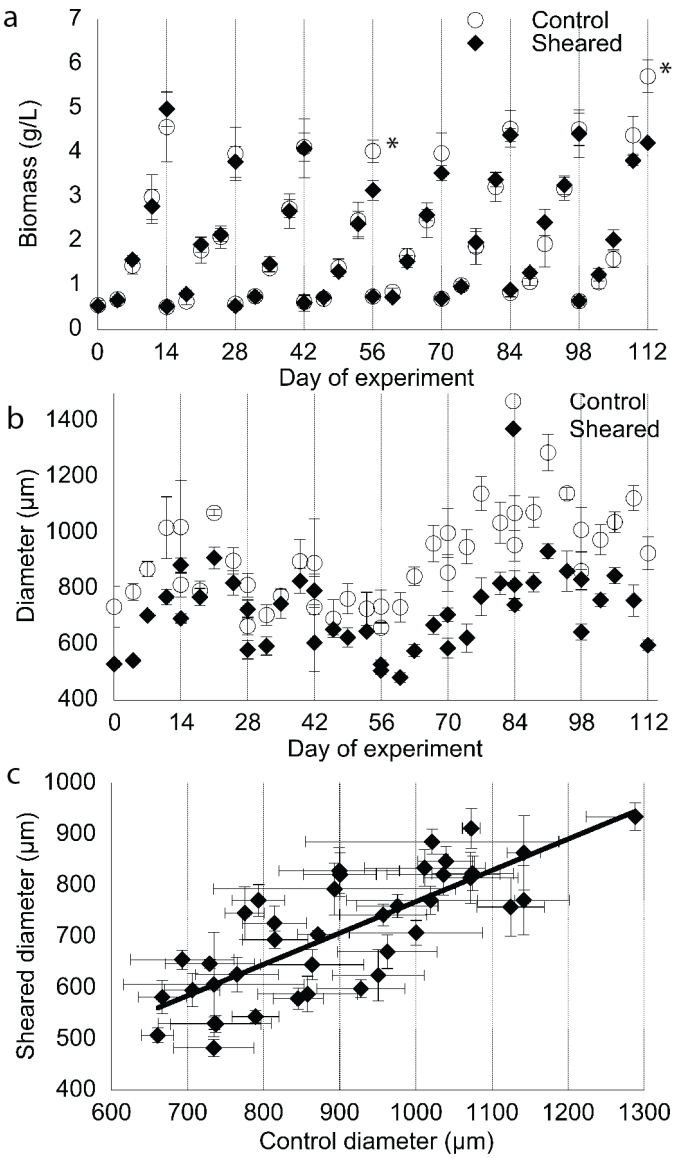

Figure 2.2. (a) Long-term growth (* indicates statistical difference from control using the Student's t-test ($p < 0.05$)) and (b) aggregation of a sheared and unsheared (i.e., control) *Taxus* (P93AF) suspension culture (of the 40 data points presented for mean aggregate size, only 9 were statistically the same). Sheared cultures were sheared 25 times on day 0 and 10 times on days 4, 7, 11 and 14. (c) Correlation between the mean aggregate size of the unsheared to the sheared culture. The relationship was found to be statistically significant using the Pearson correlation coefficient for linear correlations ($n = 40$, $R = 0.748$, critical value = 0.264). X-axis grid lines separate each generation of cell growth. Reported values represent the average of three biological replicates.

Twenty-five iterations of shear were applied to the culture on day 0 and ten iterations of shear on days 4, 7, 11 and 14 of each generation. The culture growth was stable and unaffected by shear over the four-month period, representing eight generations of culture growth (Figure 2.2a), with only two of the 40 data points being statistically different. Although the sheared population maintained a mean diameter up to 370 μm less than the unsheared culture throughout the four-month period (with an average difference of 190 ± 100 μm), the mean aggregate size of both cultures varied in an unpredictable manner (Figure 2.2b). The diameters of both cultures were statistically the same at nine of the 40 data points collected. The unsheared culture fluctuated over 600 μm between 660 μm and 1,290 μm, whereas the sheared culture fluctuated over 450 μm between 480 μm and 930 μm. Unexpectedly, there is a positive correlation between the mean aggregate size of the control culture and the mean aggregate size of the sheared culture, as determined by a Pearson correlation coefficient for linear correlations ($n = 40$, $R = 0.748$, critical value = 0.264, $p<0.05$) (Figure 2.2c). Hence, although the populations remained isolated throughout the experiment, their aggregation patterns were similar.

2.5.3. Factors that affect disaggregation

To maintain a sheared culture at a constant mean aggregate size distribution, application of shear can be tailored to the specific properties of the culture at the time of shearing (i.e., starting aggregate size distribution) using a population balance equation (PBE) model. To develop this model, the factors that affect disaggregation were explored to define relevant parameters and relationships (Figure 2.3).

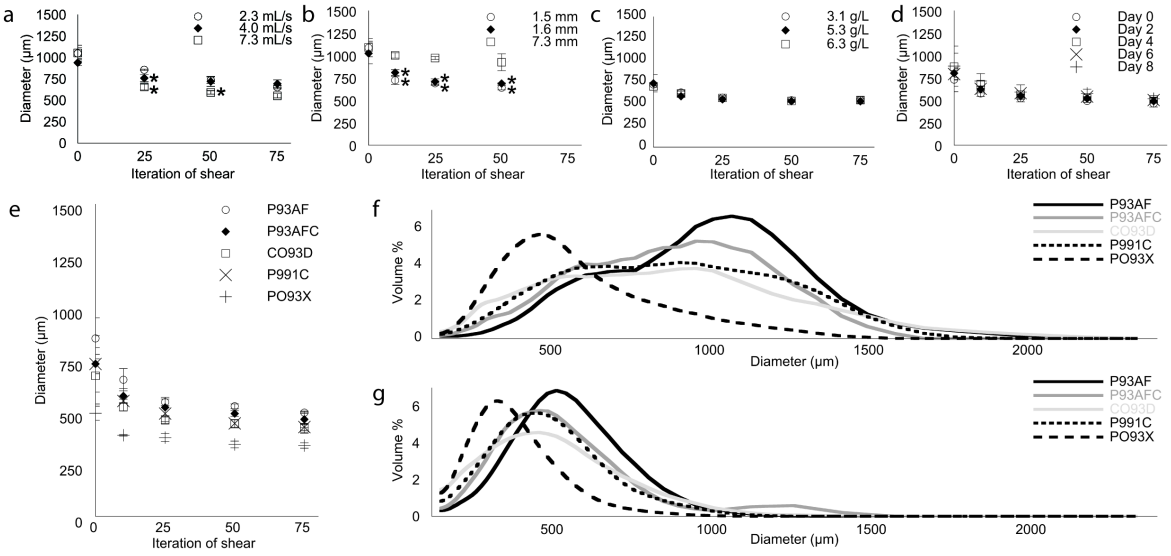

Figure 2.3. Determination of factors that affect disaggregation. The parameters that could relate to the method of shearing are (a) flowrate, which was measured at 2.3, 4.0 and 7.3 mL/s and (b) aperture diameter, which was measured at 1.5, 1.6 and 7.3 mm. The parameters that could relate to the culture properties are (c) biomass density (measured at 3.1, 5.3 and 6.3 g/L), (d) day of culture (measured on days 0-8) and (e) cell line , (f) starting aggregate size distribution and (g) aggregate size distribution after 75 iterations of shear are shown. For (a) and (b), * indicates statistically different from the largest mean aggregate size at that iteration of shear.

To determine the effect of flow rate on disaggregation, the flow rate of the Pipet Aid was varied from 2.4 to 7.3 mL/s. As expected, the culture with the fastest flow rate of 7.3 mL/s resulted in the fastest rate of disaggregation and the lowest mean aggregate diameter, reducing the mean aggregate size of the culture from a starting mean diameter of 1,050 µm to a final mean diameter of 550 µm (Figure 2.3a). Although the 4.0 mL/s flow rate resulted in a lower mean aggregate diameter than the 2.3 mL/s flow rate after 25 times shearing, the final mean aggregate diameter for both the 2.3 and 4.0 mL/s flow rates was 690 µm. Due to the fast rate of disaggregation at the fastest flow rate evaluated, a flow rate of 7.3 mL/s was used in all further experiments.

The effect of the inner pipet tip inner diameter on culture disaggregation was examined using three different pipets: a glass serological 10 mL pipet with an inner tip diameter of 1.5 mm, a plastic serological 10 mL pipet with an inner tip diameter of 1.6 mm and a broken tip plastic 10 mL serological pipet with an inner tip diameter of 7.3 mm (Figure 2.3b). The inner diameter of the pipet tip has a significant influence on the disaggregation of the culture, with the 1.5 and 1.6 mm pipet tips resulting in disaggregation from a starting mean diameter of 1,090 μm to a mean diameter of 690 μm. The 7.3 mm inner diameter pipet resulted in very little aggregate breakage, with the final culture having a mean diameter of 930 μm. The 1.6 mm pipet tip was used for further experiments.

Because cultures increase in biomass density throughout a generation of cell growth, it is important to understand the effect of culture density on disaggregation (Figure 2.3c). The culture density had no effect on disaggregation, with the highest density culture (6.3 g/L) and the lowest density culture (3.1 g/L) showing identical aggregation properties throughout the experiment from a starting mean diameter of 700 μm to a final mean diameter of 540 μm. This negligible effect on disaggregation confirms that culture density does not need to be included as a parameter in the model.

To be effective, the shearing method was applied on multiple days throughout a generation of cell growth. Throughout the 14-day growth period, cells are typically in lag phase for days 1-2, growth phase for days 3-12 and stationary phase for days 13-14 (Kolewe et al., 2012). Therefore, the effect of the day of culture must be investigated. The outcome of these culture properties on disaggregation can be seen in Figure 2.3d. The disaggregation properties of a culture did not change over the first eight days of a

generation (data for days 1, 3, 5 and 7 not shown). As a result, the day of the culture has a negligible effect on culture disaggregation and does not need to be included as a parameter in the model.

Culture aggregation can vary unpredictably within a cell line and across different cell lines. To determine the effect of starting mean aggregate size and cell line, five cell lines with varying aggregate profiles were investigated (Figure 2.3e,f,g). Three cell lines, P991C, CO93D and P93AFC, had similar starting aggregate size distributions (Figure 2.3f), with starting mean diameters of 730 μm, 680 μm and 730 μm, respectively. These cultures showed identical disaggregation profiles after 75 iterations of shear, reaching final diameters of 430 μm, 420 μm and 460 μm, respectively, after 75 iterations of shear. Cell line P93AF, which started with a significantly larger mean aggregate size of 860 μm, was reduced upon application of shear to a mean diameter 500 μm, which was significantly larger than the previous three cell lines. Additionally, cell line PO93X, which started with a significantly smaller mean aggregate size of 500 μm, was reduced to a final mean aggregate size of 340 μm. Therefore, it was determined that the initial aggregate size of the culture is the only factor that must be accounted for in the PBE model.

2.5.4. Model parameter estimation and extensibility

To estimate the model parameters involved in the breakage frequency and daughter aggregate distribution function, experimental data were collected for cultures with different initial size distributions. To obtain these data sets, experiments were performed with varying cell lines, biomass densities and culture densities. In each experiment, aggregates were sheared up to 75 times, and aggregate volume distributions

were measured after 10, 25, 50, and 75 iterations of shear. The parameters v_1, v_2, p_{max} in the daughter aggregate distribution were manually optimized to reduce computational requirements and the values that produced the best fit of the experimental aggregate volume distribution data were determined (Table 2.1).

Table 2.1. Parameter values in the optimized model. For K2 and K4, which have units of μm^3, the equivalent spherical diameter is shown in parenthesis.

Parameter	Value
v_1	9.6 x 10^6 μm^3 (500 μm)
v_2	119.7 x 10^6 μm^3 (1,200 μm)
p_{max}	15
K_1	8.27 1/s
K_2	1.12 x 10^8 μm^3 (880 μm)
K_3	0.24 1/s
K_4	1.00 x 10^4 μm^3 (40 μm)

From the resulting daughter aggregate distribution function and optimized parameters, it was determined that mother aggregates below 500 μm break into two daughter aggregates, whereas mother aggregates above size of 1,200 μm break into 15 smaller daughter aggregates with equal probability of any size (smaller than mother aggregate) being formed. This breakage hypothesis is described in further detail in the Discussion section of this paper. The number of daughter aggregates (Eq. 4) was varied linearly by aggregate volumes for aggregates between 500 and 1,200 μm (Figure 2.4a).

To best fit the experimental data, two breakage functions were defined. Model parameters K_1, K_2, K_3 and K_4 were estimated using experimental results from cell lines

P93AFC (day 0), P93AF (day 0) and P991C (day 14) by nonlinear optimization (Table 2.1). These data sets were chosen to cover a diversity of culture properties, including varying cell lines, culture ages and starting diameters and dry weights. The breakage frequencies obtained using the optimized parameters are shown in Figure 2.4b. Although a constraint was applied to $\Gamma_1(v)$ such that it must account for breakage of mother aggregates larger than 300 μm (eqn 2), the model optimization established that $\Gamma_1(v)$ comes into effect for aggregates greater than 880 μm (Figure 2.4b). From the resulting breakage functions, it was found that aggregates greater than 880 μm broke more frequently than those below 880 μm.

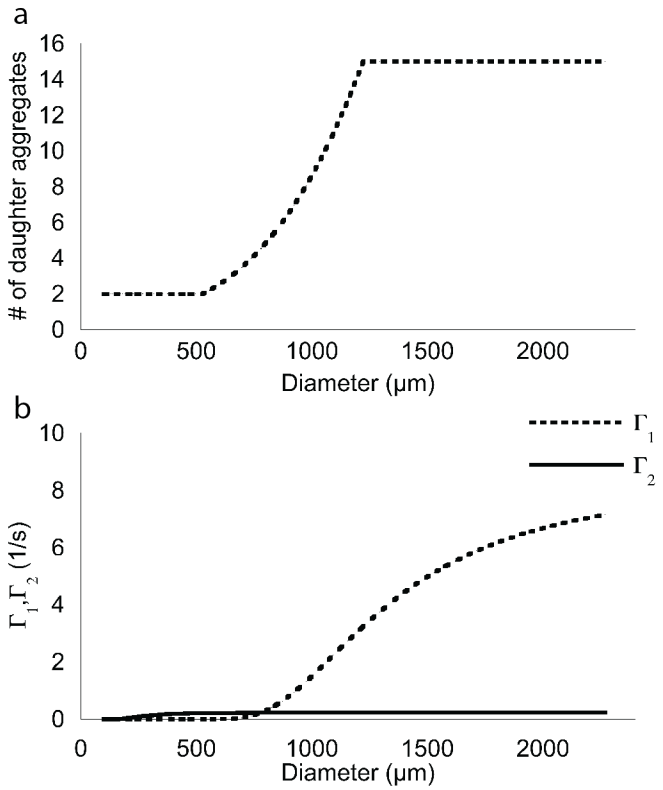

Figure 2.4. The optimized functions for the number of daughter aggregates produced as a function of aggregate diameter (a). In this function, mother aggregates below 500 µm break to form 2 daughter aggregates, whereas mother aggregates about 1,200 µm break to form 15 daughter aggregates. Linear interpolation was used between 2 and 15 daughter aggregates based on the volume of the mother aggregate. Breakage functions, where Γ_1 controls the breakage of aggregates larger than 880 µm and Γ_2 controls the breakage of particles smaller than 880 µm (b).

After optimization of the model, additional datasets were collected to check model extensibility by obtaining model predictions for additional cell lines, culture ages, dry weights and initial size distributions using the optimized set of parameters, K_1, K_2, K_3 and K_4 (Table 2.2).

Table 2.2. Objective function values for cell cultures with varying properties (starting size distribution, day of culture, culture density). Those cultures that were used in the parameter optimization are indicated with a +, whereas those that were not used are indicated with a --.

Cell line	Age of culture	Starting mean diameter (μm)	Culture dry weight (g/L)	Used in optimization?	ψ_1
P93AFC	Day 0	732	1.5	+	0.08
P93AF	Day 0	709	2.9	+	0.09
P991C	Day 14	732	10.0	+	0.09
P93AF	Day 14	854	6.1	--	0.11
P93AF	Day 14	660	9.1	--	0.24
CO93D	Day 14	676	10.9	--	0.26

The objective function value (ψ_1) is a measure of the error between the experimental and predicted data sets. In general, the low objective function values in Table 2.2 indicate strong agreement with the experimental data. Figure 2.5 shows the aggregate size distributions for the experimental datasets used in the optimization and validation of the model parameters.

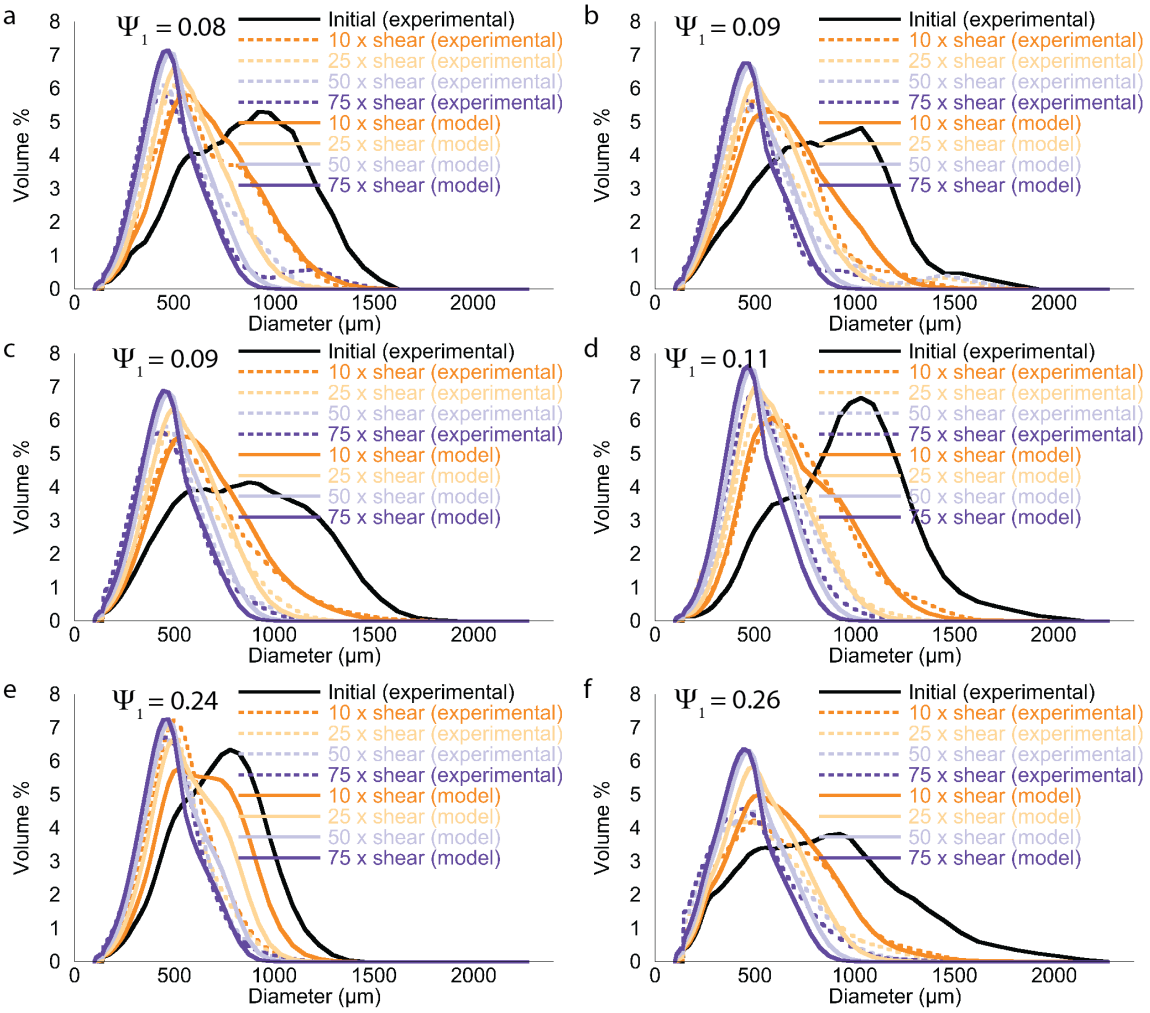

Figure 2.5. Experimental and model predicted aggregate size distributions for the experimental data sets used for model optimization (a-c) and the validation of the model (d-f). Data were collected after 0, 10, 25, 50 and 75 iterations of shear for (a) day 14 P93AFC cell line, (b) day 0 P93AF cell line, (c) day 14 P991C cell line, (d) day 14 P93AF and (e) day 14 P93AF and (f) day 14 CO93D cell line (described in Table 2).

For the day 14 P93AF culture with an objective function of 0.24 (Figure 2.5e), model predictions were in good agreement with experimental results except for the prediction after 10 iterations of shear, where the model underestimates the breakage. For the case of the day 14 CO93D cell line with an objective function of 0.26 (Figure 2.5f), smaller aggregates were formed with application of shear than predicted by the model.

This is especially true after 50 and 75 iterations of shear, where particles were formed that were below the range of the Coulter counter (as seen by the drop off in the experimental data at small particle sizes). Despite these larger objective function values, the general shapes of the predicted distributions are in strong agreement with the experimental datasets.

2.5.5. Target aggregate size distribution

Based on the experimental data sets used in the model formulation, two Gaussian distributions were defined that represented experimental data typically obtained after 1) 10-20 iterations of shear (Gaussian distribution with mean = 640 μm and variance = 54,000 μm^2), and 2) 20-30 iterations of shear (Gaussian distribution with mean = 540 μm and variance = 34,000 μm^2). A nonlinear optimization problem was formulated with the initial size distribution used as an initial condition in the PBE. The optimization problem was formulated to minimize the objective function ψ_2 (Eq. 6), which determines the error between the target and model distributions at each iteration of shear. The optimization model returns the number of iterations of shear required to reach the target distribution. Using cell cultures with different initial aggregate size distributions, the optimal number of iterations of shear was determined using the model to obtain the best fit to the two target distributions defined above (Table 2.3 and Table 2.4).

Table 2.3. Model predicted and experimental results for target 1 size distribution with mean = 640 μm and variance = 54,000. Objective function values are shown for both the model and the experimental data sets with respect to the target aggregate size distribution.

Cell line	Day of culture	Starting mean diameter (μm)	Culture dry weight (g/L)	# of passes to target 1	Target 1, ψ_2 model	Target 1, ψ_2 experimental
PO93X	Day 0	676	8.16	4	0.03	0.05
CO93D	Day 0	756	7.66	11	0.02	0.03
P93AF	Day 0	628	1.94	4	0.04	0.13
P93AF	Day 7	712	6.11	8	0.02	0.14
P93AF	Day 7	844	3.06	16	0.04	0.08
PO93XC	Day 7	628	3.66	3	0.01	0.17

Table 2.4. Model predicted and experimental results for target 2 size distribution with mean = 540 μm and variance = 34,000. Objective function values are shown for both the model and the experimental data sets with respect to the target aggregate size distribution.

Cell line	Day of culture	Starting mean diameter (μm)	Culture dry weight (g/L)	# of passes to target 2	Target 2, ψ_2 model	Target 2, ψ_2 experimental
PO93X	Day 0	676	8.16	24	0.03	0.00
PO93XC	Day 0	538	2.60	5	0.02	0.27
CO93D	Day 0	756	7.66	33	0.02	0.01
P93AF	Day 0	628	1.94	29	0.03	0.08
P93AF	Day 7	712	6.11	26	0.02	0.09
P93AF	Day 7	844	3.06	38	0.04	0.07
PO93XC	Day 7	570	8.64	12	0.01	0.29
PO93XC	Day 7	628	3.66	21	0.01	0.26

The model was able to achieve target distributions with objective function values less than 0.1 for three of the six data sets for Target 1 and five of the eight data sets for Target 2. Representative datasets for the shearing of three cell lines to reach two target particle size distributions are shown in Figure 2.6. These data sets are representative of both the low objective function values (Figure 2.6a,b,d,e) and the high objective function values (Figure 2.6c,f).

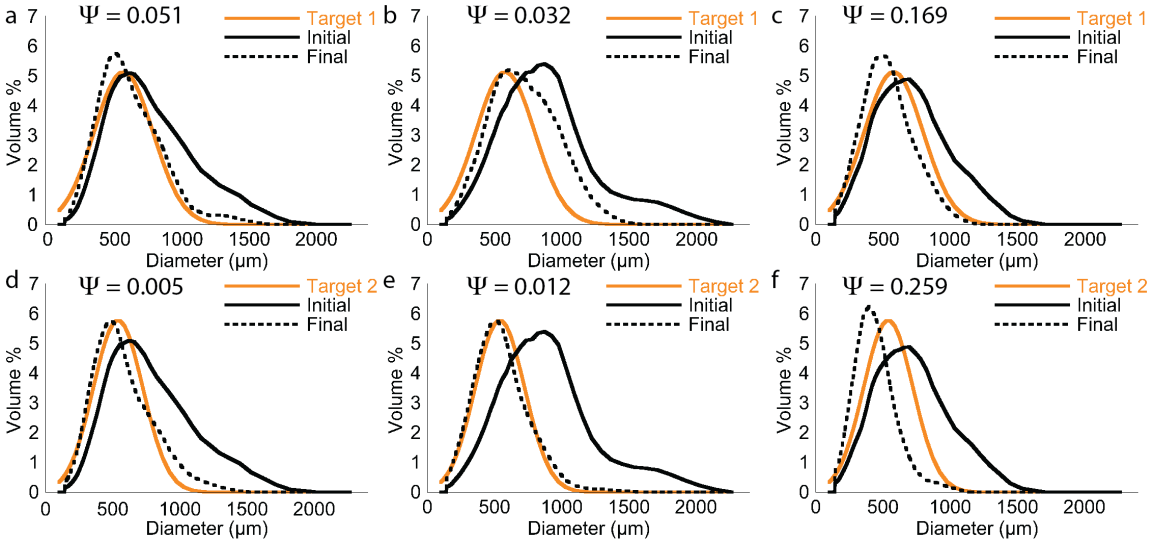

Figure 2.6. Predicted and model distributions for the lowest (a,b,d,e) and highest (c,f) objective functions obtained when using model-based design to reach two target aggregate size distributions with (1) mean = 640 µm and variance = 54,000 (a,b,c) and (2) mean = 540 µm and variance = 34,000 (d,e,f). Data correspond to a,d) the PO93X Day 0 culture, b,e) CO93D Day 0 culture and c,f) PO93XC Day 7 culture represented in Table 3.

Similar to the results presented in Table 2.1, the largest objective function values found in Table 2.3 and Table 2.4 are due to the model underestimating the amount of breakage occurring in the initial iterations of shear.

2.6. Discussion

2.6.1. Correlation found between the mean aggregate sizes of the sheared and unsheared cell populations

Development of a methodology for controlling aggregate size could provide a new, straightforward method for optimizing product yield and culture performance in plant suspension systems. Here, we applied mechanical shear over time to *Taxus* suspension cultures through manual pipetting of a batch culture, which has been shown to successfully reduce aggregate size without affecting short-term culture growth (Wilson et al., 2014b). Results demonstrated that application of a constant level of shear resulted in a decreased aggregate size compared to an unsheared control culture over eight generations of growth. Despite success in reducing overall aggregate size, the aggregate size of both unsheared and sheared populations fluctuated significantly and unpredictably over the four months of culture growth, with over two-fold changes in the mean aggregate size of both populations.

Interestingly, there was a positive linear correlation between the mean aggregate sizes of the sheared and unsheared populations over time. Cultures were maintained independently (in separate flasks under prescribed shearing conditions) over eight generations, but flasks were maintained in the same incubator with identical fresh media batches. These results indicate that culture aggregation dynamics are linked either through pre-programmed metabolism or by environmental conditions. The effect of media composition (e.g., vitamins, growth hormones, nitrogen, sugar), temperature, aeration, culture density and pH have been linked to changes in specialized metabolite accumulation (Saito and Mizukami, 2002), but no studies have reported the influence of

these factors on culture aggregation. Although attempts are made to hold these properties constant throughout a culture growth period (14 days), long-term experiments are especially susceptible to changes in environmental conditions (i.e., seasonal variability in humidity) and batch-to-batch variability in media composition. To learn more about the effect of such environmental parameters on culture aggregation, growth conditions would have to be more strictly regulated and quantified using controlled bioreactor systems over long culturing periods.

2.6.2. Model provides insight into the mechanism of shear and breakage phenomena

We found that flow rate and aperture size did have an effect on culture disaggregation, with faster flow rates and smaller aperture diameters leading to smaller aggregates; however culture density did not affect disaggregation. The negligible effect of density indicates that breakage is not due to interaction amongst aggregates, but rather to interaction between the aggregate and the aperture tip. In addition to physical contact with the aperture tip, flow through a small orifice results in an increase in shear stress, which can also contribute to aggregate breakage (Maindarkar et al., 2012). Thus, decreasing the aperture size below 1.5 mm could allow for smaller aggregates to be created; however, cell damage due to the increased stress would need to be assessed. To scale up the process from lab to production scale, pumping of the cell culture broth through an aperture could mimic the mechanism of shear developed and applied in this study. The developed PBE model could easily be adapted to this continuous shear system and operating parameters such as pump flow rate or tubing diameter could be integrated to allow for the control of detailed operating conditions.

The main factor that affected the culture mean aggregate size after shear was the starting aggregate size distribution. Regardless of the starting mean aggregate size of a culture, most cultures reached a steady-state between 420 and 550 μm after 75 iterations of shear. Those cultures that reached smaller steady state aggregate sizes typically started with an aggregate size distribution shifted towards smaller particles sizes (Figure 2.3f). This is likely because aggregates below a specific diameter require additional force to break or are subjected to less shear in the aperture. For these reason, size-dependent breakage functions, such as those used in our study, have been recommended for aggregated cell systems (Kolewe et al., 2012; Lin et al., 2008). The optimization of the two independent breakage functions in our study (Figure 2.4b) support these findings, with aggregates greater than 880 μm breaking more frequently.

In addition to gaining insight concerning the frequency of aggregate breakage, model optimization provided additional information on the breakage phenomena. The model suggested that aggregates greater than 500 μm were more likely to break into more than two daughter aggregates (Figure 2.4). Based on this result, a conceptual breakage mechanism was proposed (Figure 2.7).

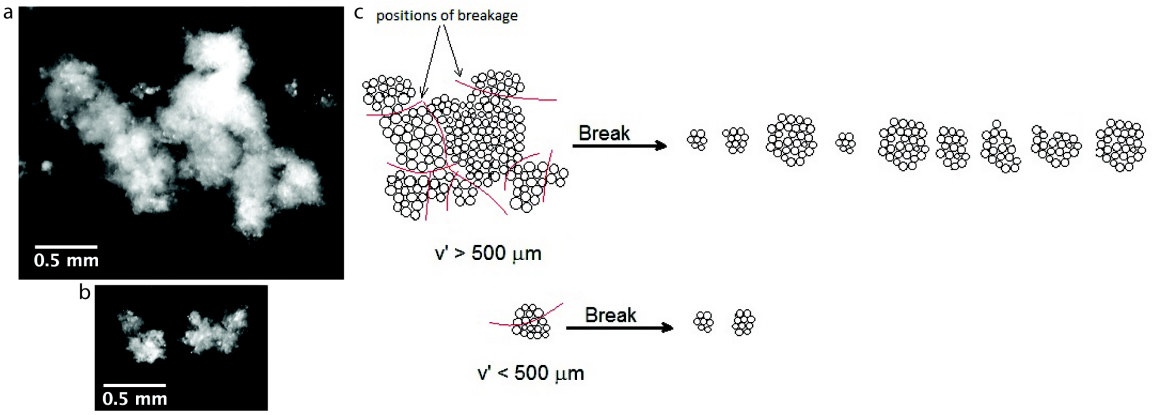

Figure 2.7. Proposed breakage mechanism for (a) large aggregates (>500 μm) and (b) small aggregates (<500 μm) (c).

As seen in Figure 2.7a, larger aggregates are expected to contain a higher number of defects, such as irregularities in shape, weakly associated cell clusters and fractures. As a result of these defects, when larger aggregates pass through the aperture, shear forces target the weak spots, leading to formation of multiple daughter particles (Figure 2.7c). On the other hand, smaller aggregates contain fewer defects (Figure 2.7b) and are exposed to lower levels of shear due to their small size compared to the aperture diameter, resulting in formation of just two daughter aggregates.

For two conditions used in the model extensibility experiments (Day 14 P93AF and Day 14 CO93D) and two conditions used in the target distribution experiments (both Day 7 PO93XC), the objective functions were significantly higher than for the other conditions (Table 2.2, Table 2.3 and Table 2.4). These cultures had starting mean aggregate sizes that were smaller than a majority of the other conditions studied, and in each case the model underestimated the amount of breakage occurring, especially in the first 10 iterations of shear. This underestimation could be due to the morphology of the smaller aggregates within an unsheared culture. For instance, smaller aggregates formed

due to cell growth could be more irregular in shape than smaller aggregates formed due to shear breakage. Therefore, to improve the ability of the model to predict the disaggregation of cultures with smaller starting aggregate sizes, breakage functions could be optimized independently for the initial iterations where aggregates are formed due to culture growth and later iterations of shear where a majority of aggregates are formed due to aggregate breakage. Alternatively, the model could be formulated for two separate populations, one containing unbroken aggregates and the other containing broken aggregates. The model could then account for the transition of unbroken aggregates into the broken aggregate population.

The aggregation dynamics of the culture at the time of shearing could affect breakage under shear. There is an unpredictable shift in mean aggregate size of a culture over time (Figure 2.2b). During the phase when the mean aggregate size of a culture is "naturally" decreasing (see days 42-56 in Figure 2.2b), the forces keeping cells together could be weaker, leading to faster disaggregation in response to mechanical shear. On the other hand, when cultures are increasing in aggregate size (see days 56-84 in Figure 2.2b), the interaction between cells in an aggregate could be stronger, resulting in less breakage in response to mechanical shear. To study the effect of natural variation in mean aggregate size on the disaggregation of a culture, a more detailed long-term study would have to be performed where culture diameter was measured both before and after application of mechanical shear. The plant cell wall primarily consists of cellulose, lignin, hemicellulose, tannin and water (Edahiro and Seki, 2006) and changes in aggregate size have been linked to changes in lignin accumulation (Edahiro and Seki, 2006; Kuboi and Yamada, 1978). Therefore, by measuring the presence of these cell wall

compounds throughout this long-term study could indicate changes in cell well structure, as well as shifts in cellular metabolism.

2.6.3. Using the model to create optimized culture aggregation properties

The creation of cell cultures with a small and stable aggregate size distribution will reduce culture variability and potentially enhance *Taxus* culture performance. We have shown that reduction of aggregate size can be achieved at a single time-point by using the PBE model to predict the amount of shear required to reach a target aggregate size distribution. Paclitaxel production is higher in smaller aggregates (Kolewe et al., 2011a; Patil et al., 2012; Patil et al., 2013), which may be due to a reduction in nutrient diffusion limitations or an increase in exposure to shear stress, which may serve as a trigger for specialized metabolism. For instance, shear has been shown to affect both cell growth and the production of specialized metabolites (Busto et al., 2013; Garcia-Ochoa et al., 2013; Han et al., 2013; Han and Yuan, 2009) and protein production (del Carmen Oliver-Salvador et al., 2013; Kwon et al., 2013) in a variety of plant cell culture systems. If such environmental cues are the cause of differences in paclitaxel accumulation amongst cultures of varying aggregate sizes, the application of shear to create a population with smaller aggregation profiles should result in higher levels of paclitaxel that are more stable over time. Studies are underway in our laboratory to assess model utility in practice to enhance paclitaxel accumulation in culture. Results from the work presented here and ongoing studies concerning long-term control of aggregate size in *Taxus* cultures will provide key insights into the influence of cell aggregation on metabolite accumulation in plants and potentially other cell culture systems. The present study is the first to demonstrate control of aggregation dynamics in plant systems and

opens new doors to engineering of plant cell suspension cultures for increased product accumulation.

2.7. Additional information

The model was applied to control the aggregation dynamics of both unelicited and elicited *Taxus* cell lines. Additionally, the long-term effect of applied shear on aggregation dynamics was studied using the model over multiple generations.

2.7.1. Methods

2.7.1.1. Maintenance of *Taxus* suspension cultures

The *Taxus cuspidata* (P93AF) and *Taxus canadensis* (CO93D) cell lines were provided by the United States Plant Soil and Nutrition Laboratory (Ithaca, NY). All chemicals were purchased from Sigma-Aldrich Co. (St. Louis, MO) unless otherwise noted. Cells were maintained and subcultured on a bi-weekly basis, as previously described (Kolewe et al., 2011a). Aggregate size distributions and cellular biomass were measured using a Multisizer 3™ Coulter counter equipped with a 2,000 μm aperture (Beckman Coulter, Brea, CA), as previously described (Kolewe et al., 2010). For analysis, a single two mL sample of well-mixed culture was analyzed from each flask at each time point. Biomass measurements and Coulter counter particle diameters obtained from the Coulter counter were converted to dry weight and true diameter, respectively, using a previously established correlation (Kolewe et al., 2010).

2.7.1.2. Mechanical shearing to maintain a target aggregate size distribution

On day 0 of the experiment, 12 replicate 125 mL flasks were created by transferring 10 mLs of a day 14 culture into 40 mLs of fresh cell culture medium. The

twelve flasks were then analyzed using the Coulter counter to determine an initial aggregate size distribution. This aggregate size distribution was then used in the shearing model previously described to determine the amount of shear required to reach a target aggregate size distribution, which was defined as a Gaussian distribution with a mean of 540 μm and variance = 34,000. Cultures were sheared according to the model and a post-shear aggregate size distribution was obtained through Coulter counter analysis. Of the twelve flasks, four flasks were maintained as unsheared controls, four flasks were treated with a constant level of shear (ten iterations of shear) and four flasks were sheared as determined by the model to reach the target aggregate size distribution. Cultures were sheared on days 0, 4, 7, 11 and 14 of each generation. Flasks were sheared by drawing the culture through a 10 mL polystyrene disposable standard serological pipet (Fisher Scientific, Pittsburgh, PA) using a Portable Pipet-Aid® XP (Drummond Scientific Company, Broomall, PA) with a flow rate of 7.3 ml/s as previously described. A single iteration of shear refers to the uptake and release of 10 mLs of culture volume. After the application of shear on each day, a one mL sample of well-mixed culture was taken and stored at -80 °C for specialized metabolite analysis.

2.7.1.3. Model design problem

The optimization problem was formulated with the number of passes through the shearing device as the decision variable. The optimized parameters K_1, K_2, K_3 and K_4were used in the PBE model and the following least-square objective function ψ_2 was used for optimization,

$$\psi_2 = \frac{\sum_{j=1}^{n}\left[\hat{n}_p(v_j) - n_{tar}(v_j)\right]^2}{\sum_{j=1}^{n}\left[n_{tar}(v_j)\right]^2} \tag{7}$$

where n_{tar} represents a target distribution and $\hat{n}_p$ represents the model predicted distribution. The target distribution was chosen based on experimental datasets to represent typical distributions achieved after 20-30 iterations of shear. The model was discretized temporally and spatially to generate a set of nonlinear algebraic equations that were used in the optimization problem as equality constraints. The number of iterations of shear was constrained to be between 0 and 100. The problem was solved in AMPL using solver CONOPT to determine the optimal number of iterations of shear to be performed to minimize the error between target and experimental aggregate size distributions. After application of mechanical shear, an experimental objective function was calculated,

$$\psi_1 = \sum_{i=1}^{N} \frac{\sum_{j=1}^{n} \left[\hat{n}_p(v_j, i) - n_p(v_j, i)\right]^2}{\sum_{j=1}^{n} \left[n_p(v_j, i)\right]^2} \tag{8}$$

where $n_p()$ is the experimental value of the volume distribution at position v_j after i iterations of shear; $\hat{n}_p()$ is the model predicted value of the volume distribution at position v_j after i iterations of shear; n is the total number of node points; and N is the number of times that the sample is sheared.

2.7.1.4. Mechanical shearing of elicited cell cultures

For elicitation of sheared cultures, 24 replicate flasks were generated (8 flasks for an unsheared control, 8 flasks for a constant level of shear and 8 flasks for the target aggregate size distribution). Flasks were maintained up to day 7 as previously described. After the application of shear on day 7, 3 x 1 mL samples of well-mixed culture were taken from each flask and stored at -80 °C for specialized metabolite analysis. Filter sterilized methyl jasmonate was then added to each flask to a final concentration of 200

μM. Flasks were then capped with with a foam cap covered in tin foil and incubated at 24 °C and 125 rpm. Cultures were sampled (3 x 1 mL well mixed culture sample), analyzed using the Coulter counter before and after shearing, and sheared on days 11, 14 and 17.

2.7.1.5. Mechanical shearing of cultures over multiple generations of growth

For cultures that were maintained for multiple generations, 10 mL of well-mixed unelicited cell culture was removed from each flask and transferred to a sterile container on day 14. This biomass was mixed with the biomass from like treatments (control, constant shear or target shear) and this culture was then used to inoculate four new flasks, which were then monitored as the next generation of the cell culture.

2.7.2. Paclitaxel measurements

Samples for paclitaxel analysis were prepped and measured through UPLC as previously described (Naill and Roberts, 2004; Patil et al., 2012).

2.8. Results

2.8.1. Application of shear over a single generation of growth with elicitation

An unsheared (control), 10x sheared and target sheared population of the *Taxus canadensis* cell line CO93D were studied over an 18-day period, with elicitation of the culture on day 7. The unelicited growth and aggregation can be seen in Figure 2.8.

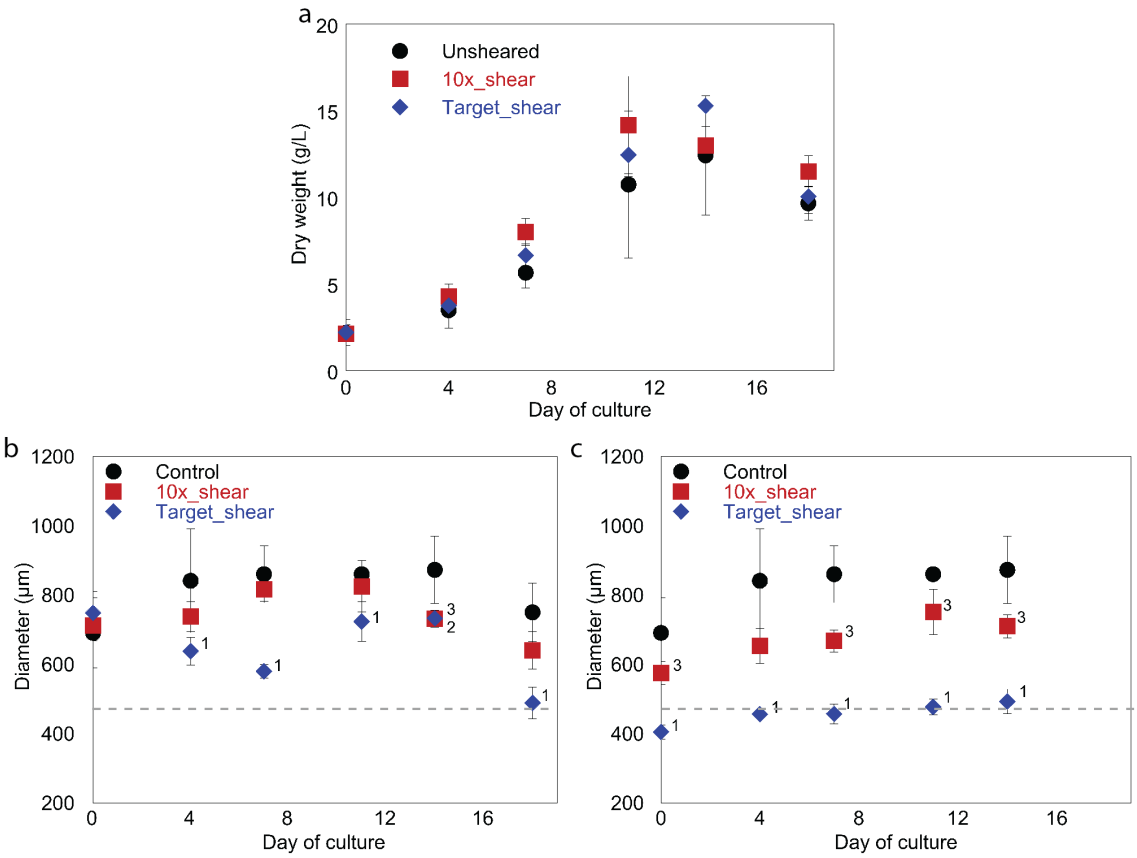

Figure 2.8. The unelicited growth (a) and pre-sheared (b) and post-sheared (c) mean aggregate size of unsheared (control), 10x sheared and target sheared cultures of the CO93D cell line. The dotted line in (b) and (c) is the mean diameter of the target distribution, which was defined in the model. Data represent an average of three biological replicates. 1 indicates that the target sheared population is statistically different from both the control and 10x sheared populations, whereas 2 indicates that this population is only different from the control. 3 indicates that the 10x sheared population is statistically different from the control. Statistical analysis was performed using a student's t-test ($p<0.05$).

Application of shear to both the 10x sheared and target sheared cultures had no effect on culture growth throughout the 18-day growth period. While the pre-sheared mean aggregate sizes were more variable than the post-sheared mean aggregate sizes, the target sheared population was significantly smaller than the control culture at all time points

both before and after shear. Additionally, the post-shear mean aggregate size of the target population remains stable throughout the experiment, only increasing from 405 to 495 μm over the course of the generation of growth. For this culture, the only post-sheared data point that is statistically different from the mean diameter of the target distribution was at day 0 of the culture. Additionally, the target-sheared population was on average 370 ± 95 μm smaller than the control culture. The 10x sheared culture increased from 575 to 710 μm throughout the course of the experiment and on average was only 150 ± 105 μm smaller than the control culture. The pre-sheared 10x culture was statistically similar to the control culture at all time points except for day 14. The mean aggregate size distributions of the cultures before and after shear can be seen in Figure 2.9.

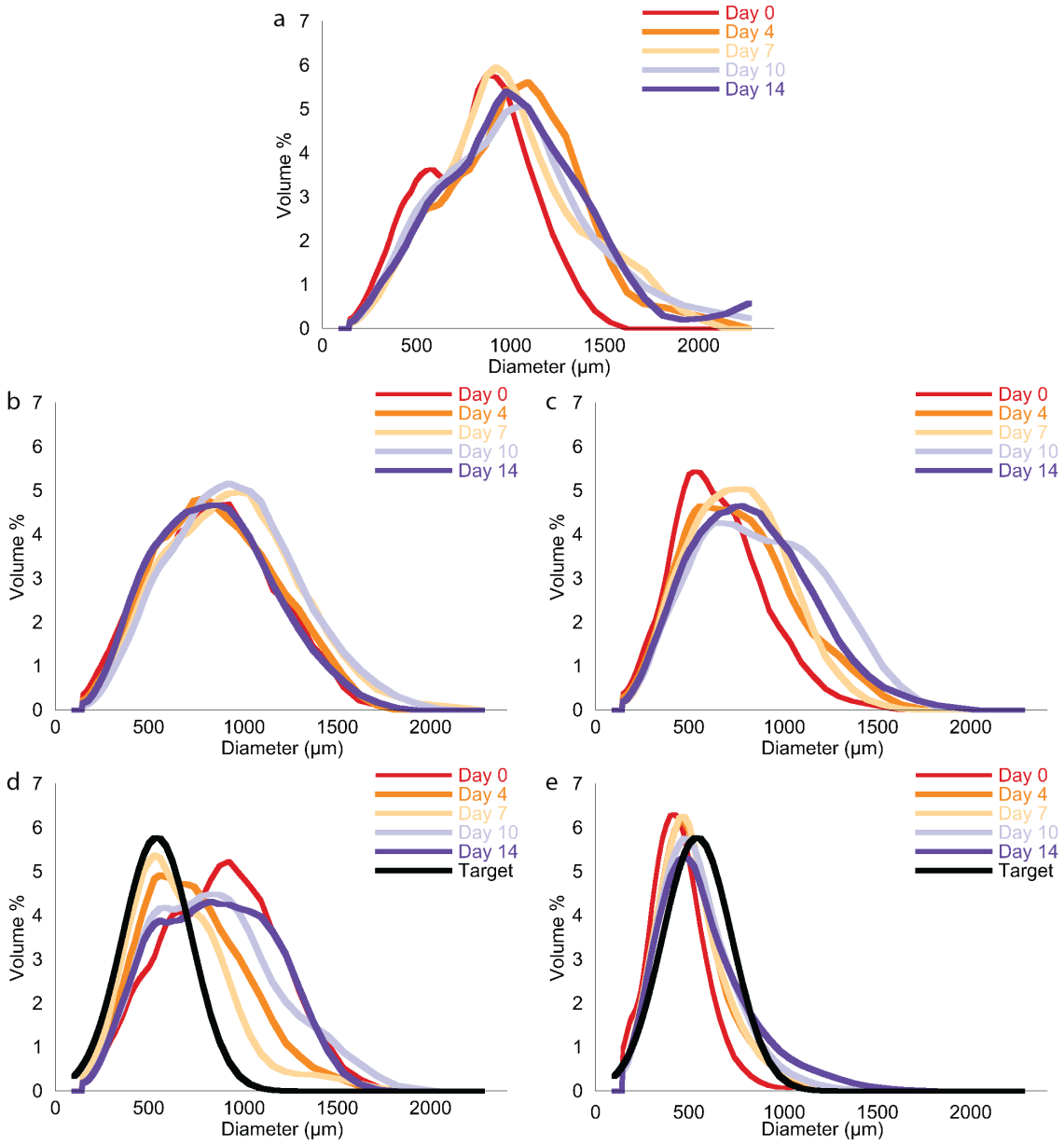

Figure 2.9. Aggregate size distributions for the control (a), 10x sheared (b,c) and target sheared cultures (d,e) before (b,d) and after shear (c,e). Data represent the average of three biological replicates. For the target sheared population, the target distribution is seen in black.

The aggregate size distribution of the control culture remained fairly constant throughout the course of the experiment, with a slight shift towards larger particle sizes between days 0 and 4. Similarly, the pre-sheared distribution for the 10x population stayed constant

throughout the experiment, indicating that aggregates within the culture increased in size between applications of shear nearly to the aggregate size distribution of the unsheared control. The target sheared population also increased in aggregate size between applications of shear, but the aggregate size distributions in the pre-sheared cultures was shifted towards smaller particles when compared to the 10x and control sheared populations (Figure 2.9). Additionally, the aggregate size distribution of the post-sheared target culture was fairly consistent throughout the course of the experiment. The objective functions associated with the experimental aggregate size distributions can be seen in Table 2.5.

Table 2.5. The experimental objective function values for the target sheared populations.

Day of culture	Experimental objective function
0	0.21
4	0.07
7	0.07
11	0.04
14	0.05

The objective function was highest on day 0 of the experiment, where the model underestimated the amount of breakage after shear (Figure 2.9e), resulting in a smaller aggregate size distribution. After shearing on day 0, the objective function was significantly smaller and the model was able to accurately predict the amount of shear required to hit the target distribution.

Cultures were elicited with MJ on day 7 and the effect of elicitation on culture growth can be seen in Figure 2.10.

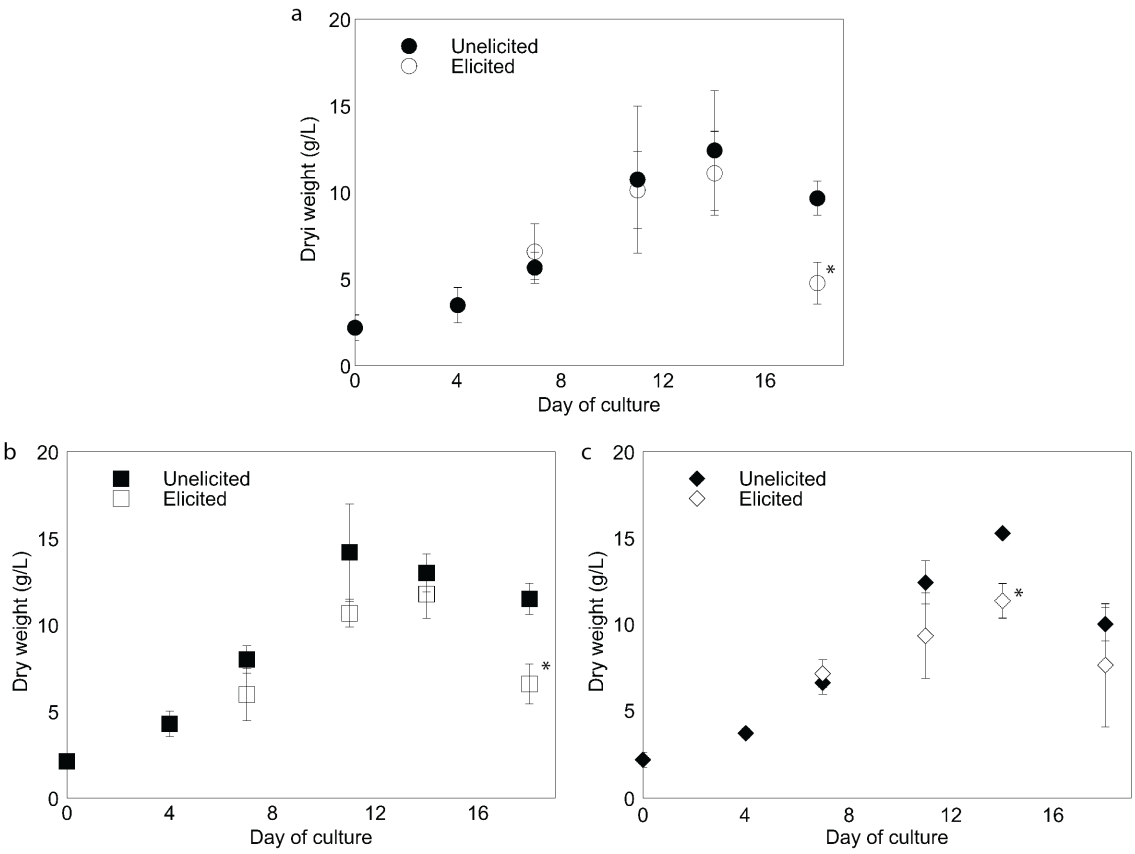

Figure 2.10. The effect of elicitation on the growth of the unsheared control (a), 10x shear (b) and target sheared (c) cultures. Data represents an average of three biological replicates. * indicates statistically different from the unelicited culture using a student's t-test ($p<0.05$).

After elicitation, biomass levels continued to increase, but all cultures experienced some level of growth inhibition. Unfortunately, cultures did not produce paclitaxel after elicitation (data not shown), so the effect of shearing on paclitaxel production could not be determined. This is not uncommon with the *Taxus* cultures, as they are highly variable in their paclitaxel production capabilities over time (Patil et al., 2012; Patil et al., 2013).

2.8.2. Application of shear over multiple generations of growth

The effect of shear on culture growth and aggregation was investigated over 5 generations of growth (2-weeks per generation) in the *T. cuspidata* P93AF cell line (Figure 2.11).

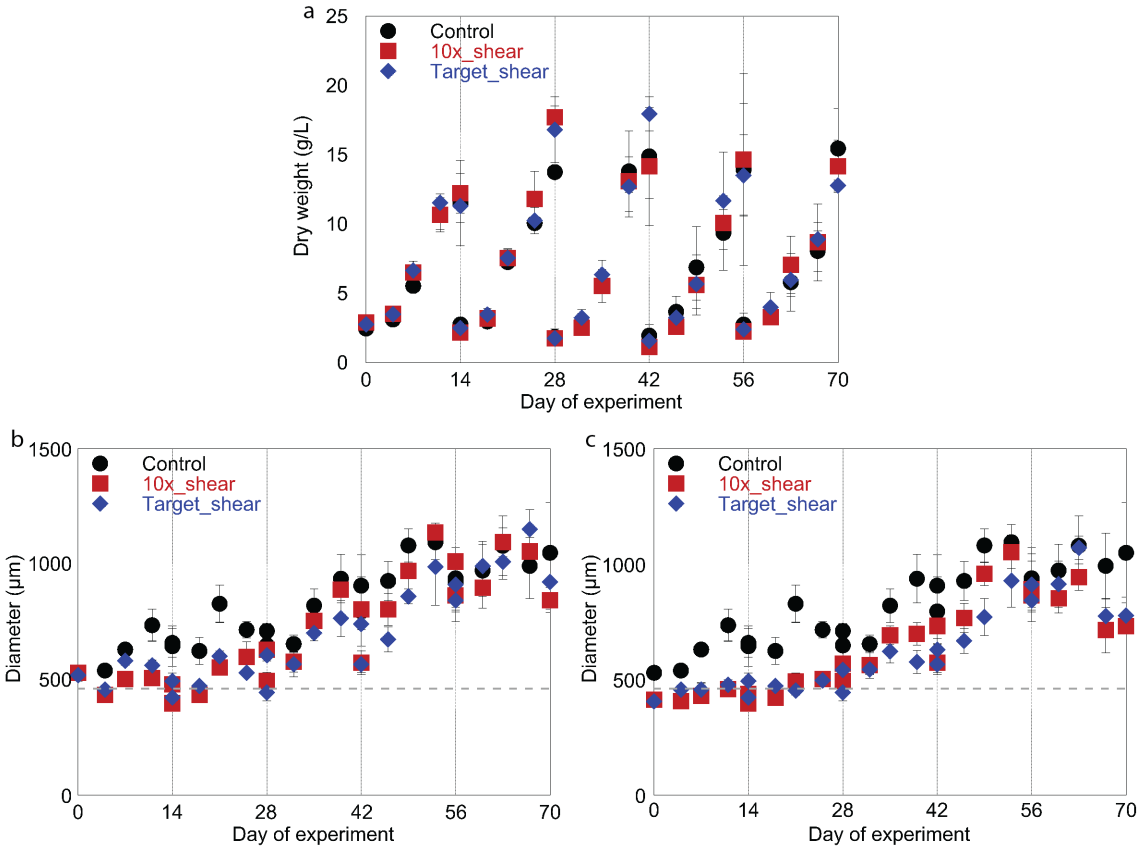

Figure 2.11. The growth (a) and pre-sheared (b) and post-sheared (c) mean aggregate size of unsheared (control), 10x sheared and target sheared cultures of the P93AF cell line over 5 generations. Data represents an average of three biological replicates.

Although growth of the cultures was unaffected by shear over the five generations, the applied mechanical shear became less effective at reducing the mean aggregate size of both the 10x and target sheared cultures after two generations of growth. As a result, the mean aggregate size of the 10x and target sheared cultures increased throughout the

course of the experiment and are statistically similar to the control for many of the time points in the last three generations of growth. Additionally, for the first two weeks of growth, the model determined that the model sheared population would need to be sheared around ten times, which resulted in mean diameters for the model shear and the 10x shear populations that were statistically the same. Interestingly, as the mean aggregate size of the control culture is increasing, the mean aggregate size of both the 10x and target sheared populations also increased. Once the mean aggregate size of the control culture started to stabilize during the last generation of growth, shearing started to have a greater effect and the mean aggregate size of both the 10x and target sheared populations became statistically different from the control. The effect of mechanical shear on the mean aggregate size of the culture can be seen in Figure 2.12.

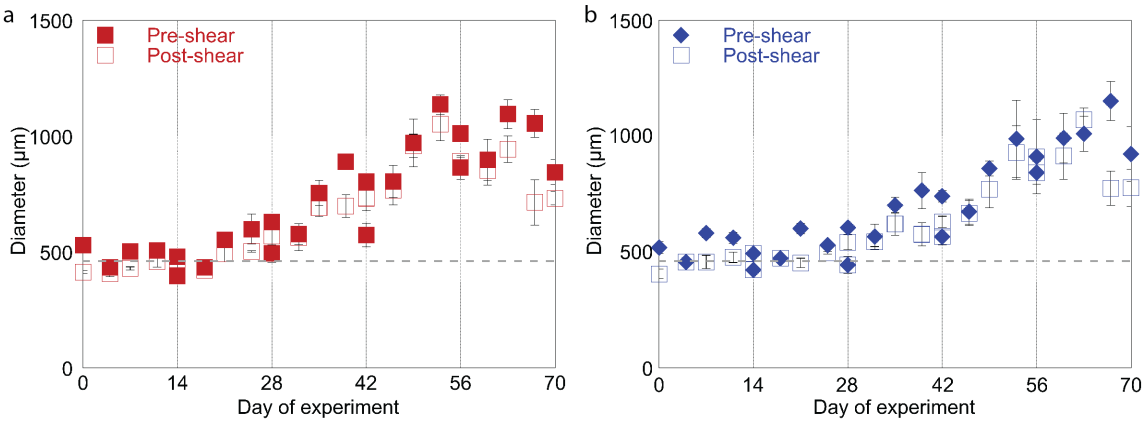

Figure 2.12. Effect of mechanical shear on the 10x sheared culture (a) and the target sheared culture (b).

From these data, it can be seen that on days where the cultures were transferred, two sets of data are shown for the pre-sheared measurements. These correspond to the 14-day old presheared cultures, as well as the newly transferred cultures (which was transferred after the application of shear to the 14-day old cells). Therefore, the mean diameter of the

freshly transferred culture should be equivalent to the mean diameter of the post-sheared culture. Occasionally, there is decrease in the mean aggregate size of the newly transferred due to the additional mechanical shear that cultures are subjected to during transferring (e.g., day 42 for the 10x sheared cultures).

The aggregate size of the culture starts small at the beginning of the experiment. As a result, the pre- and post-sheared mean diameter values are statistically the same for eight of the nine measurements for the 10x sheared culture and three of the nine measurements for the model-sheared culture. As the cultures start to grow larger throughout the course of the experiment, the shear continues to have little effect on the cultures. Once the mean aggregate size of the control population begins to stabilize around day 56, the sheared populations begin to disaggregate in response to mechanical shear. To learn more about the effect of aggregation dynamics on the utility of the shearing model, the application of shear would need to be studied through dynamic changes in the mean aggregate size of the control cultures. The decrease in effectiveness of the mechanical shearing could be due to differences in cell wall strength as cultures are undergoing changes in aggregation state (small vs. large aggregates) or due to changes in the morphology of the cultures that have been exposed to shear (Figure 2.13).

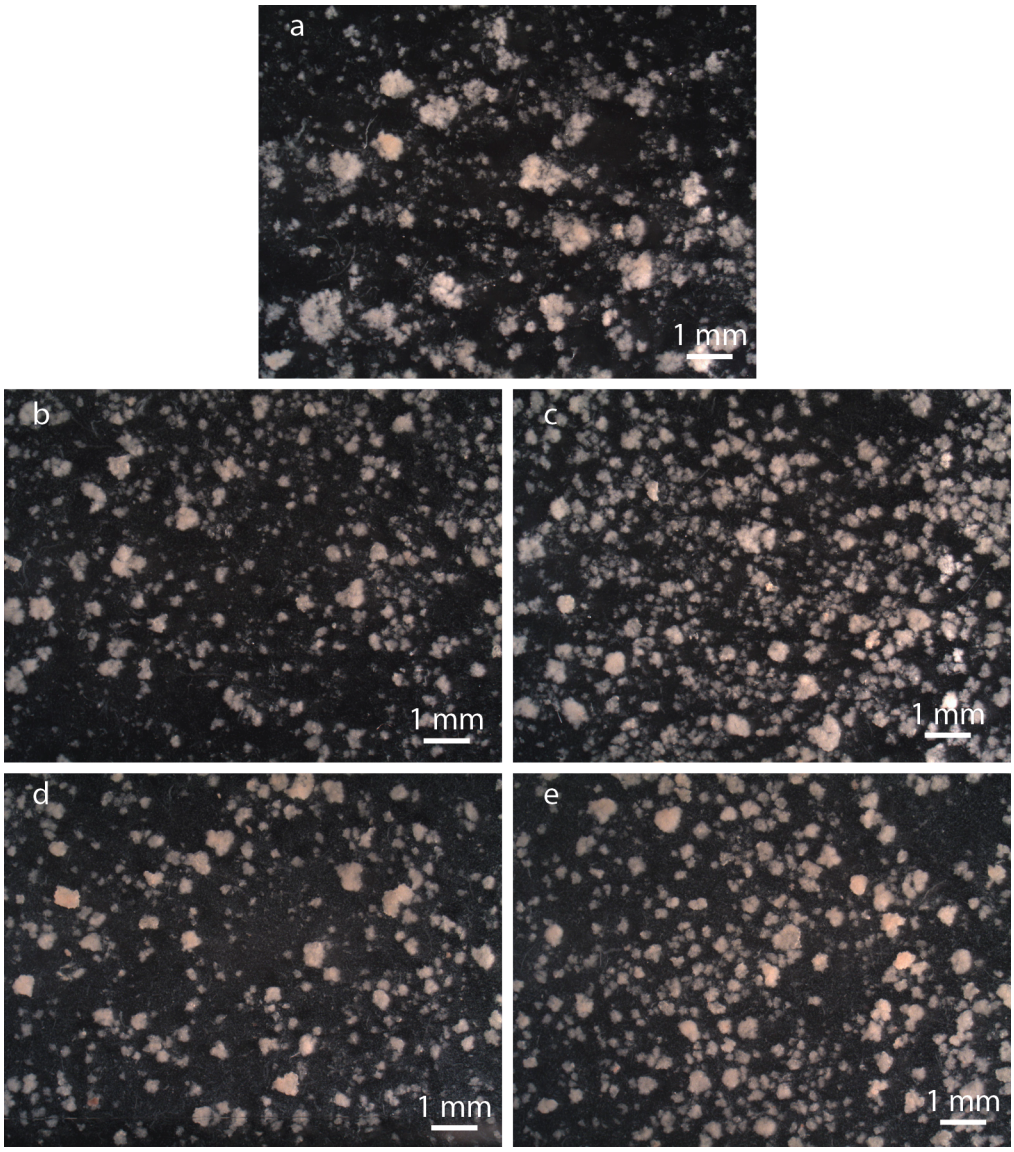

Figure 2.13. Morphology of the control (a), 10 x sheared (b,c) and target sheared (d,e) populations before (b,d) and after (c,e) after applications of shear. Image was taken at day 14 of the 5th generation of cell growth (day 70), which was the last day of the experiment.

The aggregates in the control culture appear to be more irregularly shaped and cells appear more loosely associated than those in the 10x and target sheared populations. The cultures that have been exposed to shear are more regular in shape and appear more compact. The application of mechanical shear to the cultures appears to affect aggregate morphology, which would likely influence culture disaggregation in response to shear.

Additionally, there is an increase in the amount of debris in the sheared cultures, which could indicate some level of cell damage within these cultures. Although the biomass levels were unaffected by the application of shear, analysis of specialized metabolite production (i.e., phenolics and flavonoids) could provide additional insight into the health of these cultures.

2.8.3. Conclusions and future recommendations

The data collected in these experiments provide information about the short-term and long-term effectiveness of the model at controlling culture aggregation. Interestingly, during the single generation of growth of the CO93D cell line, the mean aggregate size of the culture was successfully maintained through application of the model. When comparing the target sheared population to the 10x sheared population, there is significantly more control over the mean aggregate size in the target sheared population (Figure 2.8c). This emphasizes the need for the model to effectively determine the amount of shear required to modulate aggregation properties.

When the model was applied to a culture over five generations of growth, the ability to maintain a target aggregate size distribution through use of the model was not as effective as in a single generation. This is likely due to the large changes in aggregate size seen in the control culture over time. To control for this change in aggregate size in future long-term experiments, the model could take into account the change in the unsheared aggregate size distribution between time points. In a culture where the unsheared population is increasing in size, additional shear would need to be applied to the culture to reach a target aggregate size distribution. If the unsheared population was

decreasing in mean aggregate size, a lower amount of shear would need to be applied to achieve the target aggregate size distribution.

To learn more about the effect of shearing on the aggregate strength, mechanical testing could be performed. For instance, rheology could provide information on the interactions amongst the cells within an aggregate (Curtis and Emery, 1993). The main limitation of rheology on these types of measurements is that it will only measure the bulk properties of a population. To provide information on the strength of a single aggregate, cavitation micro rheology could be used, which is useful for the measurement of the strength of biological materials on a micron size scale (Chin et al., 2013; Cui et al., 2011; Zimberlin et al., 2010). Additionally, the effect of elicitation on aggregate strength could also be determined, allowing for modification of the model to account for cultures with differences in aggregate properties (i.e., increasing in aggregate size, decreasing in aggregation size, elicitation).

CHAPTER 3.

INTERCELLULAR CHARACTERIZATION: EXAMINING THE DISTRIBUTION OF PACLITAXEL IN AGGREGATES OF *TAXUS* SUSPENSION CULTURES THROUGH MASS SPEC IMAGING

3.1. Collaborators

Alyssa Marsico, Graduate Student, Chemistry

Richard Vachet, Professor, Chemistry

3.2. Background and motivation

One of the key characteristics of plant suspension cultures is the formation of cellular aggregates, which can range in size from 100-2,000 μm. These aggregates lead to the development of subpopulations within a culture due to diffusion limitations, differences in cell to cell signaling and shear exposure. This aggregation can have process level implications because specialized metabolite accumulation can be dependent upon the aggregation characteristics of a culture. For instance, small aggregated *Taxus* suspension cultures have been shown to have up to a 40-fold increase in paclitaxel production when compared to cultures with larger aggregates (Kolewe et al., 2011a; Patil et al., 2012; Patil et al., 2013). Similarly, a study of *Vaccinium pahalae*, which has aggregates that can be as large as 2 mm in diameter, found that over 70% of anthocyanin production was in aggregates less than 240 μm in diameter (Pepin et al., 1999). In contrast, it was found that in the cultured strawberry line *Fragaria ananassa* R, size filtered aggregates with a mean diameter of 390 μm accumulated higher amounts of anthocyanins than those with a mean diameter of 200 μm (Edahiro and Seki, 2006). Due to the large effect of aggregate size on specialized metabolism, it is important to examine

culture heterogeneity on a single cell level (within aggregates) to identify and characterize aggregate subpopulations.

To investigate the properties of single cells in an aggregated *Taxus* culture, enzymatic digestion was used to breakdown aggregates into single cells (Naill and Roberts, 2004). Through the use of a fluorescent antibody for paclitaxel, flow cytometry was then applied to determine the accumulation of paclitaxel within single cells of the *Taxus* culture (Naill and Roberts, 2005d). These methods revealed that 95% of cells within a methyl jasmonate (MJ)-elicited culture accumulated paclitaxel, but with a high degree of variability in accumulation level. Although this method provided crucial information about the heterogeneity of *Taxus* cultures, the disaggregation of aggregates into single cells does not allow information on the spatial distribution of paclitaxel within an aggregate (Figure 3.1).

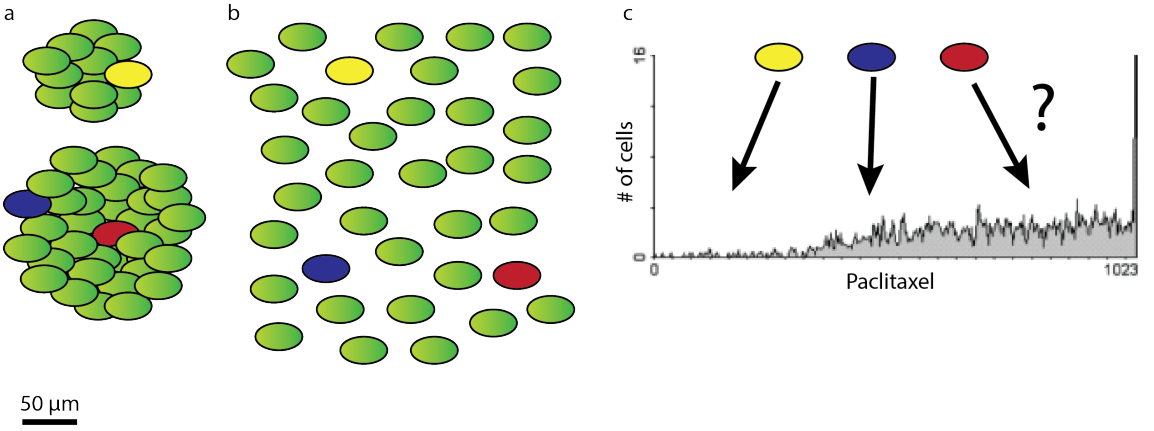

Figure 3.1. Overview of flow cytometry for paclitaxel identification (Naill and Roberts, 2005d). Aggregated cell cultures (a) were disaggregated into single cells through enzymatic digestion (b). These cells were stained for paclitaxel content using an anti-paclitaxel antibody and secondary fluorescent tag. The stained population was then characterized using flow cytometry to identify paclitaxel content of individual cells (c). The main limitation to this technique is the loss of spatial information about the origin of the single cells. For instance, the red, blue and yellow cells identified in the aggregate (a) can no longer be identified by considering only the flow cytometry data (c).

In recent years, methods have been developed to analyze the spatial distribution of a diversity of metabolites in intact plant tissue or tissue slices using mass spectrometry imaging (MSI), as recently reviewed (Bjarnholt et al., 2014). Desorption electrospray ionization (DESI) techniques are often used to image whole leaf and petals with typical resolution up to 100 µm through direct imprint onto the surface of a polytetrafluoroethylene (PTFE) or TLC plate. This technique was used to study the specialized metabolite distribution in leaves and petals of *Catharantheus roseus*, *Arabidopsis*, and several other plant species (Hemalatha and Pradeep, 2013). Differences in metabolite distribution were visualized when specific tissues were subjected to pest/pathogen attack or under stress. Additionally, DESI was used to study changes in

metabolite concentrations in *Lotus japonicas*, allowing for real time visualization of enzymatic reaction products after the leaves were wounded (Li et al., 2013a). Matrix-assisted laser desorption ionization (MALDI) can be used to achieve single cell resolution (as low as 20 μm) (Bjarnholt et al., 2014). This technique was used in *Medicago truncatula* to look at the distribution of compounds such as organic acids, amino acids, sugars, lipids and flavonoids in nodes that contain rhizobia that assist in nitrogen fixation (Ye et al., 2013). MSI has yet to be applied to cell culture systems, but could give insight into the spatial distribution of metabolites within cellular aggregates.

3.3. Experimental methods

3.3.1. Determining an appropriate matrix for ionization

Two μL of paclitaxel, 10-DAB and baccatin III (1 mg/mL in methanol stock solutions) were applied to a PTFE plate by pipetting. The methanol was allowed to evaporate at room temperature before two μL of each matrix were applied on top of the standard sample. The following matrices were evaluated: 9-aminoacridine (9AA), α-Cyano-4-hydroxycinnamic acid (CHCA), 2,5-dihydroxybenzoic acid (DHB), 1,5-dihydroxynaphthalene (DHN) and sinapinic acid (SA). After the methanol evaporated off the sample, the plate was inserted into a Bruker Autoflex III MALDI-TOF mass spectrometer (Bruker Daltonics, Bremen, Germany), which uses a Smartbeam 2 Nd:YAG laser.

3.3.2. Determining the optimal DHB concentration

DHB in 50:50 MeOH with 0.1% TFA was prepared at concentrations of 20, 40, 100, 200 and 400 mg/mL, as well as a saturated solution of DHB (where an excess of DHB was suspended in the 50:50 MeOH solution and sample was pipetted from the

supernatant). Two µL of each taxane standard (baccatin III, 10-DAB and paclitaxel in separate 1 mg/mL stock solutions) were mixed with two µL of each matrix concentration and two µL was dotted using a pipette into a grid pattern on a 25 x 75 mm stainless steel plate (Figure 3.2).

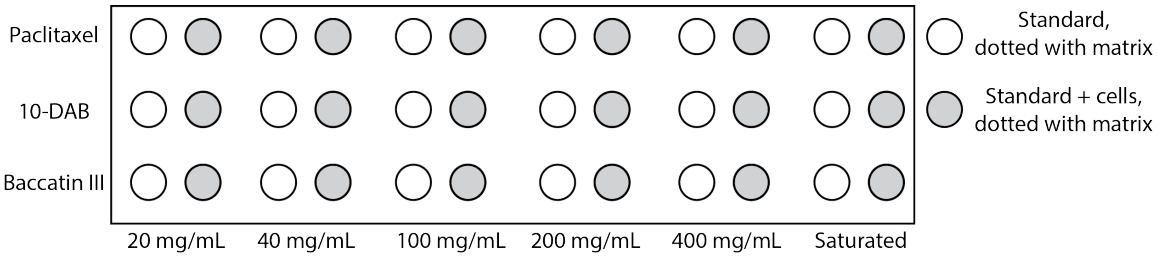

Figure 3.2. Pure standard and standard with lysed cell samples were spotted with six concentrations of DHB.

Additionally, two µL of each standard was mixed with two µL of lysed *Taxus* cells (lysed in a sonicating bath for five minutes in 50:50 MeOH:H_2O) and two µL of each matrix concentration. Two µL of this solution was then dotted on the same plate.

3.3.3. Spray coating of DHB matrix over taxane standards

DHB in 50:50 MeOH with 0.1% TFA was prepared at concentrations of 10, 30, 40 and 100 mg/mL. Two µL of each taxane standard (baccatin III, 10-DAB and paclitaxel in separate 1 mg/mL stock solutions) were dotted in eight columns on a 25 x 75 mm stainless steel plate. Four of the columns were topped with 2 µL of lysed *Taxus* cells, as described above. In a ninth column, 2 µL of standard was mixed with 2 µL of the 100 mg/mL DHB standard (Figure 3.3).

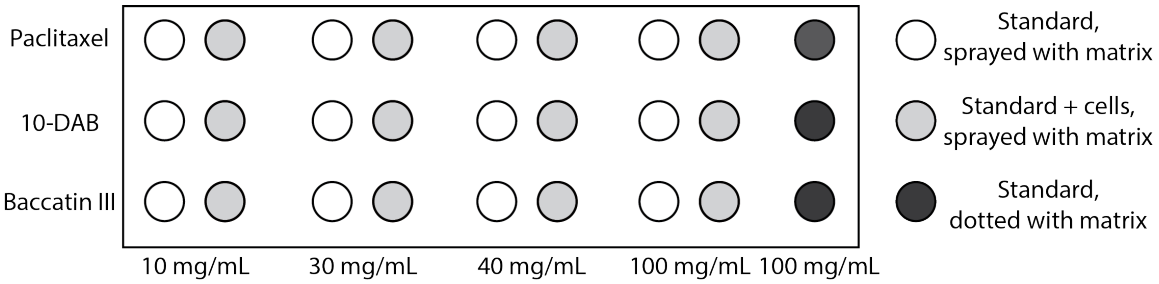

Figure 3.3. Pure standard and standard with lysed cell samples were sprayed with four concentrations of DHB. Additionally, standards were mixed with the 100 mg/mL DHB.

The plate was placed approximately 10 inches from the nozzle of an airbrush sprayer and each column was individually sprayed with a different matrix concentration (Figure 3.4).

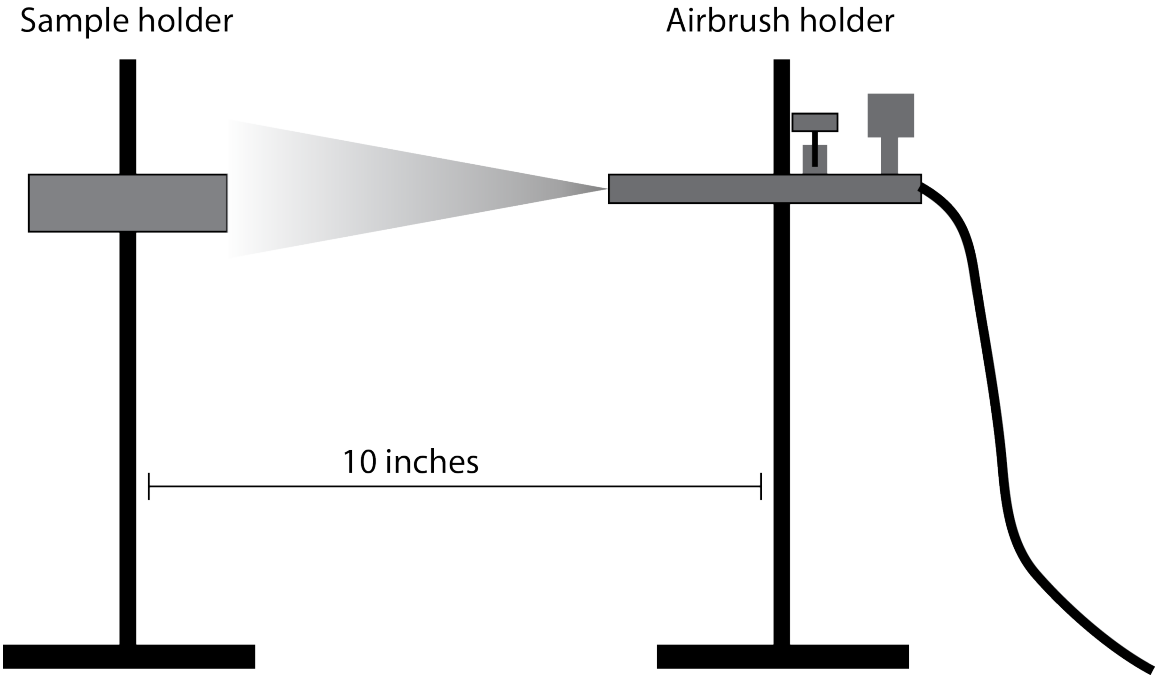

Figure 3.4. The sample and airbrush were each placed on a stand, which were approximately 10 inches apart. The matrix was then applied to the sample by airbrushing for 1 second, followed by 14 seconds to allow the methanol to evaporate off the slide. This was repeated 14 times for a total of 15 coats of matrix per sample.

For each matrix concentration, the airbrush was sprayed for 1 s at a time for a total of 15 coats of matrix per sample, waiting 14 s between each spray. After application of each

concentration of matrix, the plate was allowed to fully dry at room temperature. Tin foil was used to cover the areas of the slide that were not being sprayed. Any excess matrix solution was removed from the airbrush using a pipet and the airbrush was rinsed by spraying approximately one mL of acetonitrile through the airbrush. This procedure was repeated under the same conditions on an indium tin oxide plate. In addition to the airbrush sprayed standards, the standards were also mixed with 100 mg/mL of DHB and dotted on the plate (as described previously) to use as a control. LDI-MS imaging was performed on each sample dot seen in Figure 3.3 using a Bruker Autoflex III MALDI-TOF mass spectrometer (Bruker Daltonics, Bremen, Germany) with a Smartbeam 2 Nd:YAG laser. Fifty laser shots were measured per position and a step width of 50 μm was used between laser positions, allowing for resolution up to 50 μm within the sample. This step width could be reduced to increase the resolution of the MSI study.

3.3.4. Maintenance and elicitation of *Taxus* suspension cultures

The *Taxus cuspidata* cell line P93AF, which was obtained from the United States Plant Soil and Nutrition Laboratory (Ithaca, NY), was maintained as previously described (Kolewe et al., 2011a). All chemicals were purchased from Sigma-Aldrich Co. (St. Louis, MO) unless otherwise noted. To elicit specialized metabolite production, day 7 cultures were elicited with 200 μM MJ. On day 21, both mock-elicited and MJ-elicited cultures were filtered through a 710 μm mesh to obtain two distinct populations of aggregates: small (<710 μm) and large (>710 μm). The 710 μm size cut off was chosen based on Coulter counter analysis of the sample, where an equal distribution of biomass would fall on either side of the size cut-off.

3.3.5. Cryopreservation and cryoslicing of *Taxus* aggregates

Approximately one gram of filtered cells (see above) were transferred to a 50 mL falcon tube, excess media was removed and cells were washed with 25 mL of PBS. PBS was removed using a 10 mL pipet and the cells were resuspended in 10 mL of a fixative solution (5 mL of 37% formaldehyde, 20 μL 20% glutaraldehyde and 45 mL nanopure water). The sample was then placed in a vacuum chamber that was connected to house vacuum and placed under vacuum for 1 minute with the cap off before being capped and placed in a 4 °C refrigerator and stored for 24 hours. After the 24-hour incubation, the fixative solution was removed through pipetting with a 10 mL pipetand cells were washed by incubating the cells at room temperature (no shaking) with 10 mL of PBS for 15 minutes. The PBS was then removed through pipetting with a 10 mL pipet and replaced with 10 mL of a 2.3 M sucrose solution. Samples were capped and incubated for 24 hours at 4 °C. Fixed cells were then centrifuged for 10 minutes at 500 rpm and the sucrose solution was removed using a 10 mL pipet. Ten mL of optimal cutting temperature (OCT) solution (Fisher Healthcare™) was added to the 50 mL falcon tube and samples were stored upside down at -20 °C. Frozen samples were then removed from the falcon tube by cutting off the bottom of the tube with a razor blade. The sample was then pushed from the tube and sliced to 20 μm or 30 μm onto indium tin oxide coated glass slides (Delta Technologies, Limited, Loveland, CO) using a Leica CM 1850 cryostat at -20 °C.

3.3.6. Spiking of cells with taxane standards

Four mL of a day 13 P93AF culture were added to three wells of a six-well plate. A mixture of paclitaxel, 10-DAB and baccatin-III (stock concentrations of 1 mg/mL in

methanol) was added to each of the wells to reach a final concentration of 0, 0.5 and 50 mg/L of standard. Methanol was added to the 0 and 0.5 mg/L samples to ensure that an equal total volume of methanol was added to each culture. Cultures were incubated overnight at 125 rpm and 25 °C prior to cryopreservation and cryosclicing, as described above.

3.3.7. MSI of spiked cell samples

Spiked cell samples (0, 0.5 and 50 mg/L samples) were cryosliced to 20 μm thickness onto indium tin oxide coated glass slides and sprayed with 40 mg/mL of DHB in 50:50 MeOH:H_2O with 0.1% trifluoroacetic acid (TFA). The slide was placed approximately 10 inches from the nozzle of an airbrush sprayer and sprayed for 2 seconds, with 8 seconds for drying in between each spray. Each slide was sprayed a total of 20 times. Slides were allowed to dry at room temperature prior to analysis. LDI-MS imaging was performed on the tissue sample using a Bruker Autoflex III MALDI-TOF mass spectrometer (Bruker Daltonics, Bremen, Germany) with a Smartbeam 2 Nd:YAG laser. Fifty laser shots were measured per position and a step width of 50 μm was used between laser positions.

3.3.8. Cryopreservation of elicited *Taxus* cell samples

A day 7 culture of P93AF cells was elicited with 200 μM MJ. After 21 days in culture (14-days post-elicitation), the mock-elicited and MJ-elicited cultures were filtered over a 710 μm mesh to obtain two populations of cells: small (<710 μm) and large (<710 μm). Samples were then cryopreserved as previously described.

3.3.9. Paclitaxel measurements

Samples for paclitaxel analysis were prepped and measured through UPLC, as previously described (Naill and Roberts, 2004; Patil et al., 2012).

3.4. Results

3.4.1. Determining an appropriate matrix for ionization

To visualize the distribution of paclitaxel in aggregates of *Taxus* suspension cultures, a preliminary MALDI-MSI technique was developed. Matrices were tested for their ability to aid in the ionization of paclitaxel and two precursors to paclitaxel, 10-deactyl baccatin III (10-DAB) and baccatin III (Figure 3.5).

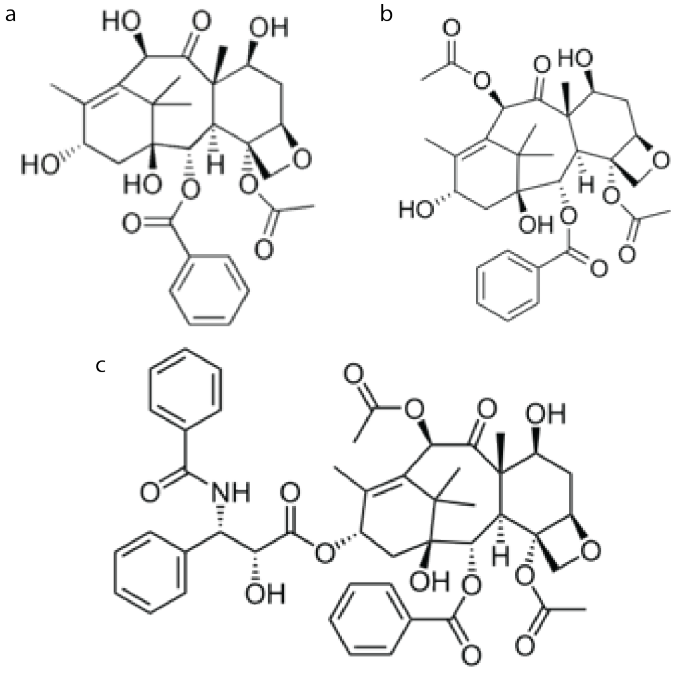

Figure 3.5. Structure of a) 10-deacetyl baccatin III (MW = 544.6 g/mole), b) baccatin III (586.6 g/mole) and c) paclitaxel (853.9 g/mole)

To analyze paclitaxel and relevant precursors using MALDI MSI, an effective matrix must be identified that is able to sufficiently ionize the compounds. For this study, one

negative ion mode matrix and four positive ion mode matrices were tested. Through analyzing the mass spectrum for each of the matrices, it was determined that DHB was the most effective at ionizing both paclitaxel and its precursors (Figure 3.6).

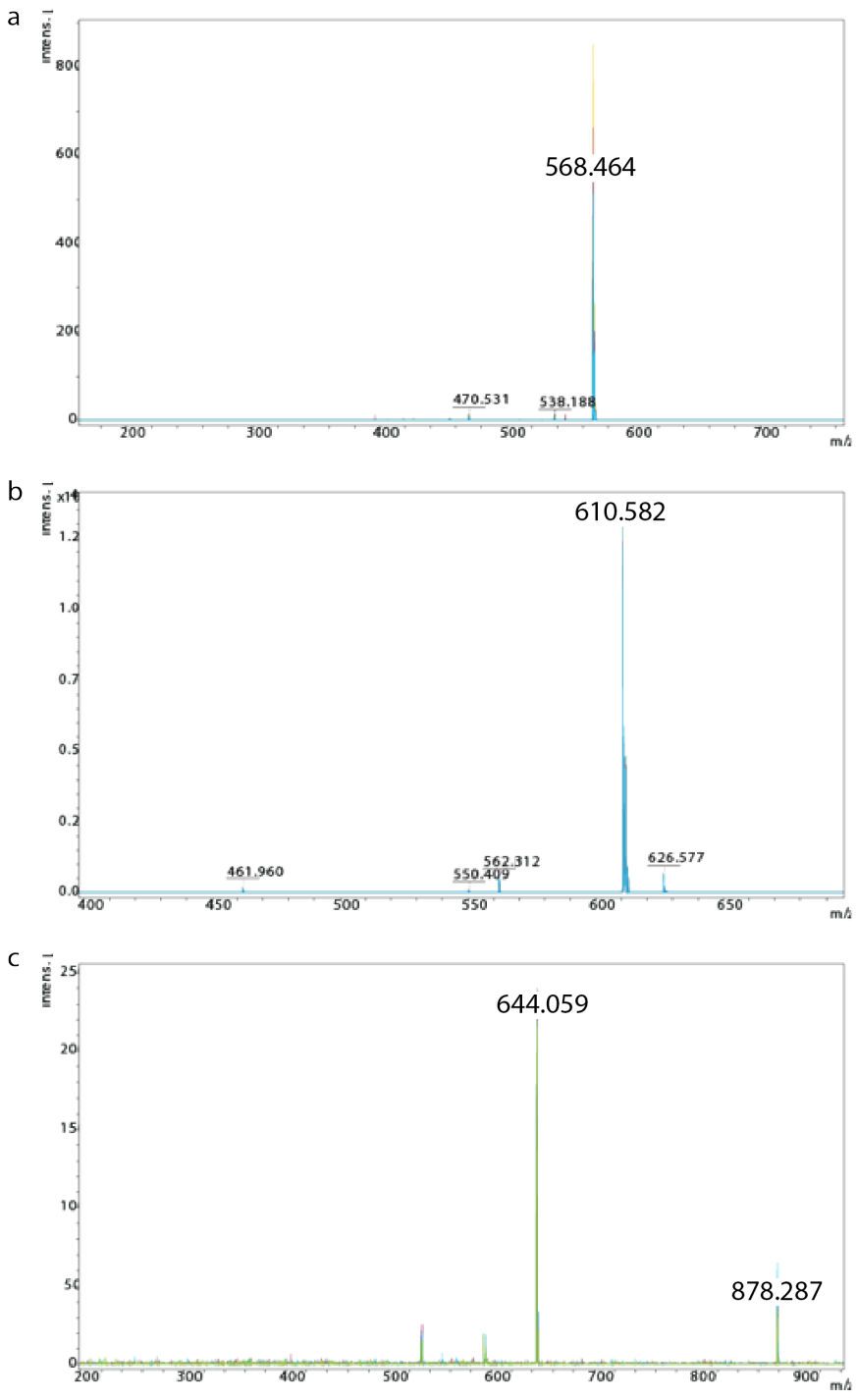

Figure 3.6. Mass spectra for a) 10-DAB, b) baccatin III and c) paclitaxel using the matrix DHB.

Both 10-DAB and baccatin III showed no fragmentation upon ionization, with peaks for the sodium adducts of each compound at 568 and 610 g/mole, respectively. Paclitaxel

ionization resulted in a peak for the sodium adduct (878 g/mole), as well as a single fragment at 644 g/mole. The fragmentation to form this peak can be seen in Figure 3.7.

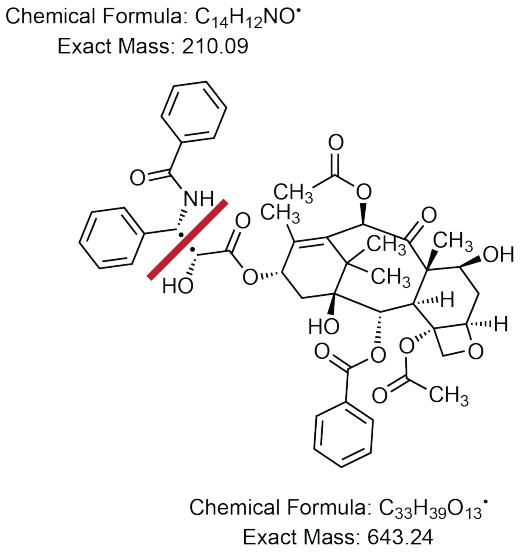

Figure 3.7. Fragmentation of paclitaxel for the matrix DHB.

The other matrices that were tested resulted either resulted in low levels of ionization or fragmentation that prevented the ability to distinguish between paclitaxel and its precursors. An example of this data for the matrix 9AA can be seen in Figure 3.8.

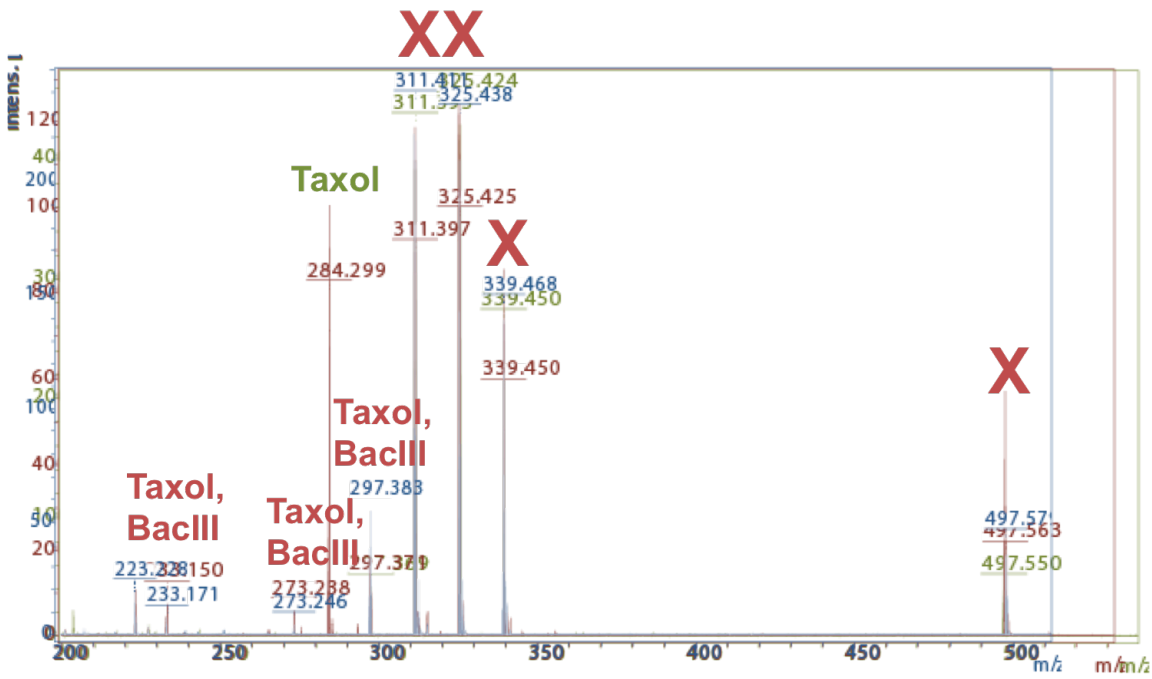

Figure 3.8. Fragmentation pattern for Taxol, 10-DAB and Baccatin III using the matrix 9AA. A red X indicates that the peak was found in all three standards. If the peak did not appear in all three standards, they were labeled with the standard or standards that produced the peak.

9AA produced only one unique fragmentation peak at 284 m/x for paclitaxel. All other peaks were overlapping across at least two of the standards. Because of the high level of fragmentation of the standard compounds, functional groups that distinguish the standards were removed resulting in peaks for backbone structures seen in all standards. To allow paclitaxel precursors to be distinguished from paclitaxel, a low level of ionization is desired. As a result, the matrix DHB was an ideal matrix. Due to the optimal fragmentation pattern of paclitaxel and its precursors with DHB, methods were developed for the spray coating of this matrix.

3.4.2. Optimal DHB concentration for standard detection

The optimal concentration of DHB for standard ionization was determined by spotting each standard with matrix at concentrations ranging from 20-400 mg/mL DHB. The results for 40, 100 and 200 mg/mL concentrations are shown in Figure 3.9.

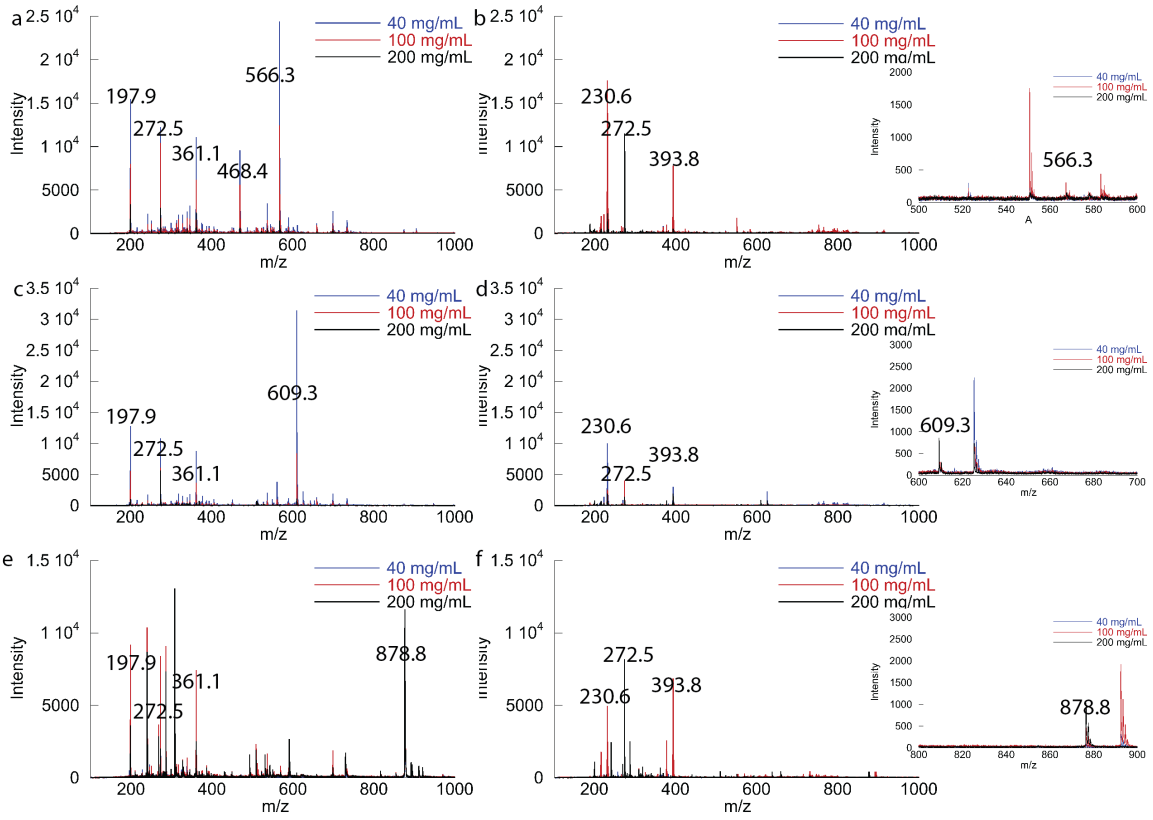

Figure 3.9. 10-DAB (m/z 566.3) (a,b), baccatin III (m/z 609.3) (c,d) and paclitaxel (m/z 878.8) (e,f) were ionized with 40, 100 and 200 mg/mL DHB in 50:50 MeOH. In b, d and f, ground cell material was added to the standard to determine interference due to cell associated metabolites. The inset on the right corresponds to the standard peak in the samples containing cells.

For 10-DAB and baccatin III, a matrix concentration of 40 mg/mL resulted in the highest intensity peak in cell free standards. When cell lysis was added to the standard, a higher concentration of 100 mg/mL was more effective for ionizing 10-DAB, as seen by the red peak at 566 m/z. For baccatin III, the 40 mg/mL matrix remained the most effective after

the addition of cell lysis, as seen by the blue peak at 609 m/z. For paclitaxel, the 200 mg/mL concentration was most effective for both cell-free and cell containing standard, as seen by the dominance of the black peak at 879 m/z. Three peaks appear in all three cell-free samples at 197.9, 272.5 and 361.1 m/z. These peaks could correspond to shared fragments of the taxane backbone or peaks related to the DHB matrix. For instance, a peak at 272.5 m/z has been shown for 2-DHB-$2H_2O$ (Amorim Madeira and Florencio, 2009). Two additional peaks (230.6 and 393.8 m/z) show up in all of the cell samples, which could be due to the ionization of a cell associated metabolite. The 400 mg/mL concentrations (data not shown) resulted in low peak intensities for all of three taxane standards. Although the intensity of the peaks is significantly lower for all three standards when cells are present, clear peaks are still visible, but the most effective matrix concentration varied depending upon the standard being analyzed. As a result, the results from this study were unable to guide the development of a spray coating method for *Taxus* samples. Therefore, a wide-range of concentrations were used in the development of a spray coating method.

3.4.3. Spray coating of DHB on taxane standards

When applying a matrix to a cryosliced cell sample, it is important to prevent the migration of compounds within the sample, which could occur due to wetting of the sample surface (Cornett et al., 2007). Because taxanes are readily soluble in the solvent used for DHB application (50:50 MeOH:Water), an airbrush can be used to minimize the size of solvent droplets on the surface of the sample. Airbrush application also leads to the formation of small, homogeneous crystals on the surface of the material (typically 50-100 nm) (Cornett et al., 2007). If the size of matrix crystals is too large, the energy from

the laser is diffused through the entire crystal, resulting in the ionization of an area larger than the diameter of the laser. As a result, small crystals are desired, which allows the resolution of the mass spec imaging to be determined by the diameter of the laser, rather than the size of the matrix crystals on the surface of the sample. The optimal concentration of DHB for spray coating of taxane standards was investigated on both stainless steel and indium tin oxide plates using concentrations ranging from 10 to 100 mg/mL (Figure 3.10).

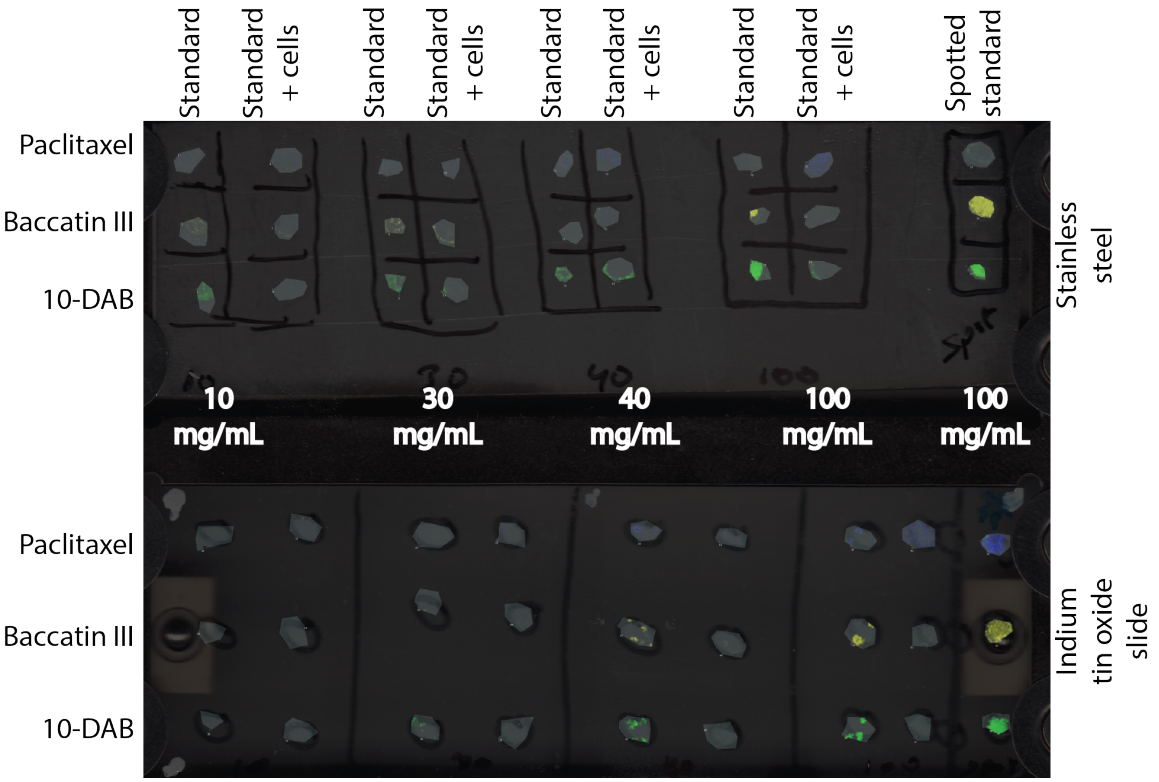

Figure 3.10. Paclitaxel (blue), baccatin III (yellow) and 10-DAB (green) were ionized with 10, 30, 40 and 100 mg/mL DHB in 50:50 MeOH spray coated onto both stainless steel and indium tin oxide slides. MALDI-MSI imaging was used for ionization of the samples with 50 µm steps. The MSI data were then analyzed for peaks corresponding to each standard, allowing for an image of the compounds on the sample, with the intensity of color corresponding to the relative concentration of the standard. For each matrix concentration, spots of pure standard (left) and standard mixed with lysed cells (right) were sprayed with matrix. In the last column, pure standards were mixed with 100 mg/mL of DHB and spotted onto the slide as a control.

The highest matrix concentration (100 mg/mL) was the most effective at ionizing all three standards on both the stainless steel and indium tin oxide coated slide. The only standard that was effectively ionized using the 10 mg/mL concentration was 10-DAB. Although the cells reduced the intensity of the standard (which supports data from the previous section), the compounds were still detected. The spotted sample of standard

mixed directly with the matrix showed the highest intensity of ionization likely due to the high degree of matrix coverage that occurs when the samples are pre-mixed together. From the results in this study, the highest matrix concentration (100 mg/mL) was used for spray coating of *Taxus* cell samples.

3.4.4. MSI of a spiked *Taxus* sample

Taxus cells were incubated for 24 hours with 50 mg/L of paclitaxel, baccatin III and 10-DAB. These samples were then cryosliced and sprayed with 100 mg/mL of DHB (Figure 3.11).

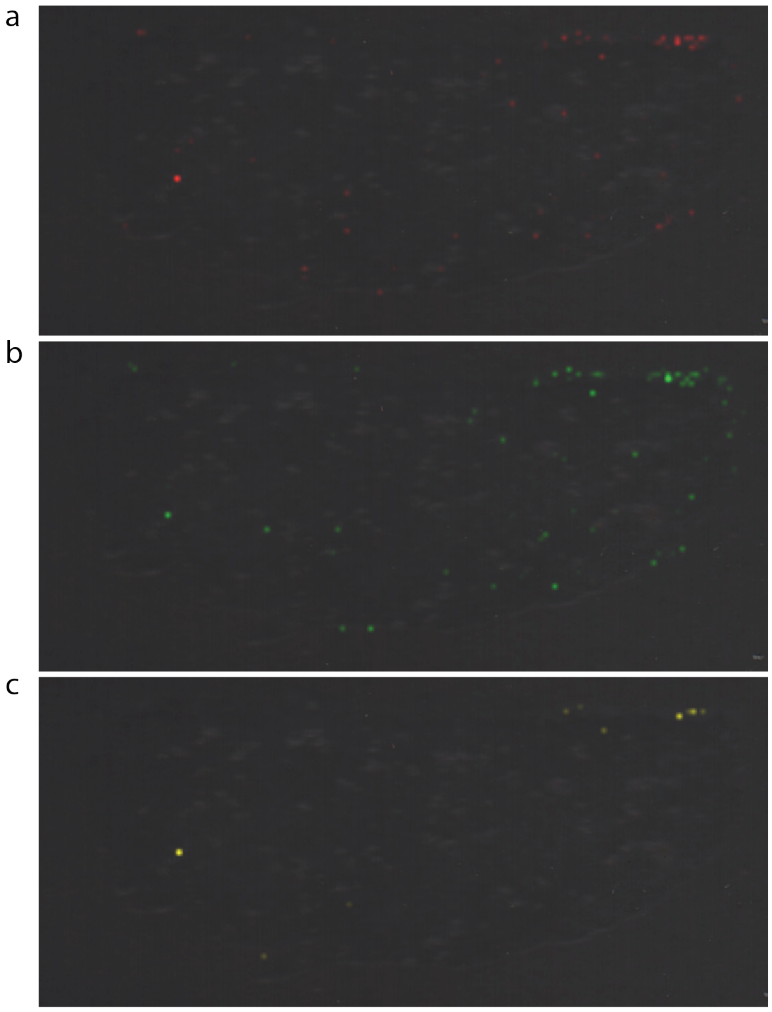

Figure 3.11. *Taxus* cells were spiked with a mixture of 50 mg/L of 10-DAB, baccatin III and paclitaxel for 24 hours before being cryopreserved and cryosectioned onto an indium tin oxide slide. Indium tin oxide coated slides were prepped for MALDI by spraying with 100 mg/mL DHB in 50:50 methanol. The distribution of standards in the tissue was then visualized with 10-DAB (red, a), baccatin III (green, b) and paclitaxel (yellow, c).

Although the MSI showed that there was standard associated with some of the cells in the sample, the intensity of the peaks was extremely low. Because the standards were grouped to specific regions on the slide, it is possible that heterogeneous application of the matrix resulted in ionization only in those specific areas. By spiking the cell samples,

all aggregates within the sample should have contained identical concentrations of all three standards. These results could indicate that 1) the concentration of standards within the sample was below the range of detection, 2) the matrix application is not suitable for detection at low concentrations or 3) application of the matrix was not effective for ionization of the cell sample.

3.5. Discussion and future work

This work aimed to develop a method for mass spectrometry imaging of *Taxus* aggregates to allow for the visualization of paclitaxel and its precursors within single cells of the aggregate. The preliminary data presented in this chapter suggests that further optimization could lead to development of a successful protocol. The most successful matrix found in this study, DHB, was dissolved in a 50:50 MeOH:water solution. This matrix was effective at ionizing paclitaxel, baccatin III and 10-DAB both when mixed directly with standards and when spray coated onto indium tin oxide coated glass and stainless steel slides. Despite this success, spraying the DHB matrix on cryosliced spiked *Taxus* samples did not allow for identification of the standards within all of the tissue. Because the spray-coated matrix was not as effective at ionizing the standards as the spotted matrix, it is possible that a higher matrix concentration must be used to allow for lower detection limits. This could be achieved by either increasing the concentration of DHB being sprayed on the sample or by increasing the number of times each sample is sprayed with the matrix. Additionally, uneven coating of the sample could have resulted in ionization of only certain regions within the sample. When plant cells are dehydrated after cryoslicing, the cell wall often shrinks, leading to an uneven surface. This uneven surface can lead to uneven matrix crystallization (Takahashi et al., 2015). As a result,

matrix application should be optimized to allow for even application of the matrix. Alternative methods such as matrix sublimation or electrospray deposition could be investigated to achieve more homogeneous matrix crystals (Goodwin, 2012)

Because paclitaxel and its precursors are highly soluble in alcohols (including the solution that matrix is dissolved in), it might be necessary to use an alternative matrix or solvent to achieve single cell resolution in *Taxus* samples. As an alternative to a traditional matrix, nanoparticles can be used to minimize the use of a solvent, and have been successful for the MSI of paclitaxel in tumor tissue (Morosi et al., 2013). In this study, a TiO_2 suspension was sprayed on the sample, taking care to prevent over spraying the tissue, which would result in the formation of droplets on the tissue surface. Using this method, a resolution of 75 μm was achieved. In this study, negative ion mode was found to reduce the noise associated with lipids, which typically have peaks between 800 and 1,000 m/z (Morosi et al., 2013).

After an ideal matrix application method has been developed and standard can be detected in spiked cell samples, MSI should be applied to MJ-elicited cultures. To prepare for this future study, MJ-elicited cell cultures were fractionated into small (< 710 μm) and large (> 710 μm) aggregates and cryopreserved. Samples of the unfiltered cultures were also analyzed for paclitaxel content and found to contain 0.55 mg/L or 0.06 mg/g dry weight paclitaxel. These samples can be cryosliced and used to determine the distribution of paclitaxel in small and large aggregates of *Taxus* cultures. It has been hypothesized that small aggregates produce higher levels of paclitaxel due to environmental conditions (shear, nutrient concentration, etc.). If this is the case, the outer

cells on a large aggregate should show similar paclitaxel content to those cells located within a smaller aggregate.

CHAPTER 4.

INTERCELLULAR ENGINEERING. ISOLATION OF TAXOL-ACCUMULATING SINGLE CELLS USING A TAXOL BINDING CASPASE SYSTEM

4.1. Collaborators

Kevin Dagbay, Graduate Student, Chemistry

Maureen Hill, Graduate Student, Chemistry

Michelle McKee, Graduate Student, Plant Biology

Jeanne Hardy, Associate Professor, Chemistry

4.2. Abstract

A major limitation to plant cell culture production systems for supply of specialized metabolites is the heterogeneity of product accumulation both within single cells and within a cell line over time. In *Taxus* suspension cultures, 95% of single cells were found to accumulate paclitaxel, but the amount of paclitaxel in each cell was highly variable. A method to select for high-paclitaxel accumulating cells could allow for the propagation of superior *Taxus* cell lines for use in bioprocesses and could open the door for a completely new approach to engineering plant cell cultures. Additionally, application of continuous selection for paclitaxel accumulation could lead to cultures with stable paclitaxel yields. To select for high-paclitaxel accumulating cells within a heterogeneous culture, a paclitaxel-binding caspase system is being developed, which will result in the apoptosis of non- or low-paclitaxel accumulating cells. Caspase proteins are known to initiate apoptosis in mammalian cells, but no sequence homolog exists in plants. Despite this, caspase-like activity has been identified in plants and inhibitors of

mammalian caspase function actively inhibit these caspase-like proteins in plants. To investigate the effect of caspase proteins on plant cells, particle bombardment was used to transiently express a mammalian caspase-3 in *Taxus* cultures. Twenty-six percent of those cells expressing the caspase protein were found to be unviable, as opposed to just 9% for GFP-only expressing cells. These preliminary data indicating that the mammalian caspase can actively initiate apoptosis in plant cells was used to obtain NSF funding for development of the paclitaxel-binding caspase selection system.

4.3. Introduction

The presence of aggregates in *Taxus* suspension cultures lead to the formation of subpopulations due to differences in nutrient availability and exposure to shear. These aggregates are one source of heterogeneity in *Taxus* cultures and smaller aggregates accumulate higher levels of paclitaxel (Kolewe et al., 2011a; Patil et al., 2012; Patil et al., 2013). Additionally, single cells within aggregates accumulate variable levels of paclitaxel, indicating an opportunity to improve culture productivity by isolating these high-paclitaxel accumulating subpopulations (Naill and Roberts, 2005d). Methods have been developed to isolate high- and low-paclitaxel accumulating single cells through fluorescence activated cell sorting (Naill and Roberts, 2005b), which could allow for the propagation of high-paclitaxel accumulating subpopulations, as well as differential gene expression studies (Figure 4.1).

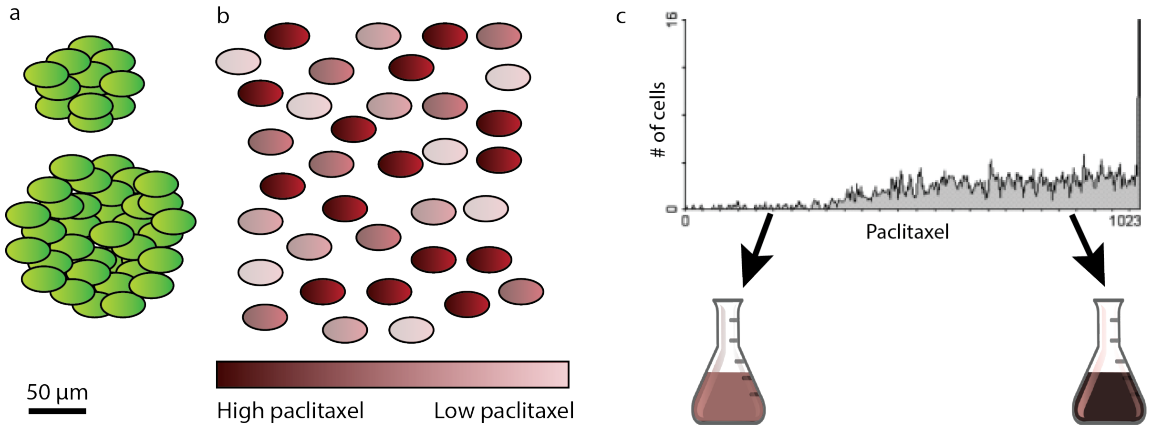

Figure 4.1 Overview of flow cytometry for paclitaxel identification (Naill and Roberts, 2005d). Aggregated cell cultures (a) are disaggregated into single cells through enzymatic digestion (b). These cells are stained for paclitaxel content using a fluorescent antibody for paclitaxel. The stained population can then be characterized using flow cytometry to identify paclitaxel content of the individual cells (c).

However, maintaining cell viability and initiating cell growth after disaggregation to single cells remains a significant challenge. Therefore, to allow for the isolation of high-paclitaxel accumulating single cells from aggregates in *Taxus* suspension cultures, this project aims to develop and use an inducible paclitaxel-binding caspase to selectively activate apoptosis in non-paclitaxel accumulating cells.

In animals, caspase proteins are heavily involved in the apoptosis cascade and are the cause of many hallmarks of apoptosis, including DNA fragmentation, cell shrinkage and membrane blebbing (Brentnall et al., 2013). Although homologs to caspase proteins are not found in plants, proteins with caspase-like activity have been identified (Belen Fernandez et al., 2015; Liu et al., 2012). Additionally, although no structural homologs of caspases exist in plants, inhibitors of animal-caspase activity have been shown to stop programmed cell death (PCD) in plant species (Fomicheva et al., 2012). This result suggests that functional analogs of caspases are involved in the PCD cascade in plants.

To further test this hypothesis, this work aimed to induce apoptosis in *Taxus* cells through the transient expression of a mammalian caspase-3 protein.

4.4. Methods

4.4.1. Plasmid construction

A pBlueScript II SK plasmid containing GFP constitutively expressed under the CaMV35S promoter was obtained from the Schnell laboratory in the Biochemistry and Molecular Biology Department at UMass Amherst. As recommended by the Schnell lab, two restriction enzyme sites, BamHI and XbaI, were selected for cloning of the mammalian caspase into the pBlueScript vector to put the caspase-3 at the N-terminal of the GFP. The caspase-3 was isolated from the plasmid pET23b-casp3-His using the primers designed in Table 4.1.

Table 4.1. Primers used to amplify the caspase-3 gene from the pET23b-casp3-His plasmid and introduce the BamHI and XbaI restriction enzyme sites

Forward primer	GGT GGT GGA TCC ATG GAG AAC ACT GAA AAC TCA GTG GAT TCA AAA TCC
Reverse primer	GGT GGT TCT AGA GTG ATA AAA ATA GAG TTC TTT TGT GAG CAT GGA AAC AAT ACA TG

After PCR amplification of the caspase-3 gene, the amplified fragment was inserted into the pBlueScript vector using the BamHI and XbaI restriction enzyme sites. The generated plasmid was confirmed through colony PCR (data not shown). To generate sufficient DNA for particle bombardment experiments, a 50 mL culture was grown up overnight and a MidiPrep was utilized to extract the plasmid DNA.

4.4.2. Preparation of gold particles for particle bombardment

Gold particles were prepared for bombardment as described in (Vongpaseuth et al., 2007). In short, 30 mg of 1.6 μm gold particles were suspended in 500 μL of 70% ethanol and vortexed for five minutes. Particles were allowed to settle for 15 minutes prior to centrifugation at maximum speed (15,000 rpm) for five seconds. The supernatant was removed and particles were washed by adding 1 mL of sterile water, vortexing for 1 minute, settling for 1 minute and pelleting the particles for 5 seconds at maximum speed. The supernatant was then removed through pipetting and this process was repeated an additional 2 times. After the 3rd wash, the supernatant was removed and particles were resuspended in 500 μL of sterile 50:50 glycerol in water.

To coat the particles with plasmid DNA, the particles were vortexed for five minutes and aliquots of 50 μL were transferred to 1.5 mL microcentrifuge tubes. While continuously agitating the particles on a vortex, 5 μL of DNA, 50 μL of 2.5 M $CaCl_2$ and 20 μL of 0.1 M spermidine were added, respectively. Particles were continuously vortexed for another 3 minutes prior to settling for 1 minute and pelleting the particles for 5 seconds at top speed. The particles were then washed by adding and removing 140 μL of 70% ethanol, followed by adding and removing 140 μL of 100% ethanol with a pipet. Particles were then resuspended in a final volume of 48 μL of 100% ethanol by gently tapping the microcentrifuge tube. This process was repeated for each plasmid being used in the bombardment.

4.4.3. Bombardment of *Taxus* cultures

Bombardment of the *Taxus* cultures was performed as previously described (Vongpaseuth et al., 2007). In short, day 7 cultures of *Taxus* cell lines P93AF and

PO93XC were plated on Gamborg B5 medium approximately four hours prior to particle bombardment. Cells were filtered over miracloth using a buckner funnel and approximating 0.5 g of cell mass was put on each plate. The cells were spread using a metal spatula to create a thin, uniform layer of cells. Six μL (approximately 500 μg) of gold microcarrier particles were loaded onto a macrocarrier disk and allowed to dry in a petri dish filled with NaCl crystals. Particle bombardment was performed using a Biolistic® PDS-1000/He Particle Delivery System (Bio-Rad, Hercules, Ca) using a rupture disk pressure of 1,100 psi and a target distance of 6 cm. Each plate was bombarded twice. All materials for particle bombardment were purchased from Bio-rad.

4.4.4. Determining GFP expression and determining cell viability

To check for GFP expression in both the CaMV35S-GFP and CaMV35S-Casp-GFP strains, plates were examined 48 and 72 hours after bombardment for GFP expression under an inverted microscope (Olympus, Center valley, PA). GFP fluorescence was viewed using 470/40 nm excitation and 495 nm long-pass emission filters (Chroma, Rockingham, VT). At 72 hours, areas containing GFP-expressing cells were removed from the solid media plate and resuspended in 1 mL of liquid Gamborg B5 medium. Cells were then stained for viability by adding 10 μL of propidium iodide (1 mg/mL in water) and incubating at room temperature for 5 minutes. After 5 minutes, 200 μL of cells were removed and placed on a glass slide and topped with a cover slip. Slides were then examined for GFP-expression and viability under the fluorescence microscope. Each GFP-expressing cell was imaged for GFP expression and viability. Images were overlaid and those cells with both GFP and propidium iodide fluorescence were counted as inviable.

4.5. Results

After 72 hours, GFP expression was identified in both the CaMV35S-GFP and CaMV35S-Casp-GFP transformed cultures of both the P93AF and PO93XC cell lines. At this time, cells were assayed for viability to determine the effect of caspase-3 protein expression on the *Taxus* cell viability (Figure 4.2).

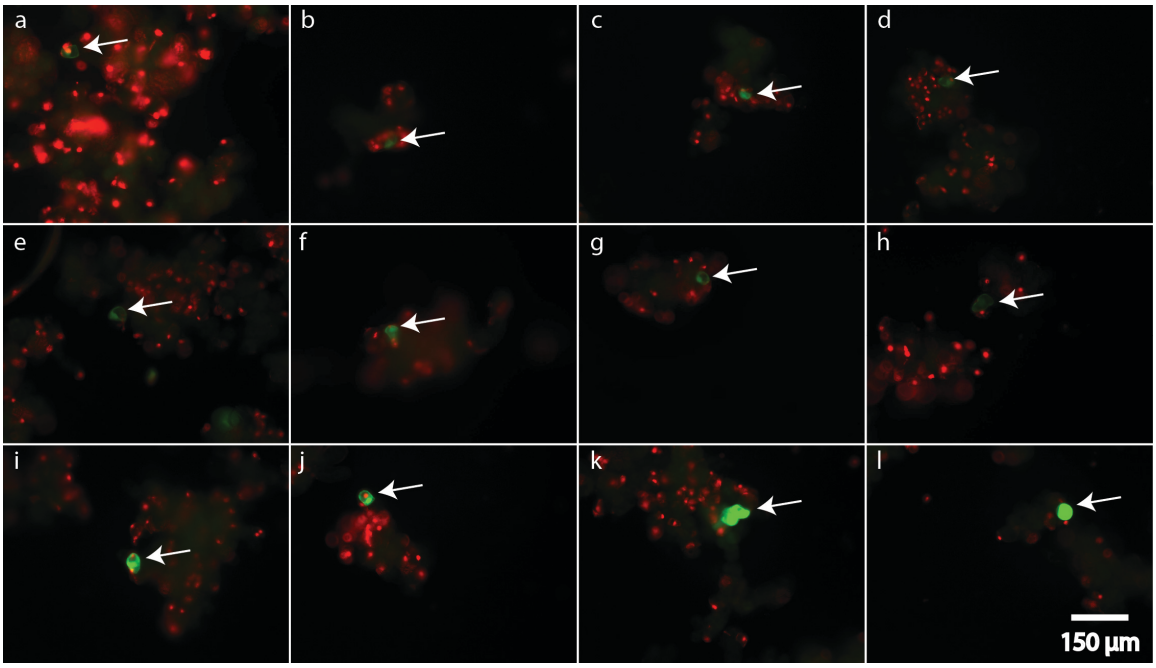

Figure 4.2. Selection of cells analyzed for GFP expression and viability of CaMV35S-Casp-GFP (a-h) and CaMV35S-GFP (i-l) expressing cells. GFP expressing cells are indicated with arrows and fluoresce green. Cells that are not viable have been stained with propidium iodide, resulting in red fluorescence in the nucleus of the cell. CaMV35S-Casp-GFP cells that are not viable can be seen in images a-e, whereas viable cells can be seen in images f-h. CaMV35S-GFP cells that are not viable can be seen in images i and j, whereas viable cells can be seen in images k and l.

All cells that were expressing GFP were imaged under the GFP and propidium iodide filters. Images were overlaid and those cells that contained both GFP and propidium iodide fluorescence were deemed inviable. It was found that five of the 19 CaMV35S-Casp-GFP transformed cells and two of the 22 CaMV35S-GFP transformed cells were

not viable 72 hours after transformation, representing 26% and 9% of the transformed populations, respectively.

4.6. Discussion

Although additional transient transformation experiments must be completed to increase the statistical significance of these results, preliminary data suggest that the caspase protein is increasing the frequency of cell death in transformed populations. Additionally, from this experiment, it can be seen that GFP expression is significantly higher in the GFP only constructs (Figure 4.2 i-l) than in the GFP-caspase constructs (Figure 4.2 a-h). This could be the result of the increased stress on the cells due to the expression of both proteins, or could be due to the initiation of an apoptotic response in those cells expressing the caspase-3 protein. In future experiments, an additional control construct will be used containing GFP and an inactive caspase-3 protein. These preliminary data were used to obtain NSF support to allow for continued investigation into the effect of human caspase proteins on plant cell systems and the engineering of caspases to select for paclitaxel-accumulating cell populations.

CHAPTER 5.

CHARACTERIZATION OF ACTIVE SPECIALIZED METABOLIC PATHWAYS IN *TAXUS* SUSPENSION CULTURES

5.1. Collaborators

Sangram K. Lenka, Post-Doctoral Associate

Rohan Patil, PhD, Chemical Engineering

Jennifer Normanly, Professor, Biochemistry and Molecular Biology

Elsbeth L. Walker, Constantine J. Gilgut Professor, Biology

5.2. Introduction

Plants are capable of producing thousands of compounds that have high value as fragrances, flavors, pesticides and pharmaceuticals. Many of these compounds, called specialized metabolites, are produced as a stress response, allowing plants to adapt to their environment. The pathways involved in plant growth and development (called conserved or primary metabolism) are well conserved across species and, therefore, very well defined. These conserved metabolic pathways form the precursor pools for specialized (formerly secondary) metabolism, leading to the production of specific classes of metabolites in plants (Figure 5.1).

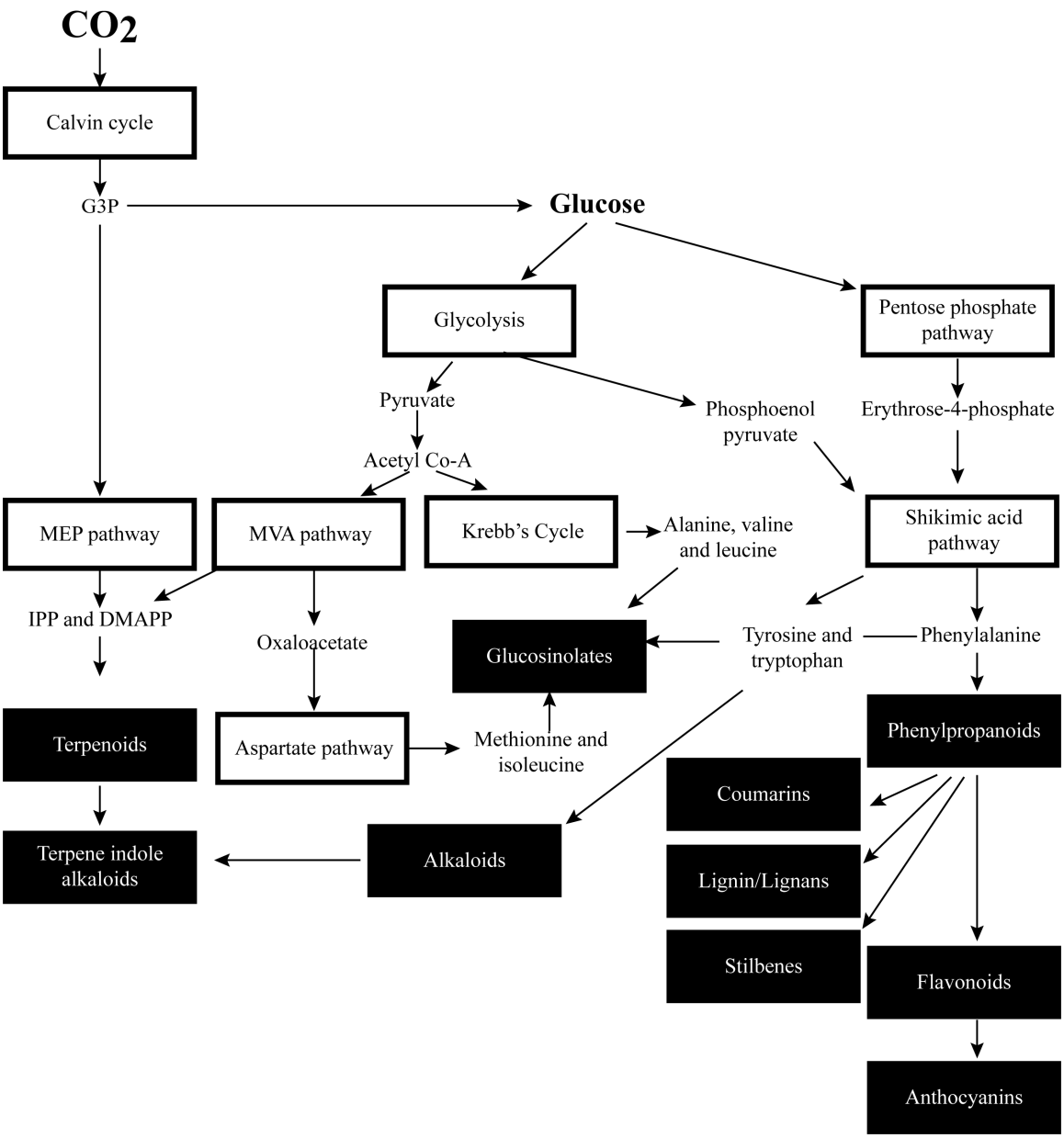

Figure 5.1. Overview of the conserved classes of specialized metabolites found in plant systems. Specialized metabolites are illustrated in black filled boxes. (Abbreviated compounds: G3P – D-glyceraldehyde 3-phosphate; IPP – isopenthenyl pyrophosphate; DMAPP – dimethylallyl pyrophosphate; Acetyl Co-A – acetyl coenzyme A)

Key classes of specialized metabolites feed off of common precursor pools, such as isopenthenyl pyrophosphate (IPP) and dimethylallyl pyrophosphate (DMAPP) from the non-mevalonate (MEP) and mevalonate (MVA) pathways and phenylalanine from the

shikimic acid pathways. The interactions between conserved and specialized metabolism are poorly understood. Recent studies have highlighted the fact that specialized metabolism cannot be neatly compartmentalized into those pathways responsible for growth and those pathways responsible for the stress response (Schwachtje and Baldwin, 2008). Additionally, as indicated in this thesis, the nomenclature defining growth related pathways as primary metabolism and defense related pathways as secondary metabolism has shifted to defining conserved metabolism (pathways conserved across all plant species) and specialized metabolism (which lead to the production of species-specific metabolites) (Pichersky and Lewinsohn, 2011).

The mechanisms that govern flux from conserved metabolism into specialized metabolism are poorly understood, complicating culture engineering efforts for the production of specific functional compounds. Additionally, specialized metabolism is further complicated because the functional compounds produced are often species specific, and as a result, the metabolic pathways to these compounds are poorly defined (Wilson et al., 2014a). It has been estimated that there are between 200,000 and 1,000,000 plant metabolites, making identification and characterization of specific metabolites an enormous bottleneck to plant metabolomics (Afendi et al., 2012; Dixon and Strack, 2003; Yang et al., 2013). Although many databases have been developed to aid in annotation, compounds cannot be accurately identified due to the lack of authentic standards for many of the complex compounds found in plant systems (Yang et al., 2013). As a result, classification of compounds often relies on MS/MS spectra in the literature or databases, which are limited and can result in incorrect compound identification (Sumner et al., 2007).

Traditional plant cell culture engineering strategies focus primarily on product yields, with little attention to competing products and the balance of flux through specialized metabolism (Wilson et al., 2014a). For *Taxus* cultures, metabolic studies have primarily focused on the production of paclitaxel in response to varying elicitor concentrations and cellular manipulations (Wilson and Roberts, 2014). As a result, little is understood about the competing products produced within these cultures. Additionally, *Taxus* cultures that are unable to produce paclitaxel are rarely investigated. We have conducted a transcriptome analysis (unpublished) in paclitaxel-accumulating *Taxus* cell line to identify active specialized metabolic pathways. The key active pathways identified in this study were the paclitaxel biosynthetic pathway, the phenylpropanoid pathway, the flavonoid pathway and the stilbenoid, diarylheptanoid and gingerol biosynthesis (Keshari Lenka, 2011). These represent major classes of specialized metabolites found in plant species and their interactions are depicted in Figure 5.2.

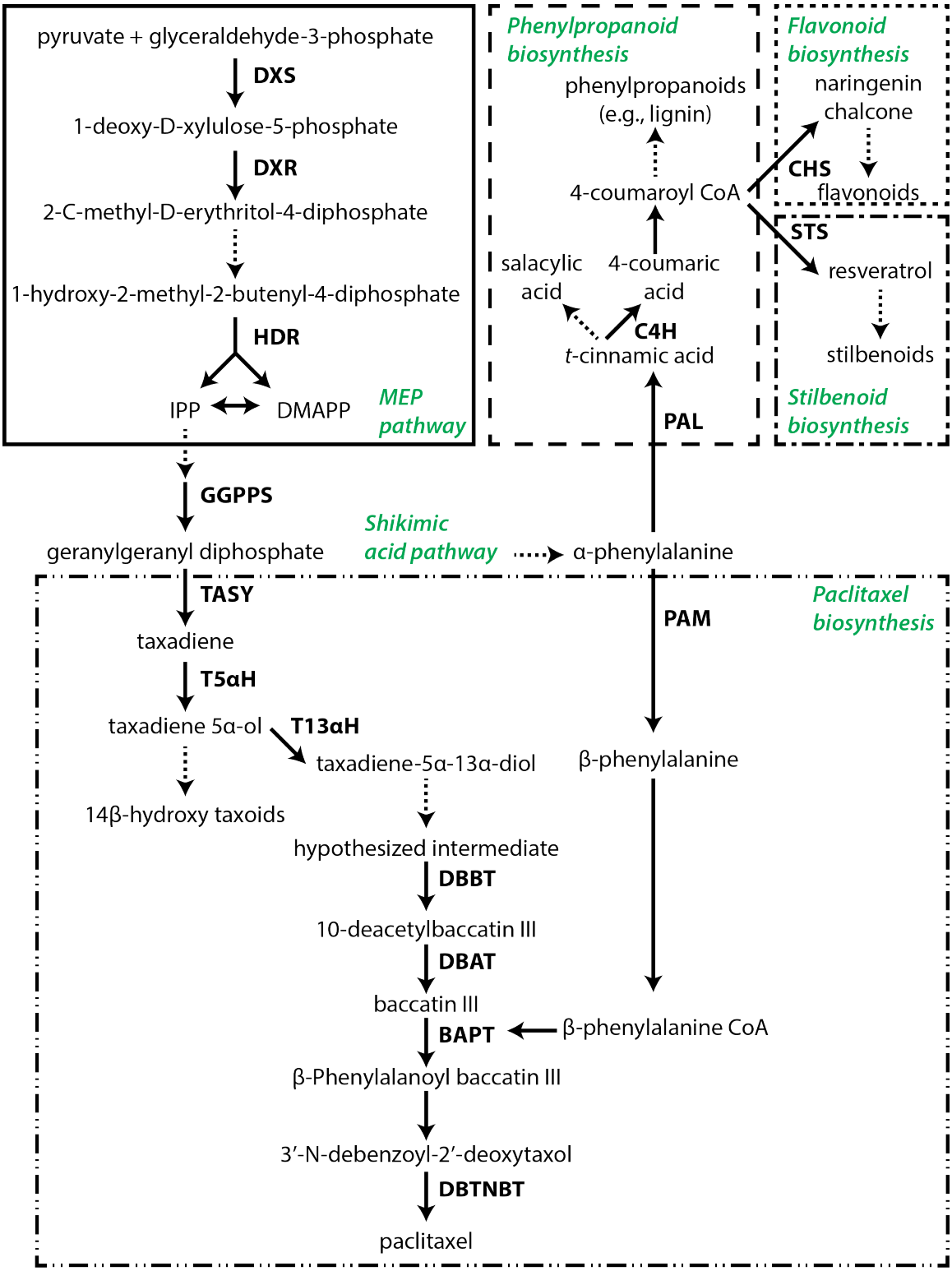

Figure 5.2. Biosynthetic pathways for key active pathways found in *Taxus* suspension cultures. (Enzyme abbreviations: DXS – Deoxy-xylulose-P synthase; DXR – 1-deoxy-D-xylulose 5-phosphate reductoisomerase; HDR – 1-hydroxy-2-methyl-butenyl 4-diphosphate reductase; GGPPS –

geranylgeranyl pyrophosphate synthase; TASY – taxadiene synthase; T5αH – taxadiene-5α-hydroxylase; T13αH – taxadiene-13α-hydroxylase; DBBT – 2α-O-benzoyl transferase; DBAT – 10-deacetylbaccatin-III-10-O-acetyl transferase; BAPT – C-13-O-phenylpropanoyl-CoA transferase; DBTNBT – 3'-N-debenzoyl-2'-deoxytaxol N-benzoyl transferase; PAM – phenylalanine aminomutase; PAL – phenylalanine lyase; C4H – cinnamate-4-hydroxylase; CHS – chalcone synthase; STS – stilbene synthase)

Phenylpropanoids and flavonoids divert flux from paclitaxel through a common precursor, phenylalanine. Methyl jasmonate (MJ) elicited cultures were shown to accumulate 122% more flavonoids and 23% more lignin than unelicited cultures (Keshari Lenka, 2011), supporting our unpublished transcriptomic data. To better understand flux in paclitaxel and non-paclitaxel accumulating cultures, it is important to develop methods that allow for the high throughput evaluation of flux through these varied specialized pathways.

In this study, assays were developed to map flux through key classes of specialized metabolites that are produced in *Taxus* cultures. These assays were then used to investigate the effect of methyl jasmonate on both paclitaxel and non-paclitaxel accumulating cultures. The rapid nature of these assays allowed them to be used to investigate the long-term variability of flux through specialized metabolic pathways in *Taxus* cultures in both unelicited and elicited states. Results from these studies will allow for development of both global and cell-line specific metabolic engineering strategies for *Taxus* cultures and open the door for additional studies with other species.

5.3. Materials and Methods

5.3.1. Maintenance and biomass measurements for *Taxus* cultures

Three *Taxus cuspidata* cell lines (P93AF, PO93X, PO93XC) and one *Taxus canadensis* cell line were obtained from the United States Plant Soil and Nutrition Laboratory in Ithaca, NY. All chemicals were purchased from Sigma-Aldrich Co. (St, Louis, MO) unless otherwise noted. Cells were maintained and sub-cultured on a bi-weekly basis, as previously described (Kolewe et al., 2011a). All biomass and aggregation data were measured using a Multisizer 3™Coulter counter with a 2,000 μm aperture (Beckman Coulter, Brea, CA), as previously described (Kolewe et al., 2010). In short, 2 x 2 mL well mixed samples of culture were analyzed from each flask at each timepoint. Biomass measurements were converted to dry weight using a previously established correlation (Kolewe et al., 2010; Kolewe et al., 2011b).

5.3.2. Effect of methyl jasmonate on paclitaxel and non-paclitaxel accumulating cultures

Eight flasks of each cell line (~100 mL of culture) were maintained in a 250 mL flask over a 21-day period. On day 7, 4 cultures were elicited with 200 μM MJ. Biomass, aggregation and specialized metabolite samples were taken on days 0, 7, 14 and 21 of the culture period. Paclitaxel samples were taken on days 7, 14 and 21 and lignin staining was performed on days 14 and 21. All samples were taken by pipetting one mL of well-mixed culture into a 1.5 mL microcentrifuge tube. Samples for specialized metabolite analysis were stored at -80 °C until they were prepped for further analysis, where as lignin samples were stained immediately with phloroglucinol (details follow).

5.3.3. Long-term effect of methyl jasmonate on PO93XC (non-paclitaxel accumulating) and P93AF (paclitaxel-accumulating) cultures

Two cell lines, PO93XC (non-paclitaxel accumulating) and P93AF (paclitaxel accumulating) were used in this experiment. For generations that were elicited with MJ, experiments were performed as above to determine the effect of MJ on non-paclitaxel and paclitaxel accumulating cultures. On day 14 of the culture period, 20 mL of well-mixed cell culture were removed from each control (unelicted) flask and transferred to a sterile container. This well mixed culture (a total of 80 mL) was then used to inoculate four new flasks, which were monitored as the next generation of the cell culture. For unelicited generations, biomass and specialized metabolite samples were taken on days 0, 7 and 14 of the generation. On day 14, well-mixed culture from each flask was combined in a sterile container and 20 mL each were transferred to 8 new flasks with fresh media to continue on to the next generation.

5.3.4. Contig generation, annotation, pathway mapping and expression analysis

T. cuspidata P93AF cells (MJ-elicited and mock-elicited) were used for contig generation, annotation and expression analysis of genes associated with specialized metabolite according to the procedure, as previously described (Patil et al., 2014b). All the annotated contigs were mapped to corresponding metabolic pathways using Kyoto Encyclopedia of Genes and Genomes (KEGG) database.

5.3.5. Preparation of samples for specialized metabolite analysis

Samples were removed from the -80 °C freezer and allowed to thaw at room temperature before being evaporated at room temperature overnight in an evaporative centrifuge. Pellets were then resuspended in 500 µL of acidified methanol (0.01 % acetic

acid in methanol), vortexed and samples were placed on a shaker at 125 rpm at 25 °C for one hour. After one hour, samples were vortexed for 10 s and pellets were disassociated using a stainless steel spatula. The samples were placed back on the shaker at 125 rpm for an additional hour before being centrifuged for 10 minutes at 15,000 rpm.

5.3.6. Phenolic content

The phenolic content was determined using a Folin-Ciocalteu reagent (Ainsworth and Gillespie, 2007). In short, 20 µL of the methanol extract was mixed with 50 µL of a 0.2 N Folin-Ciocalteu reagent and 160 µL of 700 mM sodium carbonate in a 1.5 mL centrifuge tube. The assay solution was allowed to incubate for 10 minutes before being centrifuged for 1 min at 15,000 rpm. Two hundred µL of the supernatant was then transferred to a 96-well plate and the absorbance was read at 750 nm. Absorbance values were converted to mg/mL gallic acid equivalent using a gallic acid standard curve using concentrations ranging from 0-0.2 mg/mL.

5.3.7. Flavonoid content

The flavonoid content was determined using an aluminum chloride based assay (Chang et al., 2002). Twenty-five µL of sample was mixed with 50 µL of water in a 96-well plate. Seventy-five µL of 6 g/L $NaNO_2$ was then added to each well. After 1 minute, 75 µL of 22 g/L $AlCl_3$-$6H_2O$ was added to each well. After 2 minutes, 75 µL of 0.8 M NaOH was added to each well and the absorbance was read at 490 nm. Absorbance values were converted to mg/mL catechin equivalent using a catechin standard curve using concentrations ranging from 0-1 mg/mL.

5.3.8. Lignin staining

Lignin staining was performed using an acidified phloroglucinol assay. To prepare the solution, 2 g of phloroglucinol was dissolved in 30 mL of a 20% ethanol solution. Twenty mL of 12 M hydrochloric acid was then added. For staining, a 1 mL mixed culture sample was taken and placed at the edge of a petri dish. Two hundred μL of sample was transferred to a slide for an unstained control before the supernatant was removed from the remainder of the cells using an one mL pipet. The cells were then resuspended in 500 μL of the phloroglucinol solution and allowed to incubate at room temperature for 5 minutes. Two hundred μL of each sample was then transferred to each slide and images were taken using a digital camera on the benchtop.

5.3.9. Paclitaxel measurements

Samples for paclitaxel analysis were prepped and measured through UPLC, as previously described (Naill and Roberts, 2004; Patil et al., 2012).

5.4. Results

5.4.1. Effect of MJ on non-paclitaxel and paclitaxel accumulating cultures

The effect of MJ on multiple *Taxus* cell lines was investigated. P93AF, a *Taxus cuspidata* cell line, accumulated 0.05 mg/g DW of paclitaxel throughout the 21-day growth period. CO93D, a *Taxus canadensis* cell line, accumulated about 3-fold higher levels, 0.15 mg/g DW, of paclitaxel by the end of the growth period. Additionally, two non-paclitaxel *Taxus cuspidata* accumulating cultures, PO93X and PO93XC, were studied. To look at the shift of carbon flux from conserved towards specialized metabolism, biomass measurements were taken throughout the culture growth period.

Growth inhibition was determined through the normalization of biomass levels with the mock-elicited control (Figure 5.3a).

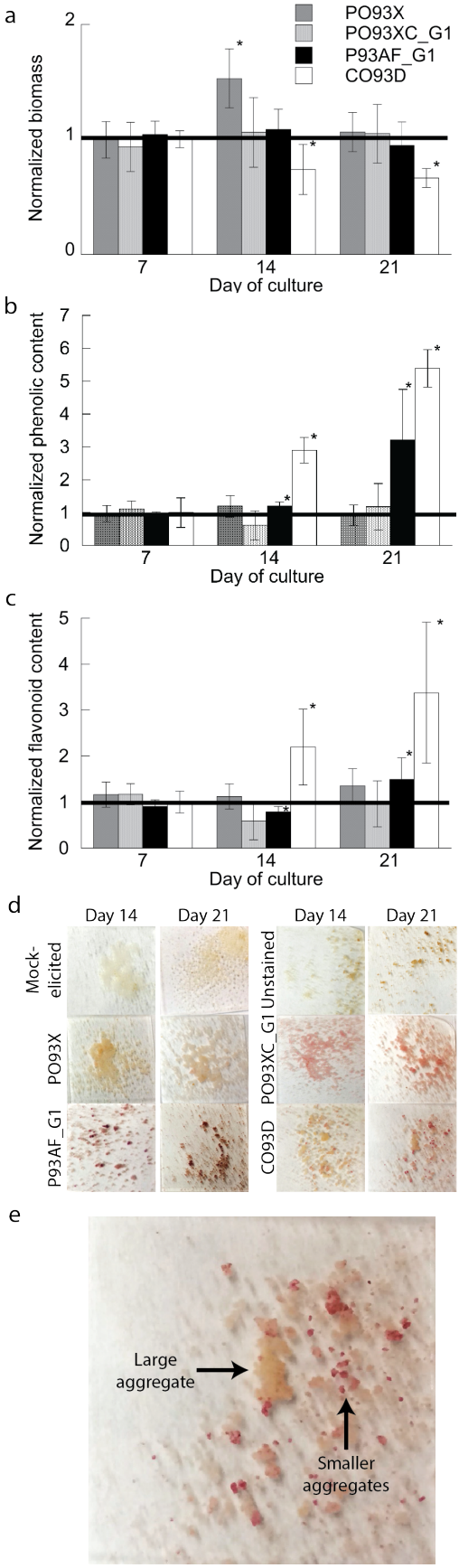
a
PO93X
PO93XC_G1
P93AF_G1
CO93D
Normalized biomass
Day of culture
b
Normalized phenolic content
Day of culture
c
Normalized flavonoid content
Day of culture
d
Day 14
Day 21
Day 14
Day 21
Mock-elicited
PO93X
P93AF_G1
Unstained
PO93XC_G1
CO93D
e
Large aggregate
Smaller aggregates

Figure 5.3. Effect of MJ on the growth (a), phenolic accumulation (b), flavonoid accumulation (c) and lignin accumulation (d,e) of non-paclitaxel accumulating (PO93X and PO93XC) and paclitaxel accumulating (P93AF and CO93D) *Taxus* suspension cultures. Growth, phenolic and flavonoid levels in MJ-elicited cultures have been normalized to the mock-elicited controls. Lignin accumulation for elicited cultures (d,e) is shown using an acidified phlouroglucinol assay, where phloroglucinol interacts with end groups on the lignin chain to form a red pigment. Mock-elicited cultures do not accumulate lignin, as shown, and unstained samples do not exhibit red pigmentation. Differential lignin accumulation in a day 21 elicited CO93D culture can be seen in the magnified image (e). * indicates statistically different from one as determined by a Student's t-test ($p<0.05$).

In the presence of MJ, the culture that produced the largest amount of paclitaxel (CO93D) exhibited growth inhibition, whereas those cultures that did not produce paclitaxel (PO93X and PO93XC) were not growth inhibited. As MJ is a global inducer of specialized metabolism, two classes of specialized metabolites, phenolics and flavonoids, were investigated (Figure 5.3b,c). MJ addition leads to the increased accumulation of phenolic and flavonoid compounds in those cultures that accumulate paclitaxel. For those cultures that do not accumulate paclitaxel, there was no increase in the production of these classes of specialized metabolites. Preliminary studies have shown that lignin, a phenylpropanoid that accumulates in the cell wall of plants, is produced by *Taxus* cultures that have been elicited with MJ (Lenka et al., Manuscript in progress.). Using an acidified phloroglucinol stain, lignin accumulation within the cultures was investigated (Figure 5.3d,e). Interestingly, all of the cultures produce lignin in response to MJ elicitation. Although lignin accumulates in all elicited cultures, the level of lignin in each aggregate can vary significantly as seen in Figure 5.3e. Smaller aggregates within this culture accumulate higher levels of lignin, whereas larger aggregates are not stained with the acidified phloroglucinol.

5.4.2. Long-term effect of MJ on PO93XC (non-paclitaxel accumulating) and P93AF (paclitaxel-accumulating) cultures

Due to the rapid nature of the assays developed in this study, long-term variability of flux through these pathways was investigated in both paclitaxel and non-paclitaxel accumulating cultures. The growth and aggregation patterns of 2 *Taxus* cultures (P93AF, a paclitaxel accumulating cell line and PO93XC, a non-paclitaxel accumulating cell line) were investigated over 9 generations of cell growth (Figure 5.4).

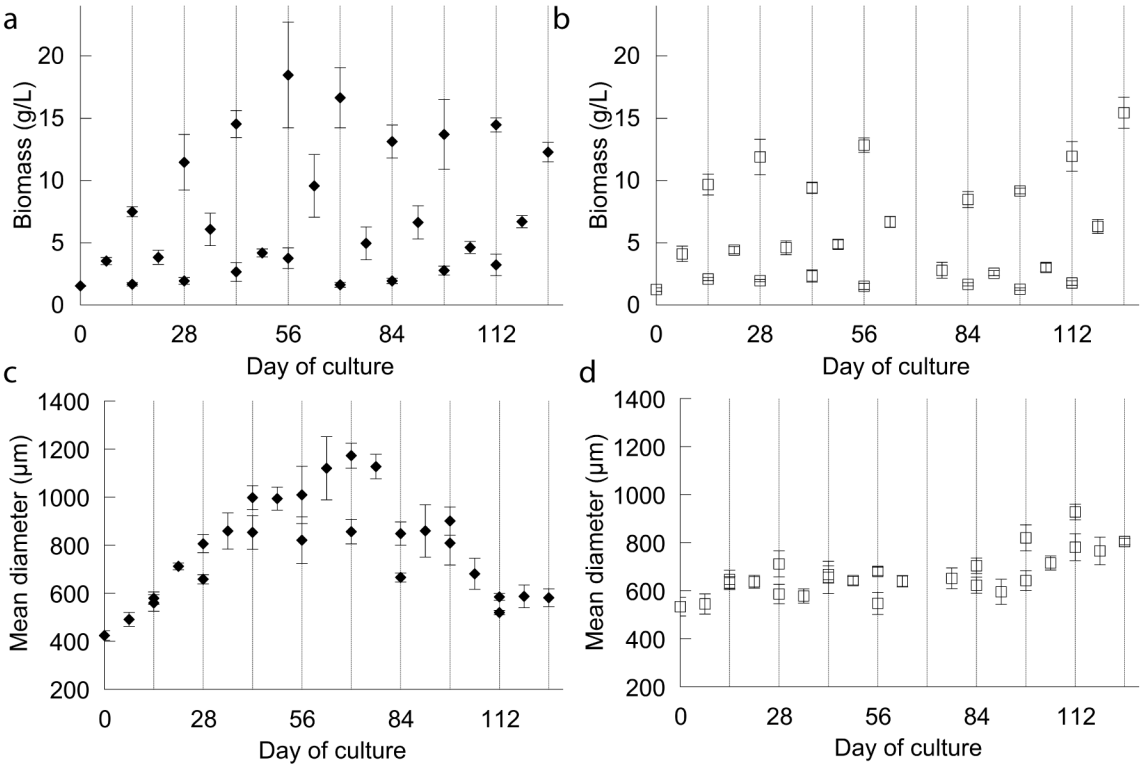

Figure 5.4. Growth and aggregation of P93AF, a paclitaxel accumulating cell line, (a,c) and PO93XC, a non-paclitaxel accumulating cell line, (b,d) over 9 generations. Each line on the x-axis represents a single generation of the culture. Reported values represent the average of three biological replicates.

Over the 9 generations, the growth of both cultures was stable (Figure 5.4a,b). Despite this observation, the aggregation dynamics of the paclitaxel-accumulating culture varied from a mean of 420 µm at the beginning of the experiment to 1,160 µm at the end

of the fifth generation of growth and then back down to 580 μm at the end of the ninth generation of growth (Figure 5.4c). Similarly, the mean aggregate size of the non-paclitaxel accumulating culture increased from 520 μm to 800 μm (Figure 5.4d). This type of variability over time is typical in *Taxus* suspension cultures (Kolewe et al., 2011a; Patil et al., 2012; Patil et al., 2013) and provides the opportunity to correlate changes observed with extent of aggregation.

5.4.2.1. Unelicited specialized metabolite accumulation

The phenolic and flavonoid contents of the cultures are shown in Figure 5.5.

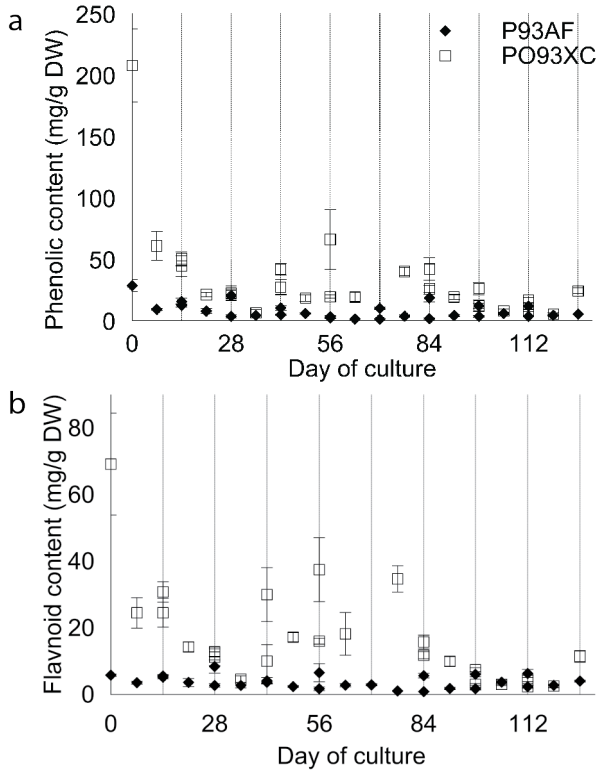

Figure 5.5. Phenolic and flavonoid content of a paclitaxel accumulating cell line, P93AF, and non-paclitaxel accumulating cell line, PO93X, over 9 generations. Each line on the x-axis represents a single generation of the culture.

The basal levels of these compounds followed similar trends in each culture over the 9 generations of growths. For the non-paclitaxel accumulating cell line, PO93XC, the phenolic content varied between 5 and 209 mg/g DW and the flavonoid content varied between 2 and 69 mg/g DW. After the first day of the culture, the phenolic and flavonoid content of the culture dropped significantly from 209 mg/g DW to 60 mg/g DW and 69 mg/g DW to 25 mg/g DW, respectively. The total contents found in the non-paclitaxel accumulating cell line were significantly higher than the content found in the paclitaxel accumulating cell line. For the paclitaxel-accumulating cell line, the phenolic content varied between 1.4 mg/g DW and 28.7 mg/g DW and the flavonoid content ranged from 0.9 to 5.8 mg/g DW. Variability in the basal accumulation of these compounds could provide insight into the capability of these cultures to accumulate high levels of specialized metabolites in response to elicitation.

5.4.2.2. Effect of MJ on growth and production of specialized metabolites

The non-paclitaxel accumulating culture PO93XC was elicited 3 times over the nine generations of growth, whereas the paclitaxel accumulating culture P93AF was elicited every other generation for a total of 5 elicited generations. The effect of MJ on the growth, aggregation, phenolic content and flavonoid content of the cultures is shown in Figure 5.6.

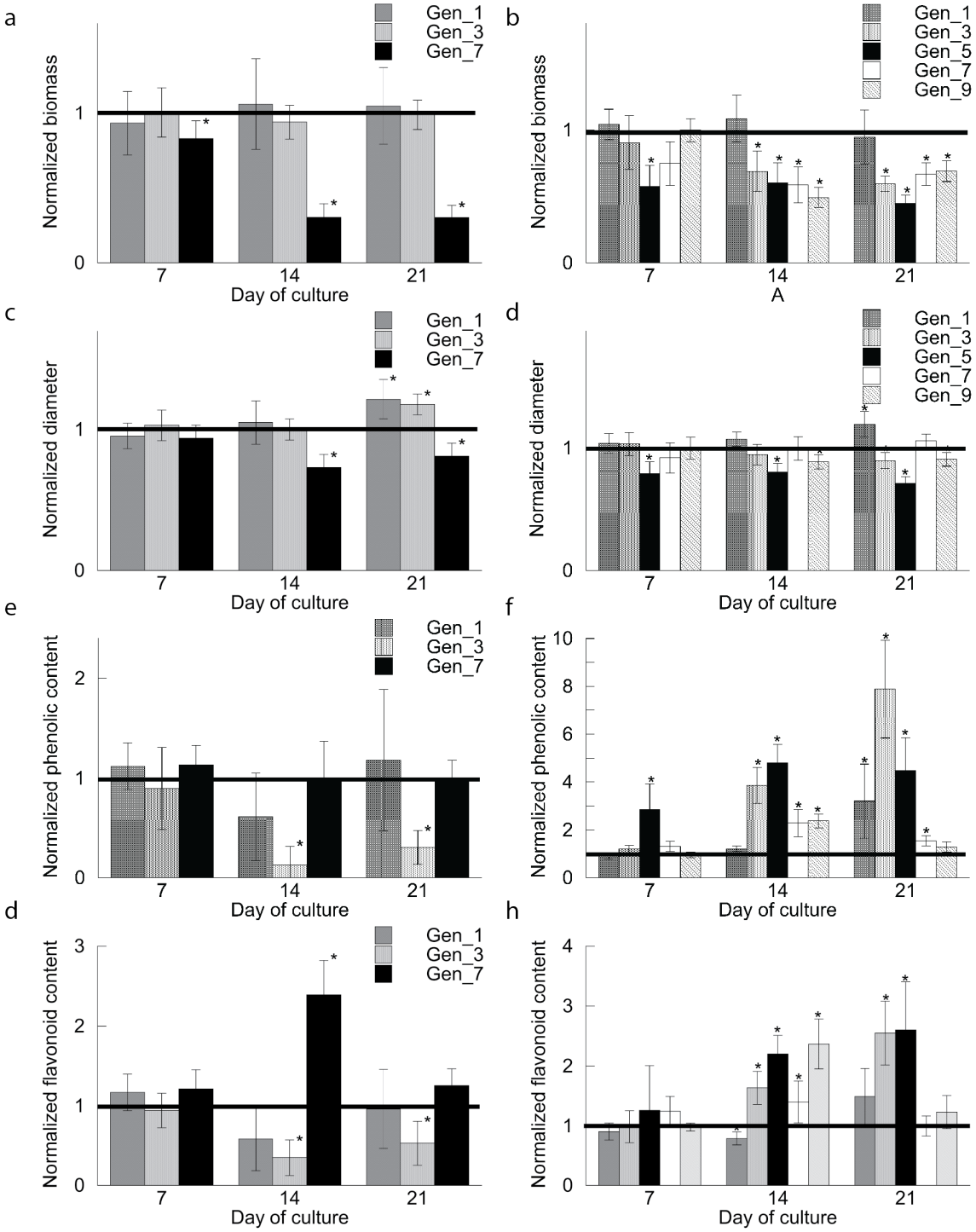

Figure 5.6. Effect of MJ on the growth (a,b), aggregate size (c,d), phenolic content (e,f) and flavonoid content (g,h) of the non-paclitaxel accumulating PO93XC cell line (a,c,e,g) and the paclitaxel accumulating P93AF cell line (b,d,f,h) over multiple generations of elicitation. All values for elicited cultures have been normalized to the control. Reported values represent the average of three

biological replicates. * indicates statistically different from one as determined by a Student's t-test ($p<0.05$).

For 2 of the 3 elicited generations, the non-paclitaxel accumulating cell line exhibited no growth inhibition. During the third elicited generation, culture growth was inhibited, with very little growth occurring after the addition of MJ (Figure 5.6a). For the paclitaxel accumulating cell line, growth inhibition was seen in all generations except for the first elicited generation. This observation is similar to the results found in short term experiment (study described above), where cultures that accumulated paclitaxel exhibited growth inhibition.

The effect of MJ on phenolic content (Figure 5.6e,f) and flavonoid content (Figure 5.6g,h) was investigated. MJ had little effect on the phenolic and flavonoid content of non-paclitaxel accumulating cultures. On the contrary, cultures that are able to accumulate paclitaxel showed a significant increase in the accumulation of both of these classes of compounds. The variability associated with these cultures becomes evident through the long-term analysis of these cultures. The paclitaxel-accumulating culture showed upregulation of phenolics and flavonoids in 3 of the 5 generations. During the first and seventh generations, accumulation of these compounds was not increased. The use of transcript level studies on these cultures would reveal more about the mechanism behind these changes in product accumulation.

Like the specialized metabolite accumulation, paclitaxel accumulation gives insight into the variability associated with these cultures (Table 5.1).

Table 5.1 Paclitaxel content (mg/g DW) in cell line P93AF over the course of nine generations of growth.

Generation of growth	Day 14	Day 21
1	0.05 ± 0.005	0.05 ± 0.004
3	0.03 ± 0.007	0.06 ± 0.006
5	0.03 ± 0.006	0.05 ± 0.009
7	0.002 ± 0.002	0.003 ± 0.002
9	0.07 ± 0.006	0.06 ± 0.02

Paclitaxel accumulation was fairly consistent in 4 of the 5 generations studied (generations 1, 3, 5 and 9), but the seventh generation showed very little paclitaxel accumulation, with one culture showing no detectable paclitaxel. Phenolic and flavonoid accumulation during this generation was also low, but growth inhibition was similar to the previous elicited generations (Figure 5.6). To learn more about the mechanisms behind these changes in product accumulation, the correlation between culture aggregation and metabolite accumulation can be investigated.

5.4.2.3. Effect of aggregation on metabolite accumulation

Interestingly, the phenolic and flavonoid content of both cells lines was shown negatively correlate with the mean aggregate size of the culture, as seen for P93AF in Figure 5.7.

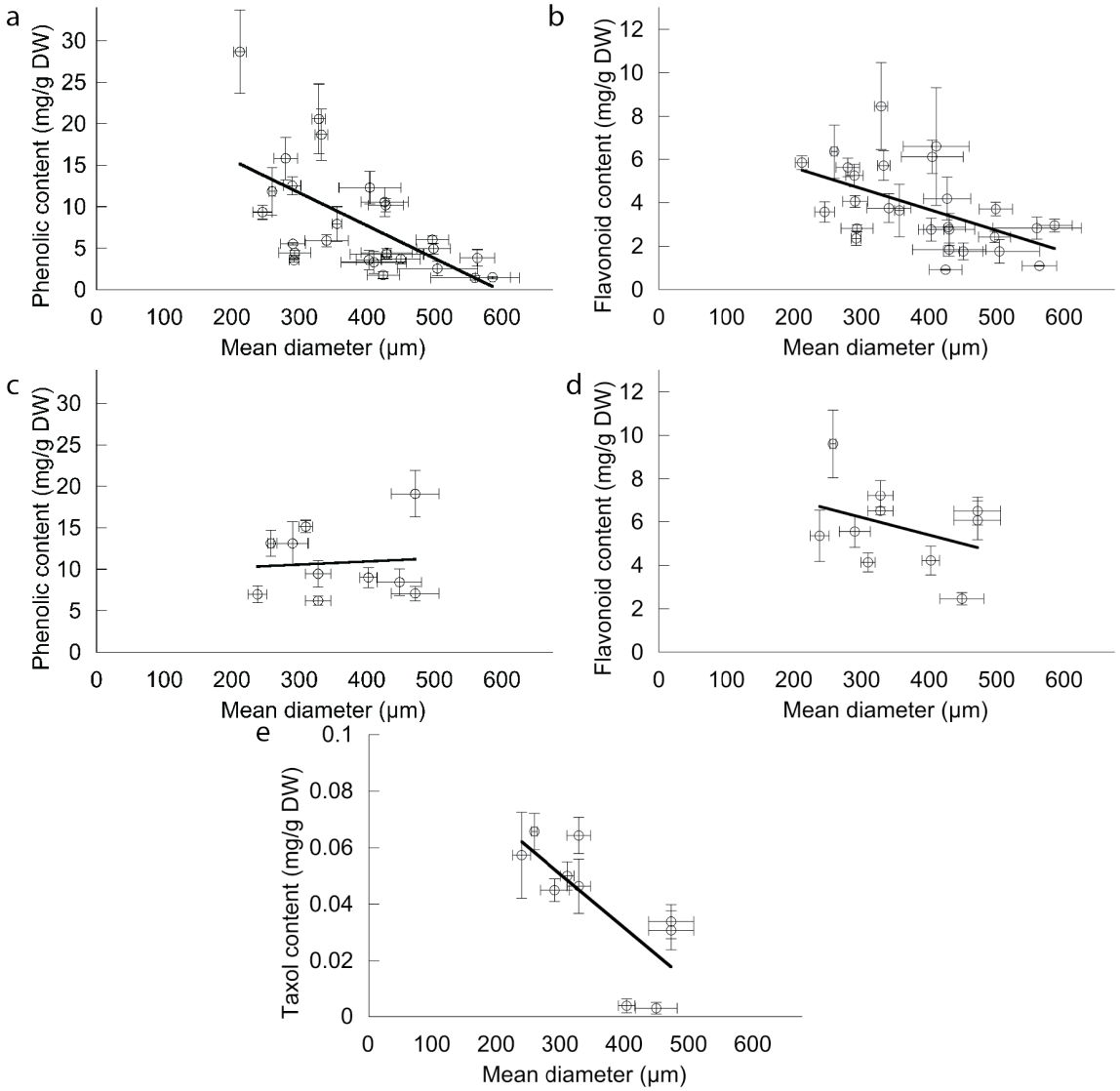

Figure 5.7. Correlation between mean aggregate size and the basal levels (a,b) and elicited levels (c,d,e) of phenolics (a,c), flavonoids (b,d) and paclitaxel (d) of the P93AF cell line. Relationships for the basal levels (a,b) were found to be statistically significant ($p < 0.05$) using the Pearson correlation coefficient for linear correlations with (A) n = 27, R = -0.614, critical value = -0.367 and (B) n = 27, R = -0.527, critical value = -0.367. Correlation between the elicited levels of phenolics (c) and flavonoids (d) and mean aggregate size were found to be insignificant using the Pearson correlation coefficient for linear correlations with (c) n = 10, R = 0.079, critical value = 0.576 and (d) n = 10, R = -0.364, critical value = -0.576. Correlation between the elicited paclitaxel content and the mean aggregate size was found to be statistically significant ($p < 0.05$) using the Pearson correlation coefficient for linear correlations with (e) n = 10, R = -0.742, critical value = -0.567.

The production of paclitaxel has been shown to negatively correlate with mean aggregate size of a *Taxus* culture (Patil et al., 2012; Patil et al., 2013), but only in an elicited state, which is confirmed here. Interesting, when the cultures were elicited with MJ, there was no correlation between the accumulation of phenolics and flavonoids and the mean aggregate size of the culture, as seen for P93AF in Figure 5.7c and d. Although the phenolic and flavonoid accumulation in response to MJ did not correlate to the mean aggregate size of the culture, the paclitaxel content was shown to exhibit a strong negative correlation (Figure 5.7e). Despite the correlations found between aggregate size and specialized metabolite accumulation in the paclitaxel-accumulating population, there were no trends found with the non-paclitaxel accumulating population. This could be because the mean aggregate size only varied between 520 and 800 μm for the non-paclitaxel population, as opposed to 420 to 1160 μm for the paclitaxel accumulating population.

5.4.2.4. Effect of aggregation on expression of key metabolic pathway genes

The transcriptomic data (presently unpublished) was mined to look at the effect of aggregation on gene expression of specialized metabolic pathways. The transcriptomic study produced gene expression datasets for small (mean diameter ~500 μm) and large (mean diameter ~ 1,000 μm) aggregates in an unelicited and elicited state both 18 and 72 hours after elicitation on day 7 (Lenka et al., Manuscript in progress.; Patil et al., 2014a). For unelicited cultures, this corresponds to a day 8 and a day 10 culture. The genes related to specialized metabolism with decreased expression levels in unelicited, large aggregate cultures can be seen in Table 5.2.

Table 5.2. Genes with decreased expression levels in unelicited, large aggregate cultures of the *Taxus* P93AF cell line.

18 hours		Fold difference
Contig number	Sequence description	(normalized)
65571	flavanone 3-hydroxylase	-3.74
90821	2-alpha-hydroxytaxane 2-o-benzoyltransferase	-3.23
19659	taxane 13-alpha hydroxylase	-3.17
139470	10-deacetylbaccatin iii-10-o-acetyl transferase	-2.98
116741	2-alpha-hydroxytaxane 2-o-benzoyltransferase	-2.93
92362	2-alpha-hydroxytaxane 2-o-benzoyltransferase	-2.58
36302	caffeic acid o-3-methyltransferase	-2.43
72 hours		Fold difference
Contig number	Sequence description	(normalized)
117154	chalcone synthase	-11.43
141549	chalcone synthase	-5.07
18122	chalcone isomerase	-4.90
117003	chalcone synthase	-4.38
65571	flavanone 3-hydroxylase	-3.90
141669	chalcone synthase	-3.33
116383	chalcone synthase	-3.33
109681	2-alpha-hydroxytaxane 2-o-benzoyltransferase	-2.80
19659	peroxidase 72	-2.74
116741	2-alpha-hydroxytaxane 2-o-benzoyltransferase	-2.16

The key pathways with lower levels of gene expression in unelicited, large aggregate cultures were diterpenoids, flavonoids and phenylpropanoids. In fact, chalcone synthase,

a key gene in the flavonoid biosynthetic pathway (Figure 5.2) had up to an 11-fold decrease in gene expression over the small aggregate cultures. This result is consistent with the specialized metabolite data presented earlier (Figure 5.7a,b), where cultures with a larger mean diameter had lower accumulation of phenolic and flavonoid compounds. The genes related to specialized metabolism that have higher levels of expression in unelicited, large aggregate cultures can be seen in Table 5.3.

Table 5.3. Genes with increased expression levels in unelicited, large aggregate cultures of the *Taxus* P93AF cell line.

Day 8 culture Contig number	Sequence description	Fold difference (normalized)
63242	phytoene synthase 2	2.08
95991	peroxidase 12	2.03
Day 10 culture Contig number	Sequence description	Fold difference (normalized)
63242	phytoene synthase 2	2.25

The key pathways that were upregulated in unelicited, large aggregate cultures were phenylpropanoids and carotenoids, with the peroxidase 12 that is associated with phenylpropanoids no longer differentially expressed in the day 10 culture.

Because elicitation has a large effect on specialized metabolism, the difference between small and large aggregate cultures in an elicited state becomes more complex. The genes related to specialized metabolism that have lower expression levels in large aggregate cultures can be seen in Table 5.4. Although these genes have lower expression levels in large, elicited cultures, a majority of the contigs are upregulated in response to MJ. Therefore, the fold-difference in expression in unelicited vs. elicited small and large cultures was also determined for each contig identified as differentially expressed in small vs. large elicited cultures.

Table 5.4. Genes with decreased expression levels in elicited, large aggregate cultures of the *Taxus* P93AF cell line. Additionally, the degree of upregulation of each contig in response to MJ elicitation in large and small aggregate cultures is identified. * indicates minimal levels of expression in an unelicited state.**

Lower expression in large aggregate, elicited cultures			Large, Upregulated with MJ		Small, Upregulated with MJ	
	Day 8 culture		**Day 8**	**Day 10**	**Day 8**	**Day 10**
Sequence description	Contig #	Fold difference	Fold difference	Fold difference	Fold difference	Fold difference
chalcone isomerase	18122	-2.81			2010.98	17.24
flavanone 3-hydroxylase	65571	-2.37	2.94			15.41
	Day 10 culture		**Day 8**	**Day 10**	**Day 8**	**Day 10**
Sequence description	Contig #	Fold difference	Fold difference	Fold difference	Fold difference	Fold difference
p-coumarate 3-hydroxylase	120868	-7.34			13.57	
taxane 13-alpha-hydroxylase	91441	-2.4	88.49	30.68	128.84	105.72
	93532	-2.04	***	15.02	***	262.09
	93580	-2.3	***	13.56	417.22	297.92
	114558	-2.09	720.30		***	502.99
	115650	-2.28	14.75		8.93	9.38
	116097	-2.41	1389.38	30.94	***	203.15
	116177	-2.06	11.73	5.38	7.43	7.81
	116422	-2.05	***	7.14	***	723.31
	117162	-2.09	278.91	4.34	***	1147.61
	125837	-2.02	51.54	27.95	51.87	56.45
	127442	-4.15		135.66		100.66
	127837	-3.8		47.13		113.49
	139497	-2.09	470.37	27.52	134.08	1085.87
	145821	-2.2	349.28	***	***	92.16
	149319	-3.51				***

	150590	-2.18	***	5.3	322.84	1334.64
taxadiene 5-alpha	92364	-2.65	355.24	8.08	671.14	307.2
hydroxylase	133694	-2.46	414.48	445.87	***	***
	116452	-2.45	159.89	106.51	***	128.47
	115314	-2.35	133.76	7.57	102.62	303.04
	116299	-2.18	***	18.75	***	347.3
	78204	-2.11	134.38	3.86	145.69	96.94
	116364	-2.08	330.07		371.53	308.62
2-alpha-hydroxytaxane 2-	109681	-2.45	26.94	132.01	12.2	8.96
o-benzoyltransferase	116032	-2.29	14.86	179.09	5.98	7.43
	92362	-2.06	4.27	6.93	2.89	4.21
	116741	-2.04	7.45	18.98	3.87	4.81
	90821	-2.01	5.44	6.73	2.79	3.9
taxoid 7-beta-hydroxylase	115327	-2.24	50.71	4.61	6.44	44.29
	115099	-2.13	24.34	1202.78	57.25	82.13
taxoid 2-alpha-	114222	-2.19	23.78	142.23	18.89	39.32
hydroxylase	117191	-2.13	13.15	3.48	10.18	24.2
taxadiene synthase	59384	-2.19	759.94		873.17	131.91
mac perforin domain						
containing protein	64550	-2.03				

On day 8, the only pathway with lower expression in elicited, large aggregate cultures is the flavonoid pathway. In fact, the chalcone isomerase contig 18122, which has 2.81-fold lower expression levels in large aggregate cultures, was not upregulated in response to MJ in cultures with large aggregates. Because the phenolic and flavonoid data were not collected until a week after elicitation, the effects of early differences in gene expression were likely not captured in the metabolite data. On day 10 (72 hours after elicitation with MJ), the diterpenoid and phenylpropanoid pathways have lower expression in large

aggregate cultures than in small aggregate cultures. The p-coumarate 3-hydroxylase contig, which has 7.34-fold lower expression levels in large aggregate cultures and is involved in lignin biosynthesis, is not upregulated after MJ elicitation in cultures with larger aggregate.

The day 10 transcript data show that several genes involved in paclitaxel biosynthesis were expressed at lower levels in large aggregate cultures, which supports the paclitaxel accumulation data, where large aggregate cultures accumulate lower levels of paclitaxel (Figure 5.7e). Despite the identified genes having lower expression levels in large aggregate cultures, all genes that are differentially expressed in small and large aggregate cultures (with the exception of the chalcone isomerase gene, the p-coumarate 3-hydroxylase and the mac perforin domain containing gene) are upregulated in response to MJ. For example, taxane 13-alpha-hydroxylase contig 91441 had 2.4-fold lower expression levels in large aggregate, elicited cultures when compared to small aggregate, elicited cultures. Despite this observation, the gene was upregulated in large aggregated cultures by 88.49 fold in day 8 cultures, and 30.68 fold in day 10 cultures in response to MJ elicitation.

The pathways that had higher expression levels in elicited, large aggregate cultures can be seen in Table 5.5.

Table 5.5. Genes with increased expression levels in elicited, large aggregate cultures of the *Taxus* P93AF cell line, as well as the degree of upregulation of each contig in response to MJ elicitation in large and small aggregate cultures.

Higher expression in large aggregate, elicited cultures			Large, Downregulated with MJ		Small, Upregulated with MJ	
		Day 8 culture	**Day 8**	**Day 10**	**Day 8**	**Day 10**
Sequence description	Contig #	Fold difference	Fold difference	Fold difference	Fold difference	Fold difference

peroxidase 25	14070	2.70	-2.11		-4.57	
taxane 13-alpha hydroxylase	117036	2.58	97.49	18.30	14.04	49.30
peroxidase 12	95996	2.54	4.23			
taxadiene 5-alpha hydroxylase	113816	2.32		***		3.24

		Day 8 culture	**Day 8**	**Day 10**	**Day 8**	**Day 10**
Sequence description	Contig #	Fold difference	Fold difference	Fold difference	Fold difference	Fold difference
peroxidase 25	14070	5.70	-2.11		-4.57	
cinnamate 4-hydroxylase	114388	3.14	1112.17	39.37	4875.52	56.29
taxadiene 5-alpha hydroxylase	113383	3.00	538.36	5.88	***	307.48
	134507	2.92	4958.29	161.81	2347.35	48.53
cationic peroxidase 1	114398	2.92	1361.07	2.77	4590.04	64.26
Chalcone synthase	91644	2.82	1687.55	2.96	2950.80	80.70
Cytochrome P450 protein	90926	2.80	1774.61	5.10	3148.12	50.24
	93768	2.69	2.90	2.90	4.15	4.15
peroxidase 12	90730	2.64	2.12	148.81	3.08	
	99310	2.57			2.15	
	90973	2.33	2.30		3.14	
	97035	2.16	2.52		3.59	
	95991	2.16	2.98		6.98	
	94226	2.11	3.17		4.63	
10-deacetylbaccatin iii-10-o-acetyl transferase	147215	2.10	8.66	30.23	7.41	6.07
protein	94619	2.04	2.34		3.40	

In both day 8 and 10 cultures, genes involved in the diterpenoid and phenylpropanoid pathways were upregulated in large aggregate cultures. Additionally, cinnamate 4-

hydroxylase and chalcone synthase, key genes in the phenylpropanoid and flavonoid pathway, respectively, were upregulated 3-fold in large aggregate cultures. The taxane 13-alpha-hydroxylase and taxadiene 5-alpha hydroxylase genes that were upregulated in large aggregate cultures are also shown in the down-regulated table, which indicates that there are many homologs of this gene present in *Taxus* cultures, which is common in plant systems (Lyons and Freeling, 2008). Again, nearly all genes found differentially expressed in large and small aggregate cultures were affected by MJ elicitation, with the exception of the peroxidase 12 contig 91996, which was not upregulated in small aggregate cultures.

5.5. Discussion

Plants produce thousands of specialized metabolites as part of an innate defense response. Due to the complexity of the compounds being produced, metabolomic studies are expensive and annotation of specific metabolites is difficult due to a lack of reliable standard compounds. In this study, methods were developed to examine flux through specific specialized metabolic pathways that are active in *Taxus* metabolism. The assays were chosen based on the results of a transcriptome level study, where transcripts from the paclitaxel, phenylpropanoid and flavonoid pathways were found to be upregulated in response to MJ elicitation (Figure 5.2).

5.5.1. Effect of MJ on paclitaxel and non-paclitaxel accumulating cultures

Through these assays, it was determined that paclitaxel accumulating cultures exhibit growth inhibition in response to MJ (Figure 5.3a). Growth inhibition indicates a shift from conserved towards specialized metabolism (Yang et al., 2012). This trend has been seen previously with paclitaxel accumulating cultures, where elicitation results in

reduced growth through inhibition of progression through the cell cycle (Patil et al., 2014a). Those cultures that were unable to produce paclitaxel exhibited no growth inhibition, which could indicate the inability of these cultures to reprogram metabolism after elicitation. Additionally, the concentrations of phenolic and flavonoid compounds increased after MJ elicitation in those cultures that are able to accumulate paclitaxel, but not in those that could not accumulate paclitaxel (Figure 5.3b,c).

MJ has been shown to upregulate transcripts involved in lignin biosynthesis in both *Arabidopsis* tissue samples (Pauwels et al., 2008) and *Vinis vinifera* cell culture (Martinez-Esteso et al., 2011). The production of lignin *in vitro* in both unelicited and elicited states has recently been reviewed (Karkonen and Koutaniemi, 2010). Interestingly, all *Taxus* cultures were found to increase the accumulation of lignin in response to MJ elicitation (Figure 5.3d,e). In the cell line CO93D (non-paclitaxel accumulating), it appears that smaller aggregate cultures accumulated higher levels of lignin (Figure 5.3e). This could be confirmed through the quantitative analysis of lignin content using an acetyl-bromide assay (Chang et al., 2008). Both cell wall associated lignin and extracellular lignin can be produced in cell culture (Karkonen and Koutaniemi, 2010). Although it is hypothesized that the lignin produced in these cultures is cell wall associated (due to staining and a lack of precipitant in the cell culture medium), additional studies with *Taxus* would have to be performed to confirm this hypothesis. Since lignin does not accumulate in unelicited cultures, silencing of the lignin biosynthetic pathway would be a viable option for increasing flux towards paclitaxel without affecting the health of the cultures.

5.5.2. Long-term variability of *Taxus* suspension cultures

The long-term study on a non-paclitaxel accumulating and a paclitaxel accumulating cell line provided insight into the extreme variability associated with plant cell culture systems. Whereas the growth of both the paclitaxel and non-paclitaxel accumulating cultures was stable throughout the 9 generations of growth studied (Figure 5.4a,b), the aggregation dynamics of the cultures varied dramatically throughout the culturing period (Figure 5.4c,d). The cause of changes in aggregation has yet to be elucidated in plant cell culture systems, but the effect on specialized metabolite accumulation makes this an important factor to consider when characterizing and designing a culture production system.

Results from this study the long-term specialized metabolite study support the result from non-paclitaxel and paclitaxel accumulating cultures, where cultures that are able to produce paclitaxel exhibit growth inhibition after the addition of MJ. Interestingly, the non-paclitaxel accumulating culture exhibited growth inhibition in one generation; however, production of specialized metabolic compounds were not highly upregulated. Based on this result, it would be interesting to examine the mechanism of MJ elicitation in the non-paclitaxel accumulating culture. Elicitation can lead to the production of specialized metabolites or lead cells towards apoptosis (Kim et al., 2005). Although studies on paclitaxel-accumulating *Taxus* cell cultures have shown that cells are not undergoing apoptosis (Patil et al., 2014a), no studies have been performed on cultures that are unable to produce paclitaxel. For cultures that exhibit growth inhibition without the accumulation of other metabolites, it could be possible that cells are undergoing apoptosis.

Similar to the previous study, the basal levels of phenolics and flavonoids were higher in the non-paclitaxel accumulating cultures than in the paclitaxel accumulating cultures. Paclitaxel-accumulating cultures exhibited increased levels of these compounds in response to MJ, whereas non-paclitaxel accumulating cultures showed no increase. This result indicates that specialized metabolic pathways are active in both paclitaxel-accumulating and non-paclitaxel-accumulating cultures, but there is a difference in the reprogramming of metabolism after MJ elicitation. As mentioned previously, the method for elicitation has not been optimized for all of the cell types being used in this study. Therefore, further studies could vary the concentration or type of elicitors to determine the appropriate levels for each cell line. With proper elicitation strategies, paclitaxel accumulation could potentially be obtained in cultures that typically do not accumulate paclitaxel in response to standard MJ elicitation protocols.

5.5.3. Paclitaxel accumulation does not correlate with growth inhibition or the production of other specialized metabolites

One of the most interesting results from this study was the lack of paclitaxel in the seventh generation for the paclitaxel-accumulating cell culture (Table 5.1). This culture showed similar levels of growth inhibition after MJ elicitation to generations 3, 5 and 9 (Figure 5.6b). Additionally, phenolics were increased 2-fold and flavonoids were not significantly increased in the seventh generation of growth, as opposed to up to 8-fold increased accumulation for phenolics and 3-fold increased accumulation for flavonoids in the 2 previous elicited generations (Figure 5.6f,h). Although this result may seem to indicate that the production of phenolics and flavonoids is tied to the production of paclitaxel, the ninth generation of growth contradicts this hypothesis. In the ninth

generation, the accumulation of both phenolics and flavonoids are not significantly increased after elicitation, but the production of paclitaxel is recovered back to the levels seen in generations 1, 3 and 5 (Figure 5.6f,h, Table 5.1). This result indicates that paclitaxel accumulation cannot be clearly correlated to growth inhibition or production of phenolic or flavonoid compounds.

5.5.4. Aggregate size dependence of basal and elicited metabolite accumulation is supported by transcriptome data

Finally, the basal accumulation levels of phenolics and flavonoids were tied closely to the aggregation of both cell lines studied in this experiment (Figure 5.7). As the aggregate size of the cultures increased, the phenolic and flavonoid contents decreased. Additionally, although the increased accumulation of phenolic and flavonoids in response to MJ was not affected by culture aggregation, the increased accumulation of paclitaxel was found to be aggregation dependent. As supported by previous studies (Kolewe et al., 2011a; Lenka et al., Manuscript in progress.; Patil et al., 2012; Patil et al., 2013), smaller aggregate cultures accumulate higher levels of paclitaxel. These data are supported by transcriptome data, where unelicited cultures with larger aggregates had lower levels of expression for genes related to flavonoid and phenylpropanoid biosynthesis than unelicited cultures with smaller aggregates. Additionally, genes related to paclitaxel biosynthesis had lower expression levels in elicited, larger aggregate cultures than in elicited, smaller aggregate cultures.

In an elicited state, there were some differences in phenylpropanoid and flavonoid gene expression between small and large aggregate cultures, mainly with respect to those genes involved in lignin biosynthesis (e.g., cinnamate 4-hydroxylase, chalcone synthase,

p-coumarate 3-hydroxylase and chalcone isomerase). Despite this result, there were no differences in phenolics and flavonoid content between elicited small and large aggregate cultures. This could be because production of these compounds is not solely regulated by gene expression, as was previously seen with the effect of paclitaxel biosynthetic gene expression on paclitaxel accumulation in *Taxus* cultures (Patil et al., 2012). Additionally, the phenolics and flavonoids assays consider only methanol soluble compounds. Therefore, the presence of cell-associated compounds, such as lignins, will not contribute to the measurements in these assays. Because unelicited cultures do not accumulate lignin (Figure 5.3), phenolic and flavonoid measurements in an unelicited state would likely be more representative of the culture properties. Qualitative data suggests that lignin accumulation is dependent on aggregate size (Figure 5.3e). Therefore, key differences in metabolite accumulation (as suggested by the transcriptome data) could be seen if cell-associated compounds were accounted for. For instance, the use of a quantitative lignin assay would allow for the measurement of cell-associated lignins within the sample.

5.6. Conclusion

From these studies, we were able to gain insight into the complex metabolism of *Taxus* cultures in both paclitaxel-accumulating and non-paclitaxel accumulating cultures, as well as in unelicited and elicited states. This is one of the first studies to look into the metabolism of non-paclitaxel accumulating cultures and provides interesting insight into the ability of these cultures to support paclitaxel production in the future. For instance, although these cultures were unable to produce paclitaxel, they were able to shift metabolism towards the production of lignins in response to MJ without negatively affecting culture growth. If the paclitaxel biosynthetic pathway were to be activated in

these cultures, it could be possible to shift metabolism towards paclitaxel production while maintaining culture growth, potentially improving overall culture performance.

In paclitaxel accumulating cultures, the production of basal levels of phenolics and flavonoids was found to be size dependent, whereas the elicited levels of these compounds was size independent. These data were supported by transcript data for this paclitaxel-accumulating cell line. The link between aggregation and specialized metabolite production has not been fully elucidated and it is still unknown whether or not aggregation has a direct effect on metabolite production or if changes in cellular metabolism simultaneously affect both specialized metabolite production and aggregation. Perhaps the most interesting conclusion from this study was that the production of paclitaxel could not be directly correlated to growth inhibition or the production of phenolics of flavonoids. This result highlights the complexity of plant specialized metabolism and indicates that product accumulation could be linked to compound specific regulators in addition to the global regulators of specialized metabolism.

CHAPTER 6.

INTRACELLULAR ENGINEERING: DEVELOPMENT OF AN *AGROBACTERIUM*-MEDIATED TRANSFORMATION METHOD FOR *TAXUS* SUSPENSION CULTURES

6.1. Collaborators

Joyce Van Eck, Associate Professor, Boyce Thompson Institute for Plant Research

Patricia Keen, Research Technician, Boyce Thompson Institute for Plant Research

Nicole Raia, B.S. Chemical Engineering, University of Massachusetts

6.2. Abstract

The FDA approved anti-cancer compound paclitaxel is currently produced commercially through the use of *Taxus* plant cell suspension cultures. One major limitation to the use of plant cell cultures as a production platform is the low and variable product yields, Therefore, methods to increase and stabilize paclitaxel production are necessary to ensure product security, especially as the demand for paclitaxel continues to rise. Although a stable transformation method for *Taxus* suspension cultures has been developed, stable transformant yields were low (around 1% of experiments) and the method was unable to be translated to the *Taxus cuspidata* and *Taxus canadensis* cell lines used in this study. Therefore, a new method for *Agrobacterium*-mediated transformation of *Taxus* callus and suspension cultures was developed through identification of the optimal *Agrobacterium* strain, inclusion of a modified antioxidant cocktail and increased recovery time for cells after transfection. With the established method, over 200 stably transformed *Taxus* cultures were recovered from both callus and suspension cultures of multiple *Taxus* cell lines. Additionally, two transgenic lines have

been maintained with stable transgene expression for over five years. This method represents an improvement over existing transformation methods for *Taxus* cultures and can be used for metabolic engineering for improved paclitaxel production.

6.3. Background and motivation

Plants produce a vast source of diverse chemical compounds with many commercial applications including fragrances, flavors, dyes, pesticides and pharmaceuticals. Between 1960 and 1982, the United States Department of Agriculture, in agreement with the National Cancer Institute, led the collection and screening of plant-derived compounds for anti-cancer activity (Cragg and Newman, 2009). During this search, paclitaxel, a compound found in the bark of *Taxus brevifolia*, was discovered. Currently, paclitaxel is FDA approved for the treatment of breast, lung and ovarian cancers, as well as AIDS-related Kaposi's sarcoma (Vongpaseuth and Roberts, 2007). Additionally, paclitaxel based treatments are being developed for further forms of cancer, Alzheimer's disease post-heart surgery patients, skin disorders, renal and hepatic fibrosis, limb salvage and inflammation (Vongpaseuth and Roberts, 2007; Zhang et al., 2014). Initially, the commercial supply of paclitaxel was obtained via harvesting bark of the Pacific yew tree, but this process was limited due to the slow growth rate of the tree, low product yields and species availability. As a result, alternative methods of supply including total synthesis, semi-synthesis and plant cell culture have been developed (Wilson and Roberts, 2012). In 2002, Bristol-Myers Squibb switched from semi-synthesis to plant cell culture production methods for Taxol®, making paclitaxel one of the few commercial products in the world supplied through plant cell culture technology (Mountford, 2010).

Although paclitaxel production through plant cell culture is sustainable, plant cell production systems are limited by low and variable product yields, making the use of engineering strategies to optimize production desirable (Wilson et al., 2014a). To allow for metabolic engineering of *Taxus* plant cell suspension cultures (the current culture format used for paclitaxel synthesis at scale), reliable stable gene transfer methods must be developed and readily available. The first report of a stable transformation method for *Taxus* suspension cultures used *Agrobacterium rhizogenes* ATCC 15834 containing the binary vector pCAMBIA 1301 and *Agrobacterium tumefaciens* EHA105 containing the binary vector 1305.2 to transform *Taxus cuspidata* cell lines (Ketchum et al., 2007). In addition, *Taxus chinensis* cultures were transformed with *A. rhizogenes* 25818 containing the vector pCAMBIA 1301 (Ketchum et al., 2007). Although multiple stably transformed *Taxus* cell suspension lines were achieved and maintained for at least nine months, only 1% of experiments yielded a stably transformed transgenic cell line, limiting the utility of the method. A modified version of this protocol was developed and applied in metabolic engineering experiments to upregulate 10-deacetylbaccatin III-10 β-*O*-acetyltransferase (DBAT), a key step in paclitaxel biosynthesis, in suspension cultures of *T. chinensis*, which resulted in a 1.7 fold increase in paclitaxel production (Zhang et al., 2011). Additionally, modified methods have been used for: 1) upregulation of 9-cis-epoxycarotenoid dioxygenase (a gene involved in the regulation of abscisic acid biosynthesis) (Li et al., 2012a), 2) upregulation of neutral/alkaline invertase (a gene involved in sucrose hydrolysis) (Dong et al., 2015), 3) down-regulation of 14 β-hydroxylase (Li et al., 2011), and 4) characterization of a WRKY-transcription factor

involved in the regulation of paclitaxel biosynthetic pathway genes, including DBAT (Li et al., 2013b).

While these reports provide the first methods for *Taxus* transformation and metabolic engineering, a higher efficiency protocol is necessary for high-throughput gene expression studies to facilitate optimized metabolic engineering for enhanced paclitaxel production. Here, we report on factors found to enhance the recovery of stable transgenic lines of *Taxus* including the *Agrobacterium* strain, modification of an antioxidant cocktail and recovery time after transformation, which allowed for development of a method that is consistent and highly efficient.

6.4. Materials and methods

6.4.1. Suspension and callus cultures

Taxus suspension cultures established from embryo-derived callus were obtained from Dr. Donna Gibson's group at the USDA/ARS, Ithaca, NY. Three cultures (P991C, PO93X, P093XC, P93AF) were derived from *T. cuspidata* and one culture (C093D) was established from *T. canadensis*. Suspension cultures were maintained and sub-cultured on a bi-weekly basis in Gamborg B5 (Phytotechnology Laboratories, Shawnee Mission, KS) medium with the antioxidants ascorbic acid, citric acid and L-glutamine (referred to here as standard medium, or SM) as previously described (Kolewe et al., 2011a). To create callus cultures, suspension cultures were filtered through Miracloth© (EMD Millipore, Billerica, Ma) over a buchner funnel and vacuum was pulled for approximately five seconds to remove cell culture medium. Approximately 0.5 g of cells were then transferred to individual calli on solid medium consisting of SM with the addition of 4 g/L Gelzan (Phytotechnology Laboratories). Approximately 6-8 calli were evenly

distributed across each plate. Callus cultures were maintained in the dark at 24 ^{o}C and subcultured monthly by transferring approximately 0.5 g of cells to form each new callus. All chemicals were purchased through Sigma-Aldrich Co. (St. Louis, MO) unless otherwise noted.

6.4.2. Bacterial strains and binary vector

Initial transformation efforts were started using the methods found in (Ketchum et al., 2007). From preliminary results that yielded no successful transformants (data not shown), modifications were implemented to the reported methods for enhanced transformation efficiency and recovery of transgenic material. Four *Agrobacterium tumefaciens* strains (C58C1, EHA105, GV3101, LBA4404) were tested that contained the pCAMBIA1301 vector (http://www.cambia.org/daisy/cambia/585.html). This vector contains the hygromycin phosphotransferase II gene (hptII) as the plant selectable marker driven by the Cauliflower Mosaic Virus 35S (CaMV35S) promoter and the beta-glucuronidase (GUS) gene driven by the CaMV35S promoter. Two days prior to initiation of transformation experiments, the *Agrobacterium* selected for each experiment was streaked onto LB medium containing 50 μg/mL kanamycin and the appropriate antibiotics for the *Agrobacterium* strain (10 mg/L tetracycline for C58C1, 15 mg/L rifampicin for EHA105, 30 mg/L gentamycin for GV3101 and 15 mg/L rifampicin for LBA4404) and maintained in the dark at 28 ^{o}C. A single colony was selected to initiate an overnight culture in YEP (10 g yeast extract, 10 g Bacto peptone, 5 g NaCl per liter) containing the appropriate antibiotics and placed in an orbital shaker incubator at 250 rpm and 28 ^{o}C until the OD_{600} was approximately 0.6. Acetosyringone was added to the culture at a final concentration of 200 μM 30 minutes prior to infection. The

Agrobacterium culture was spun down, medium removed, and resultant pellet resuspended in standard medium (SM), as previously defined. For some experiments, the standard antioxidant mixture of ascorbic acid, citric acid and L-glutamine was replaced with an alternative antioxidant mixture of 5 mg/L silver nitrate, 40 mg/L cysteine and 20 mg/L ascorbic acid.

6.4.3. Effect of cefotaxime and hygromycin on callus cultures

Cells from one *T. canadensis* cell line (CO93D) and four *T. cuspidata* cell lines (P93AF, PO93X, PO93XC and P991C) were plated on SM containing 4 g/L gelzan and either 300 mg/L of cefotaxime or 300 mg/L of cefotaxime and 10 mg/L of hygromycin. About 0.1 g of cells were plated as individual calli, with approximately 15 calli per 150 mm x 15 mm petri plate. Images of the plates were taken once a week for three weeks using a gel-electrophoresis UV light box and GeneSnap software. Using ImageJ software, two-dimensional area analysis was performed. This involved tracing the outline of each callus on the plate, measuring the area, and normalizing the area to week 0 cultures (Figure 6.1).

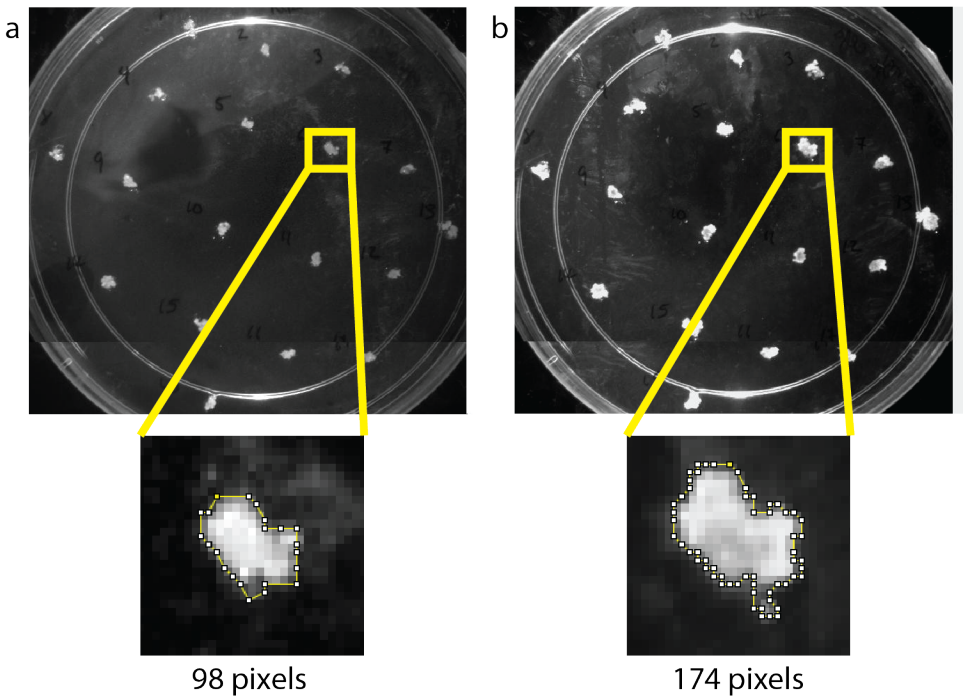

Figure 6.1. ImageJ Two-Dimensional Area Analysis. Images of the week 0 (a) and week 3 (b) callus plates are uploaded to ImageJ software. Each callus is traced using the freehand selection tool and then measured to determine its area. This area is then normalized to the area of the callus at week 0 to determine the fraction of callus growth.

6.4.4. Transformation of *Taxus* suspension and callus cultures

Suspension cultures were transferred to fresh SM seven days prior to infection. For each transformation experiment, cultures were abraded by drawing the culture up and down 15 times through a wide-bore ten mL pipet. Cells were allowed to settle and culture medium was removed and replaced with SM containing the resuspended *Agrobacterium* pellet (described above). The entire solution was transferred to the flask containing the remaining suspension culture and incubated in the dark at 24 ^{o}C for 24 hr shaking at 125 rpm.

The media containing *Agrobacterium* was then removed and cells were washed by resuspending cultures in 50 mL of SM containing 300 mg/L cefotaxime. Cells were

agitated for 15 min at 125 rpm at 24 ^{o}C. The wash was repeated three additional times. To improve recovery after transformation, a modified antioxidant solution containing 5 mg/mL silver nitrate, 40 mg/mL cysteine, 20 mg/mL ascorbic acid and 300 mg/L was used. Washed cells (approximately 1 – 2 mL) were plated onto each of six 150 mm x 15 mm petri plates containing solid SM (4 g/L gelzan) supplemented with 300 mg/L cefotaxime. Plates were wrapped with Nescofilm (Fisher Scientific, Pittsburgh, Pa) and maintained in the dark at 24 ^{o}C. After new calli growth was observed on the plates (approximately 4-8 weeks post-transformation), growing calli were individually selected and transferred to selective solidified SM that contained 10 mg/L hygromycin with 300 mg/L cefotaxime. Each transgenic event was then maintained as a separate callus by bi-monthly transferring of approximately 0.5 g of biomass to a new petri dish containing solidified SM media with 10 mg/L hygromycin and 300 mg/L cefotaxime. All callus cultures were maintained in the dark at 24 ^{o}C.

For *Agrobacterium* infection of callus, three week-old callus was divided into approximately three mm sections one week prior to infection. Immediately before infection, calli received a desiccation treatment by removing the lids from the Petri plates and allowing cultures to remain open in a laminar flow hood for 15 min. Approximately 45 calli were transferred to a 15 mL Falcon tube then covered with an excess of *Agrobacterium* resuspended in SM media and incubated for five minutes at 24 ^{o}C and 125 rpm. The inoculation medium was removed with a 10 mL sterological pipet and calli were transferred to petri plates (100 mm x 15 mm) containing sterile 7 cm Whatman filter paper (Fisher Scientific). The plates were wrapped with Nescofilm and incubated in the dark at 24 ^{o}C for three days. Calli were then transferred to solid SM containing

cefotaxime (300 mg/L). After growth was observed (approximately 4-8 weeks after co-incubation), the growing calli were transferred to solid media containing cefotaxime (300 mg/L) and hygromycin (10 mg/L). Cultures were stored in the dark at 24 ^{o}C and transferred biweekly to solid SM 300 mg/L cefotaxime and 10 mg/L hygromycin.

6.4.5. Histochemical GUS assays

Sections of actively growing calli were periodically assayed for GUS expression. A GUS assay solution consisting of 0.25 mL/mL of 1.6 mM K-ferri and K-ferro, 21.4 mg/mL sodium phosphate dibasic, 11.0 mg/mL monosodium phosphate, 0.5 µl/mL Triton X-100, 3 mg/mL EDTA, 0.8 mg/mL X-glucoronidase and 0.2 mL/mL methanol was created. Calli or washed cells from suspension were placed in separate wells of a 48-well plate and 0.5 mL of assay solution was added to each well. The calli were then vacuum infiltrated in a vacuum chamber for three hours and transferred to a 37 ^{o}C incubator overnight. After overnight incubation, the GUS assay solution was removed and replaced with 500 µl of 70% ethanol. If GUS expression was observed, the remainder of the calli was allowed to grow and designated as a transgenic line.

6.4.6. Analysis of growth, GUS expression and gene integration in transformed cultures after five years

Callus cultures from two transformation events produced through the *Agrobacterium*-mediated transformation of a PO93XC suspension culture were transferred monthly to solid SM media containing cefotaxime (300 mg/L) and hygromycin (10 mg/L) over a five-year period. Suspension cultures were initiated from callus cultures of the two transformed and one un-transformed control by resuspending 2.5 g of callus biomass into 50 mL of SM and 300 mg/L cefotaxime. Additionally, 10

mg/L hygromycin was added to the transformed cultures. Cultures were placed in an incubator at 125 rpm and 24 ^{o}C for one hour to allow the callus cells to disaggregate. To assist in disaggregation, cultures were then sheared 20 times by pipetting with a plastic 10 mL pipette. Cultures were grown for three weeks to increase biomass levels. After three weeks in culture, 10 mL of well-mixed culture was transferred to 40 mL of fresh media containing 300 mg/L cefotaxime (control and transformed cultures) and 10 mg/L hygromycin (transformed cultures). Culture growth and aggregation was monitored on day 0, 4, 7, 11 and 14 using a Beckmann Coulter Multisizer 3 (Kolewe et al., 2010). Genomic DNA was extracted from the cultures on day 7 using the method described in (Cenis, 1992). The primers used to confirm gene integration into the chromosome, as well as identify the original plasmid are shown in Table 6.1 (Shekhawat et al., 2008).

Table 6.1. Primers for confirmation of chromosomal integration (primers A and B) and plasmid identification (primers A and C).

Primer A	5’ AACAGGTATGGAATTTCGCCGATTT 3’
Primer B	5’ TTTATCCTAGTTTGCGCGCTATATTT 3’
Primer C	5’ CCTAGATCTCTTCGGTAATGAAAAA 3’

By using primers A and B, a 450 bp section of the β-glucoronidase gene can be amplified. Using primers A and C results in the amplification of a 1,585 bp section of the β-glucoronidase gene, as well as a region outside of the T-DNA section of the pCAMBIA1301 plasmid. These primer sets were used here to confirm integration of the β-glucoronidase gene into the chromosome of the *Taxus* cultures and a plasmid control (pCAMBIA1301 isolated from *Escherichia coli* strain DH5α) was used to confirm that the genomic samples were not contaminated with plasmid DNA (Shekhawat et al., 2008).

6.5. Results and discussion

6.5.1. Effect of hygromycin on callus cultures

The ability to recover stable transgenic lines can be affected not only by the type and concentration of selection agent, but also by the timing of transfer of infected material post cocultivation to selective medium. In preliminary transformation experiments, 2.5 mg/L hygromycin was used in selective SM based on the report by (Ketchum et al., 2007). However, over time, growth of the non-transformed controls of *T. cuspidata* and *T. canadensis* was observed, indicating that 2.5 mg/L hygromycin was not an effective concentration for selection of transformed cultures. The effect of higher concentrations of hygromycin (10 mg/L) on callus growth of *T. canadensis* cell line C093D and *T. cuspidata* cell lines P93AF, P093X, P093XC, and P991C was investigated (Figure 6.2).

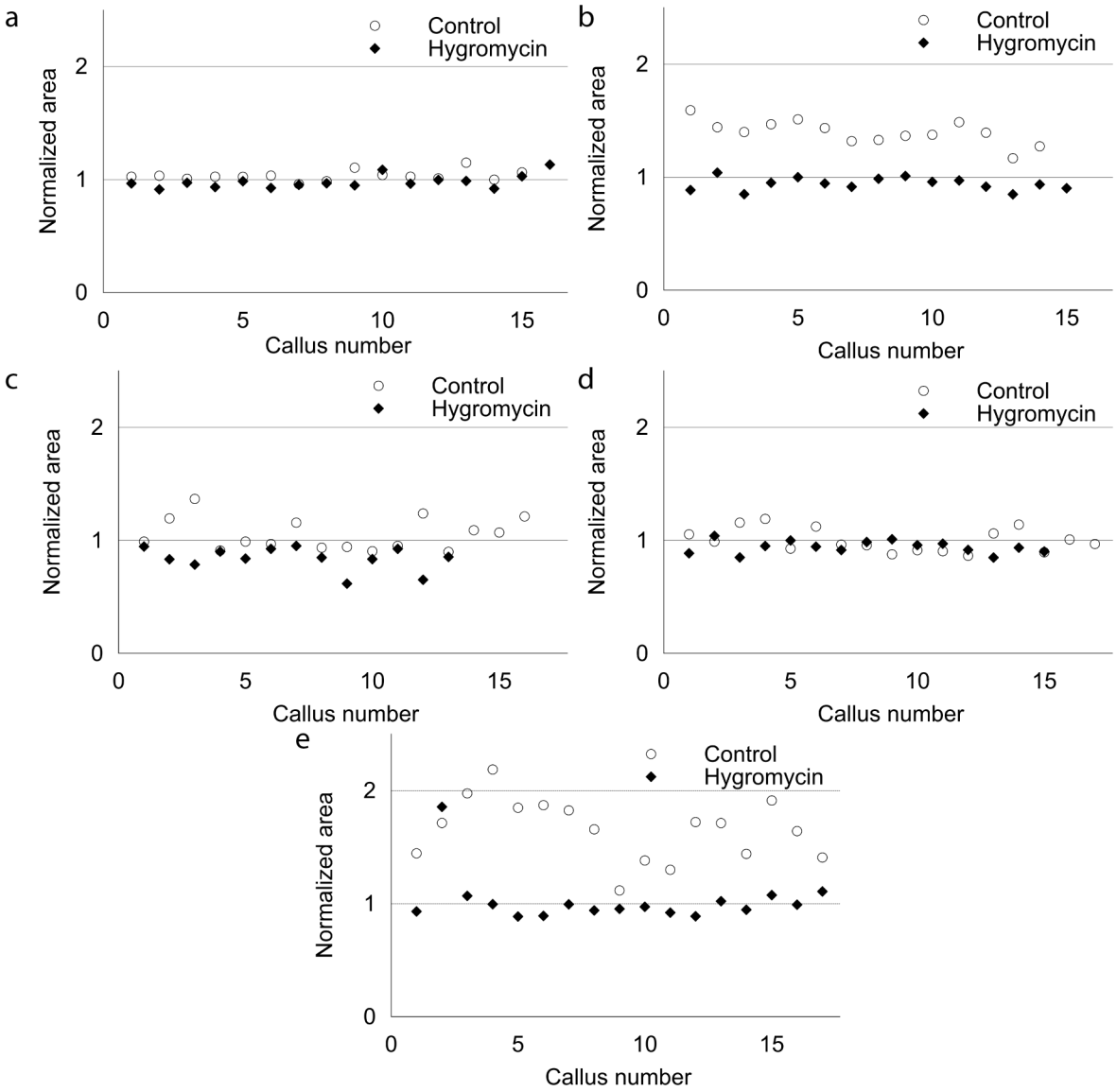

Figure 6.2. Effect of hygromycin on two-dimensional growth of callus cultures after three weeks in culture. C093D (a), P93AF (b), P991C (c), PO93X (d), and PO93XC (e) cells were placed on solid media containing either 300 mg/L cefotaxime (control) or 300 mg/L cefotaxime and 10 mg/L hygromycin (experimental). Samples were imaged once a week for three weeks. Two-dimensional area analysis using ImageJ allowed the determination of the fraction of growth for each calli in each sample. The area of each callus was normalized to day 0 data.

From the two-dimensional analysis of growth, hygromycin at a concentration of 10 mg/L effectively stopped the growth of all cell lines investigated. Although the

imaging measurement only analyzed growth in two dimensions, three-dimensional growth was only observed in those cultures with significant two-dimensional growth; hence two-dimensional growth analysis can be used as a direct indicator of overall culture growth. Because the CO93D and PO93X cultures had little growth on both the control and hygromycin media, these cell line should be repeated to ensure that 10 mg/L hygromycin is sufficient for stopping culture growth. Of the 17 PO93XC calli grown on hygromycin (Figure 6.2e), only one callus exhibited an increase in biomass area, indicating the ability to grow on the antibiotic medium. Because no additional escapes were found in the other cell lines analyzed, a concentration of 10 mg/L was deemed acceptable and used in all future experiments.

6.5.2. Effect of *Agrobacterium tumefaciens* strain

The type of *Agrobacterium* strain has been shown to have a significant effect on the successful transformation of various plant species including lentil and blueberry (Akcay et al., 2009; Song and Sink, 2004), which can be attributed to the pathogenicity of the strain to the host range of the strain. Four different *Agrobacterium tumefaciens* strains (C58C1, EHA105, GV3101, LBA4404) were evaluated to determine their effectiveness on the recovery of transgenic lines from cell cultures of *T. cuspidata* and *T. canadensis*. *Agrobacterium* strains EHA105 and C58C1 were found to be the best for recovery of transgenic lines.

6.5.3. Effect of antioxidants on the recovery of transgenic cell lines

Taxus suspension cultures are very sensitive to perturbations of the environmental conditions under which they are maintained. Infection with *Agrobacterium* resulted in stress on the *Taxus* cultures. Inclusion of a “cocktail” of silver nitrate, cysteine, and

ascorbic acid in the infection, cocultivation, and wash solutions was found to be key in the recovery of transgenic lines. This cocktail was also reported to be effective for rice transformation (Enríquez-Obregón et al., 1999).

6.5.4. Effect of transfer to selective media post cocultivation

It was found that delaying transfer of callus post cocultivation to hygromycin-containing SM until there were signs of growth had a significant effect on the recovery of transgenic cell lines. In early experiments, cells of the infected cultures were transferred to selective SM after a three-day cocultivation period; however, growth was never observed. After several failed experiments, the transfer to selective SM was delayed until the first signs of growth were observed on non-selective medium after the cocultivation period (typically between three and five weeks after cocultivation). As a result of this delay, growth was observed in the infected material, and cells were found to be positive for GUS expression (Figure 6.3).

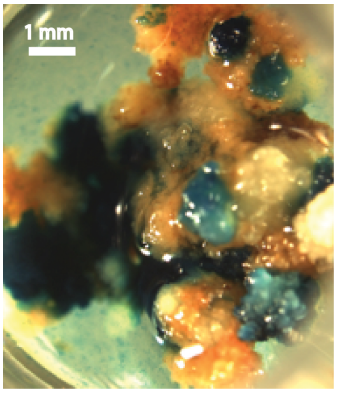

Figure 6.3. GUS expression in transformed cells from the *T. cuspidata* cell line PO93XC using the *Agrobacterium* strain EHA105. Image was taken after growth was recovered on non-selective medium (prior to moving cultures to selective medium).

The need for a delay could be attributed to the slow growth of *Taxus* cells (with doubling times ranging from 13-23 days under ideal conditions (Fettneto et al., 1994;

Hirasuna et al., 1996)), especially following infection with *Agrobacterium*. For effective plant cell growth, a critical culture density is required. Research has shown that cells below a critical density can undergo programmed cell death, which can be reversed through the addition of conditioned medium, indicating a necessity for signaling molecules in the medium (McCabe et al., 1997). After growth recovery on non-selective medium, calli contain large masses of GUS-positive cells, as seen in (Figure 6.3). To date, a total of 209 independent transgenic lines that were positive for GUS expression have been recovered from transformations of *T. cuspidata* line PO93XC.

6.5.5. Establishment of transgenic suspension cultures and long-term maintenance

After growth on selective medium for seven months, transformed cultures of *T. cuspidata* line PO93XC were transferred to suspension in liquid medium with 300 mg/L cefotaxime and 10 mg/L hygromycin. GUS expression was observed in all cells of the suspension culture, indicating stable GUS and hpt expression by the culture (Figure 6.4).

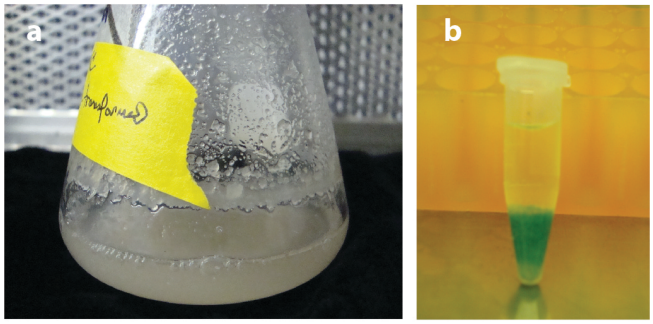

Figure 6.4. GUS expression in a suspension culture of a transformed *Taxus* culture.

Transformed cultures were maintained as callus on selective SM and transferred monthly over a period of three years. After five years, calli from two individually transgenic events were initiated into suspension. GUS expression was observed in all cells in both suspensions, indicating stable GUS and hpt expression (Figure 6.5).

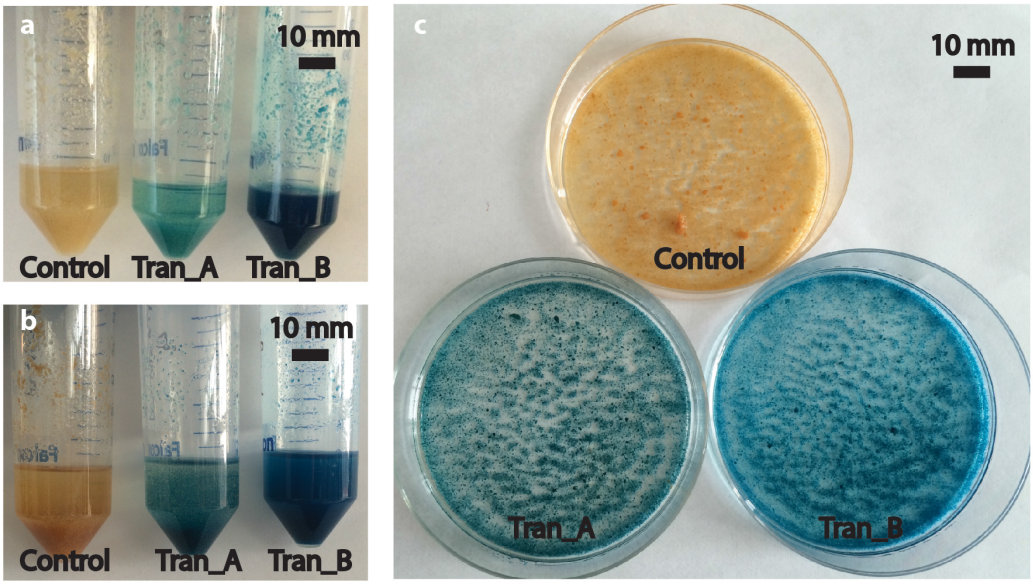

Figure 6.5. GUS expression in suspension cultures initiated from two individual transgenic events and one non-transformed control after three hours of vacuum infiltration (a), and overnight incubation in the GUS assay solution (b,c).

Interestingly, after three hours of vacuum infiltration in the GUS assay solution, a significantly higher level of GUS staining was observed in transgenic culture B as compared to transgenic culture A (Figure 6.5a). This result suggests differential levels of protein accumulation within the cultures. When performing an *Agrobacterium*-mediated transformation, the number of copies of the gene integrated into the genome cannot be controlled. Additionally, incorporation of the gene into a region of the chromosome that is hypermethylated can result in transcriptional gene silencing, decreasing the overall expression level of the gene (Vaucheret et al., 1998). For example, by specifically inserting a gene into different regions of the *Arabidopsis* chromosome, nearly a 10-fold difference in gene expression was observed and nearly 50% of transformants were affected by transgene silencing (Day et al., 2000). Despite differences in expression level between the cultures, all cells within both transformed cultures show high levels of GUS-

expression after 24-hours in the GUS assay solution (Figure 6.5b,c). This long-term stability of gene expression is crucial for development of stably genetically engineering *Taxus* cell lines for use in bioprocesses.

The growth and aggregation patterns of the two transgenic suspension cultures were monitored over a 14-day growth period (Figure 6.6).

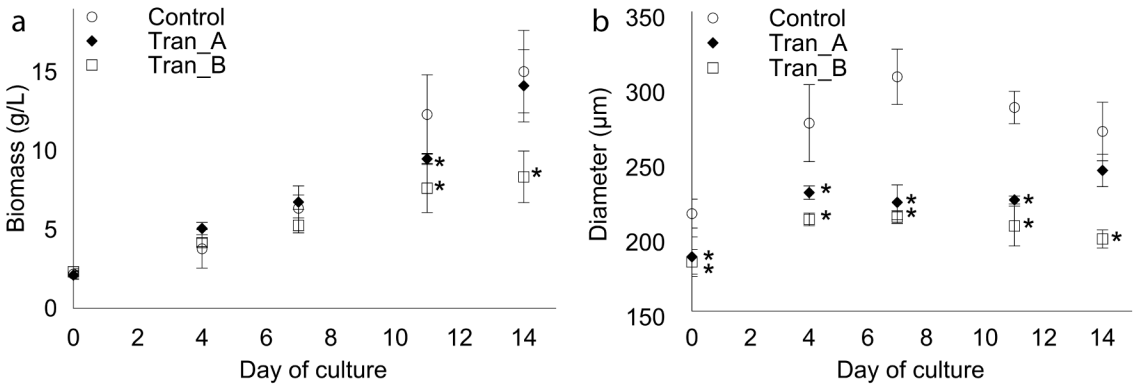

Figure 6.6. Growth of transformed cultures

The growth of transgenic culture A was identical to that of the control throughout the 14-day growth period. On the other hand, the growth of transgenic culture B was significantly lower than both the control and transgenic culture A. Additionally, the mean aggregate size of both transgenic cultures was significantly lower than the culture throughout the growth period. Aggregation in *Taxus* cultures is poorly understood, but has been shown to affect accumulation of specialized metabolites (Kolewe et al., 2011a; Patil et al., 2012; Patil et al., 2013). Differences in aggregate size between the control and transgenic culture could be due to inherent variability associated with the cultures or due to differences in cellular metabolism.

To confirm integration of the gene into the genome, PCR of the genomic DNA was performed (Figure 6.7).

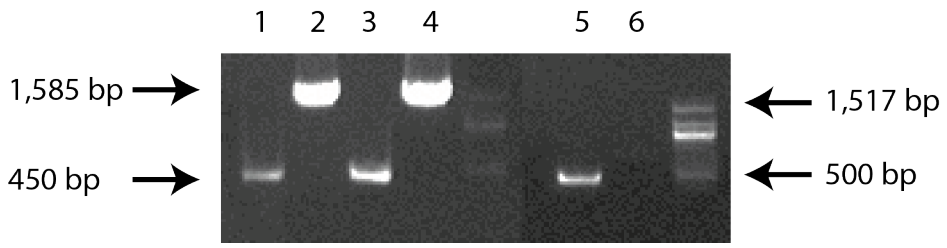

Figure 6.7. PCR of the control and transgenic from the PO93XC cultures, as well as plasmid DNA (pCAMBIA1301 isolated from *E. coli*). Lanes 1 and 2 show the plasmid DNA with primers A+B and A+C, respectively. Lanes 3 and 4 show a mixture of plasmid and transgenic culture B DNA with primers A+B and A+C, respectively. Lanes 5 and 6 show the transgenic culture B DNA with primers A+B and A+C, respectively.

Results from PCR show stable integration of the GUS gene into the genome of transgenic culture B, as indicated by the 450 bp product from PCR with primers A+B. The PCR also confirms that there is no plasmid DNA contamination due to the lack of a band in the PCR of transgenic culture B DNA with primers A+C. These results confirm the stable transformation of transgenic culture B for a five-year period.

6.6. Conclusion

One of the main limitations of the commercial application of plant cell culture is low and variable product yields. To successfully genetically engineer cultures for increased product yields, reliable and high-throughput stable transformation methods must be developed. Although a previous transformation method for *Taxus* suspension cultures has been developed, successful transformation was only achieved in 1% of experiments (Ketchum et al., 2007). Additionally, this method could not successfully translat to the *T. cuspidata* and *T. canadensis* cell lines used in this study. Here we present a new method for the transformation of *Taxus* suspension cultures, which included supplementation with an antioxidant cocktail and an increase in the recovery

time after transformation, enabling the recovery of over 200 stably transformed *Taxus* cell lines. Stable gene expression of the reporter beta-glucuronidase (GUS) gene was observed for over three years in culture. This consistent and highly efficient transformation method represents an improvement over existing *Taxus* suspension culture transformation methods and could be more easily translated to other *Taxus* cell culture lines to enable future metabolic engineering efforts.

CHAPTER 7.

CHARACTERIZATION AND ENGINEERING OF SOMATIC EMBRYOGENESIS CULTURES

7.1. Introduction

There is a critical need to develop technologies for the cultivation of high value plants to replenish supplies for forestry, agricultural, health and horticultural needs (i.e., combat deforestation, lumber, landscaping, lignocellulosic biofuel feedstocks, medicinal plants, etc.). Somatic embryogenesis (SE) is a promising platform for large-scale, commercial propagation due to its ability to create genetically identical seed populations, allowing for cloning of superior plants and ensuring product quality (Lelu-Walter et al., 2013). In the US, timber milling and logging is a $100 billion industry (Athey et al., 2011). This technology is ideal for meeting rapidly increasing acreage demands for commercial timber, such as the Loblolly pine, which currently occupies over 30 million acres in the U.S. and is projected to increase to 55 million acres by 2040 (Antony et al., 2011). Currently, commercial technologies are being developed using SE to create populations of conifer embryos with optimized phenotypes for growth and wood quality (Gupta and Hartle, 2015; Pullman et al., 2015). A major limitation to commercialization of this process is the significant variability in the yields of embryos that are able to germinate into successful seedlings. By establishing a greater understanding of both the growth dynamics and development of SE cultures on a fundamental level, a more consistent embryo and germination yield will be achieved, leading to a new, cost effective pathway for the production of manufactured seed.

Somatic embryogenesis is an asexual process through which non-embryogenic plant tissue develops into somatic embryos, which can then be germinated (Park, 2002). *In vitro*, SE takes place through three distinct phases of multiplication and development (Figure 7.1).

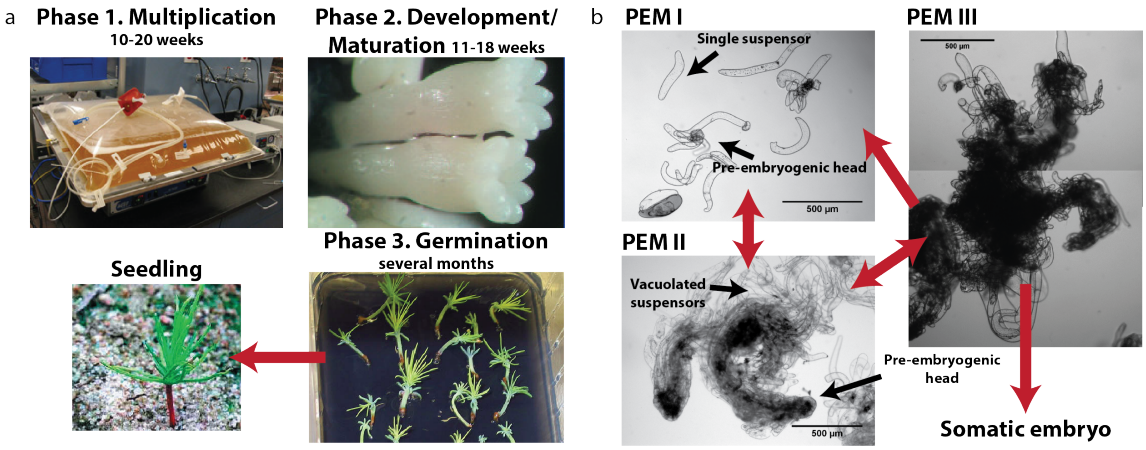

Figure 7.1. (a) Growth phases of somatic embryogenesis where cultures are multiplied in Phase 1 for 10-20 weeks, transferred to solid medium in Phase 2 for development and maturation (11-18 weeks) before germination in stage 3, which takes several months. (b) Hypothesized growth cycle of cell types within a multiplication culture (Filonova et al., 2000). PEM I's consist of a small pre-embryogenic head and filamentous tail of suspensor cells. These can develop to become PEM II's, which have a more developed pre-embryogenic head and complex tail of vacuoles. These can either separate to form additional PEM I's or become the more complex PEM III's. It is hypothesized that only PEM III's can develop into somatic embryos.

In the first phase, embryonic suspensor masses (ESM) are propagated in a multiplication culture, allowing for scale-up and multiplication from cryopreserved stock. Multiplication cultures contain two classes of cells: pre-embryogenic heads and the more vacuolated suspensors. In the second phase, cultures are transferred to a solid development medium, which initiates the transition from pre-embryogenic material into

somatic embryos. In the third phase, embryos are isolated and placed on specific medium to germinate. The key limitation for process optimization is the lack of fundamental knowledge regarding how cultures transition through each phase of development, leading to variable yields of germination competent embryos and severely inhibiting commercialization (Montalban et al., 2010).

Currently, somtic embryogenic culture success is evaluated at the end of the development stage (after 11-18 weeks) by quantifying the number of high quality embryos, as well as at the end of the germination stage (after several months) by determining the number of viable germinates. Through developing methods to predict culture success while in the multiplication stage of SE, the number of unsuccessful cultures propagated through the late stages of development can be minimized. A hypothesized growth cycle for specific cell types within the multiplication phase of *Picea abies* SE cultures has been proposed (Figure 7.1b) (Filonova et al., 2000). In this hypothesized growth cycle, pre-embryogenic masses (PEM) are characterized into three specific classes. PEM I's, which consist of a small pre-embryogenic head and a single filament of vacuolated cells, are hypothesized to develop into the more complex PEM II's. PEM II's contain a larger, more developed pre-embryogenic head and a complex tail of vacuolated cells. PEM II's can transition towards the more complex PEM III's or tissue can separate from the PEM II to form additional PEM I's. PEM III's are the most complex, containing larger masses of pre-embryogenic heads and vacuolated tissues. Again, tissue from the PEM III's can separate to form additional PEM I's and II's. Additionally, it is hypothesized that PEM III's are the only tissue type that have the

ability to differentiate into somatic embryo tissue, which can further develop into a mature embryo.

While this hypothesized growth cycle is a promising start for determining the ideal cell morphologies for a high embryo-yielding maintenance culture, it was developed through the isolation of specific cell types in an agarose gel (Filonova et al., 2000). By isolating tissue in an agarose gel, many of the important cell-cell interactions and singalling pathways are interrupted, which could affect cell development. Therefore, a method to study the different classes of PEM in culture could allow for a better understanding of the maintenance growth cycle and the capability of specific cell types to differentiate into somatic embryos. Because the 3 different types of PEM tissue have distinct morphologies, a method to characterize the morphology of tissue structures in a multiplication culture could allow for prediction of culture success by identifying the proportion of tissue representing each class of tissue. Here, a method to characterize the size of aggregates within an SE multiplication culture using a Coulter counter was developed. These methods were used to determine the morphology of four Loblolly pine SE genotypes. Additionally, eight cultures of a single genotype were followed through seven weeks of growth in the maintenance phase to provide insight into culture phenotypes. The method developed not only provided important information on the biomass density of cultures, but also allowed for characterization cellular morphology and is ready to be used to fully study any SE culture.

7.2. Materials and Methods

7.2.1. Loblolly Pine SE culture multiplication and sampling

Loblolly Pine SE cultures from six individual genotpypes (referred to as genotypes A-F) were maintained by an industry partner and well-mixed culture samples were shipped overnight in a cooler with ice packs for analysis at UMass. Cultures were received at UMass in 15, 50 or 500 mL sterile containers and stored at 4 °C until analysis. Storage at 4 °C for several days was shown to have a negligible effect on culture morphology as measured by the Coulter counter (data not shown).

7.2.2. Establishment of a Coulter counter method for aggregate size characterization

Aggregate size distributions and cellular biomass were measured for four unique genotypes (genotypes A-D) using a Multisizer 3™ Coulter counter equipped with a 560, 1,000 or 2,000 μm aperture (Beckman Coulter, Brea, CA), as previously described (Kolewe et al., 2010). For analysis on the 2,000 μm aperture, five replicate two mL samples were analyzed from each culture sample. For the 560 and 1,000 μm apertures, two replicate two mL samples were analyzed. Data were analyzed using a 7-point weighted moving average (WMA).

$$WMA(x_n) = \frac{1(x_{n-3}) + 2(x_{n-2}) + 3(x_{n-1}) + 4(n) + 3(x_{n+1}) + 2(x_{n+2}) + 1(x_{n+3})}{16}$$

where *n* is the number of the bin being analyzed and *x* is the number of particles in that bin. Due to the limited number of counts obtained in analysis of samples with a large particle size, the weighted moving average is used to obtain a more representative

aggregate size distribution (Kolewe et al., 2010). Microscope images of cultures were obtained using an inverted microscope (Olympus, Center valley, PA).

7.2.3. Size fractionation

Cultures of genotype A were filtered using nylon mesh or polypropylene mesh as previously described (Kolewe et al., 2010). In short, cells were poured over the nylon mesh and biomass was washed through the filter using a wash solution of Gamborg B5 basal medium. The biomass remaining on the filter after a minimum of two wash steps was backwashed with Gamborg B5 medium into a beaker for analysis.

7.2.4. Biomass correlation

A mixed culture of genotype E was separated into six size fractions by filtering the culture over seven nylon mesh or polypropylene filters. The nylon mesh sizes employed were 300, 500, 710, 1,000, 1,320, 1,680 and 2,000 μm in diameter, to create bins containing aggregate sizes 300-500 μm, 500-710 μm, 710-1,000 μm, 1,000-1320 μm, 1,320-1,680 μm and 1,680-2,000 μm. Each fraction was diluted 2-fold two times to create a total of three biomass concentrations. After the dilutions were created, all of the fractions and dilutions were analyzed on the Coulter counter by taking four replicate two mL samples. Additionally, three dry weight measurements were taken for each fraction and dilution by pipetting 20 mL of culture over filter paper in a vacuum flask. A vacuum was pulled on the sample for approximately five seconds and the filter paper was placed in an oven at 50 °C overnight. The remaining biomass weight was recorded as the dry weight.

7.2.5. Long-term characterization of biomass

Eight cultures of a single genotype (genotype F) were maintained at an industry partner over a 7-week period. Four individual treatments were applied to the cultures, with two replicate cultures of each treatment. Fifty mLs of well-mixed culture samples were collected bi-weekly and sent to UMass for size characterization at week 3, week 5 and week 7 of the experiment. During the first week of sampling, 12 replicate two mL samples from each culture were run on the Coulter counter. For the third and fifth week of sampling, six replicate two mL samples were analyzed on the Coulter counter.

7.3. Results

7.3.1. Coulter counter analysis of Loblolly Pine SE cultures

A Coulter counter method was developed through the analysis of four distinct genotypes of Loblolly pine SE multiplication cultures to ensure broad applicability. The aggregate size distributions obtained using the 2,000 μm aperture can be seen in Figure 7.2a.

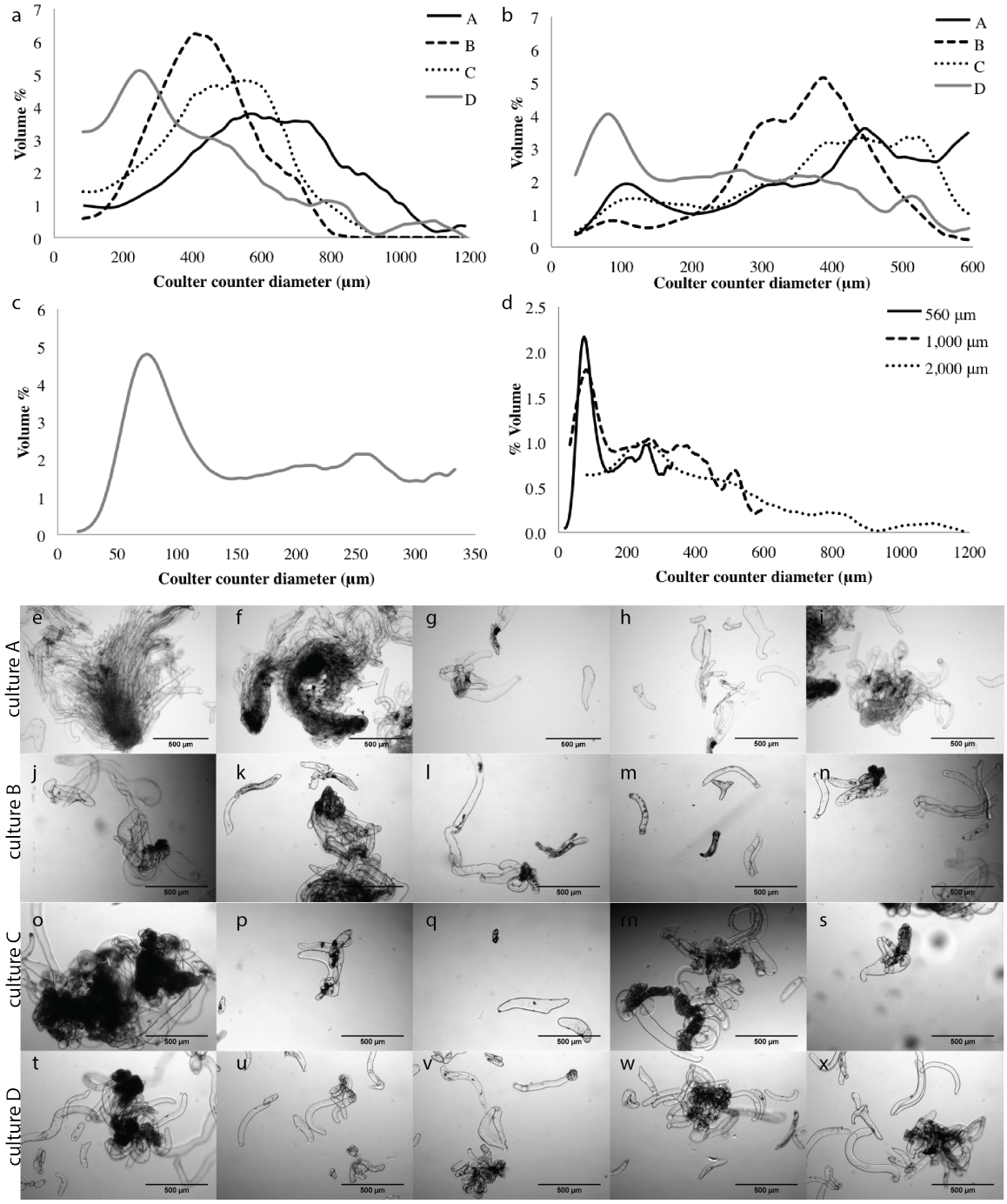

Figure 7.2. Aggregate size distributions of four distinct genotypes of Loblolly Pine obtained using the a) 2,000 µm aperture (data represent an average of five replicate two mL samples), b) 1,000 µm aperture (data represent an average of two replicate two mL samples), c) and the aggregate size distribution of Genotype D on the 560 µm aperture (data represent an average of two replicate two mL samples). To compare across apertures for Genotype D, data for each aperture were normalized

to the volume % at 230 µm (b). Data represent an average of two replicate two mL samples. Microscopy was used to confirm that the morphology of the genotypes A (e-i), B (j-n), C (o-s) and D (t-x) were consistent with the Coulter counter distributions.

Distinct aggregate size profiles were obtained through analysis of the four genotypes on the Coulter counter. The mean aggregate size and standard deviation (representative of the broadness of the peak) for each genotype are shown in Table 7.1.

Table 7.1. Mean aggregate size measured by the 2,000 µm aperture on the Coulter counter for each genotype. The mean aggregate size is a volume weighted average and the standard deviation is a measurement of the error associated across the five experimental replicates.

Genotype	Mean aggregate size (µm)	Standard deviation (µm)
A	600 ± 30	290 ± 20
B	440 ± 10	140 ± 10
C	470 ± 10	180 ± 10
D	390 ± 60	220 ± 60

The 2,000 µm aperture is able to accurately measure particle sizes between 70 and 1,200 µm in diameter. From the distributions in Figure 7.2a, it can be seen that Genotype D contains particles below this 70 µm cut-off. Therefore, the 1,000 µm aperture was used to measure the particle size distributions of all of the genotypes to ensure that all particles were being measured and accounted for (Figure 7.2b). The 1,000 µm aperture is able to accurately measure particles between 30 and 600 µm. All genotypes contain a population of particles with a mean diameter around 100 µm, with Genotype D having the largest proportion of particles at this size. These particles likely correspond to single suspensors, which are present in all cultures. To further analyze Genotype D and ensure that all particles were accurately quantified, this genotype was analyzed using a 560 µm aperture, which can accurately measure particles between 10 and 330 µm (Figure 7.2c). Using the

560 μm aperture, the full peak of particles with a mean diameter around 100 μm was obtained. To overlay data from all three apertures, the data were normalized to the volume percentage of particles found at 230 μm, which was a particle size accurately measured across all three apertures. (Figure 7.2d). Data from all three apertures are in strong agreement, with the smaller apertures showing increased levels of accuracy at smaller particle diameters.

To ensure that the aggregate size distributions were representative of the morphology of the genotypes, microscope images of each genotype were obtained. The microscope images for Genotype A, which had a mean aggregate size of 600 μm, can be seen in Figure 7.2e-i. This genotype contained the largest particles measured in this analysis, as represented by the particle size distributions in Figure 7.2a and the mean aggregate size in Table 7.1. These data are supported by the presence of large tissue seen under the microscope, which consist of both pre-embryogenic heads and complex vacuole structures (Figure 7.2e,f). The structures seen in Figure 7.2f could be characterized as PEM II's (Figure 7.1b) and PEM III's can be seen in Figure 7.2e and g. Genotype B had a mean aggregate size of 440 μm and had the most narrow aggregate size distribution, as indicated by the standard deviation of 140 μm in Table 7.1 (Figure 7.2j-n). This is supported by the cellular morphology seen in the microscope images, which lack the presence of large, complex tissue structures. Genotype C had a mean aggregate size of 470 μm and a standard deviation of 180 μm (Figure 7.2o-s). This genotype had more complex structures (PEM II's and III's) than those found in Genotype B (Figure 7.2o,r), but also had the presence of small structures (Figure 7.2p,q,s), some of which were below the aggregate size cut-off of the 2,000 μm aperture (Figure 7.2a).

Genotype D contained the smallest aggregates analyzed and contained a significant population of particles that were below the cut-off of the 2,000 μm aperture (Figure 7.2t-x). Although this genotype contained some more complex structures (Figure 7.2t,w,x), it contained a large population of single vacuole cells (Figure 7.2u,v,x). Overall, the microscope images confirm the data collected from the 2,000, 1,000 and 560 μm apertures for each genotype.

7.3.2. Further validation through size segregation and microscopy

To further validate the Coulter counter distribution, Genotype A was filtered through nylon mesh to create three size fractions: a) >700 μm, b) 300-700 μm and c) < 300 μm. These samples were run through the Coulter counter and the morphology of the size populations was examined through microscopy (Figure 7.3).

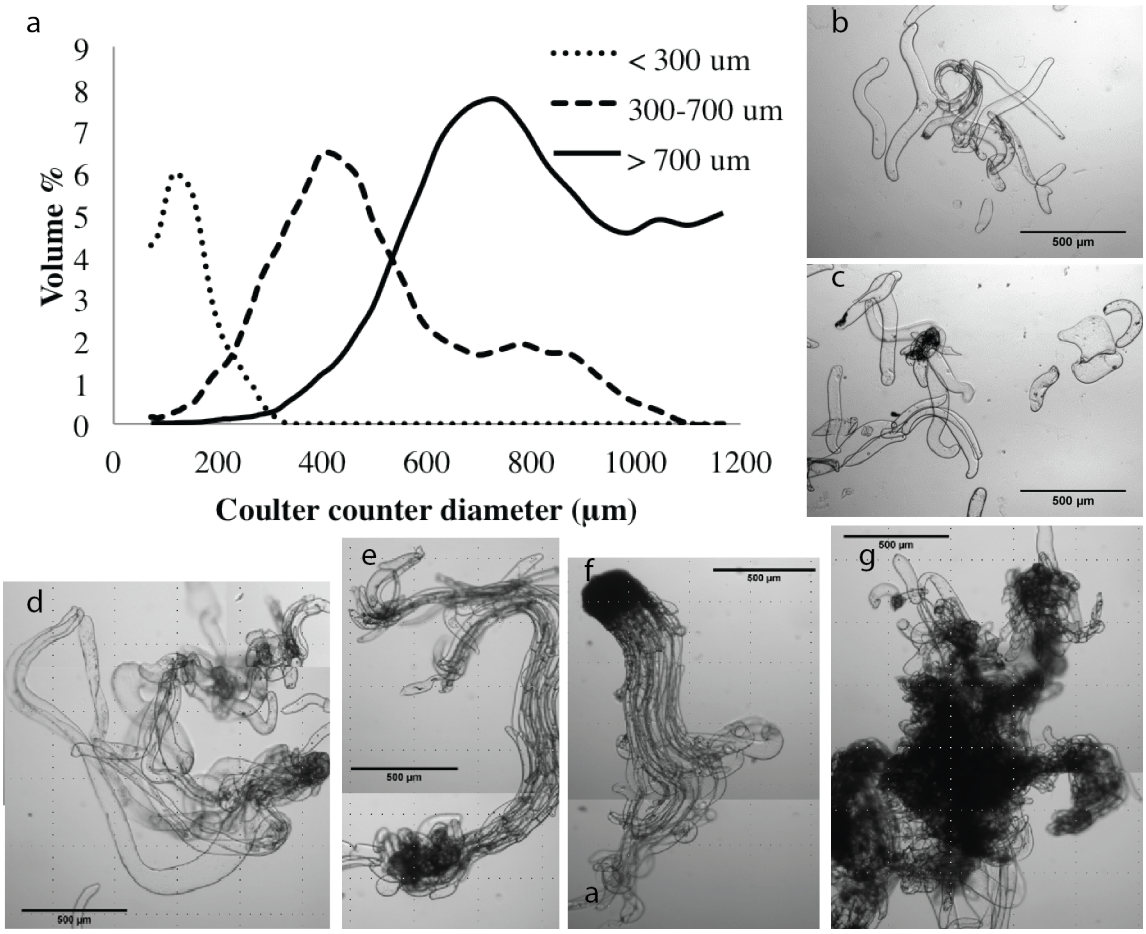

Figure 7.3. Genotype A was size segregated into three different size bins containing particles <300 µm (b,c), 300-700 µm (d,e) and >700 µm (f,g). Size bins were analyzed using the Coulter counter (a) and cell morphology for the bins was verified through microscopy (b-g).

Size fractionation verified that the Coulter counter accurately characterizes the particles based on size. Additionally, microscopy was effectively utilized to determine the phenotypic differences between the size fractions. The <300 µm size bin (Figure 7.3b,c) consisted primarily of single suspensor cells and small pre-embryogenic heads (PEM I's). The 300-700 µm bin (Figure 7.3d,e) contained more complex cell structures, with larger suspensors and organized suspensor tails (PEM II's). The >700 µm bin (Figure 7.3f,g) contained the most complex structures, with long, organized suspensor tails and complex masses of pre-embryogenic tissue (PEM III's).

7.3.3. Biomass correlation

A correlation between the measured Coulter counter volume and a traditional dry weight measurement can be developed to allow for comparison of Coulter counter data amongst data sets. Because of the differences in morphology and cell types (both pre-embryogenic heads and vacuolated suspensors), size segregation allows for the isolation of specific cell types to determine their effect on the biomass correlation. A mixed cell culture of Genotype E was filtered through seven filter sets to establish six populations of cells containing distinct cell populations (Figure 7.4a).

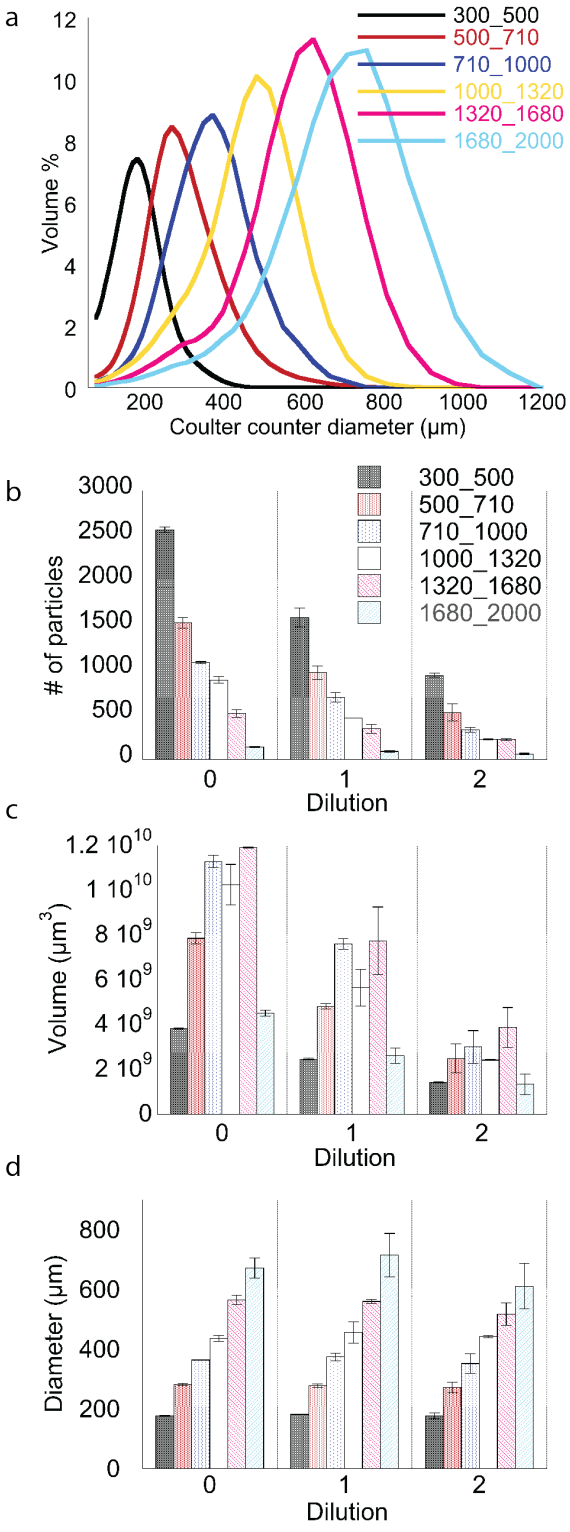

Figure 7.4. The aggregate size distributions for the undiluted size fractions (a) and number of particles (b), volume of particles (c) and mean diameter (d) for the 0-, 1- and 2- fold dilutions of

Genotype E. The genotype was size segregated into six different size bins containing particles 300-500 µm, 500-710 µm, 710-1,000 µm, 1,000-1320 µm, 1,320-1,680 µm and 1,680-2,000 µm.

These size fractions were then diluted two times to determine the effect of dilution on the particle size measurements, as well as to establish a linear biomass correlation for each size fraction (Figure 7.4b,c,d) to be used for future analyses. As expected, the highest number of particles was counted in the smallest aggregate sizes, with counts of 2,500 particles per run. The largest size bin contained the fewest particles, with counts as low as 60 for the 2-fold dilution. Although low particle counts can result in high levels of variability across replicates, the standard deviations remained low across the number, volume and mean diameter measurements. The largest volume of particles was found in the intermediate size bins (710-1000, 1000-1320 and 1320-1680 µm). The lowest volume of biomass was found in the smallest and largest size bins, with each bin containing less than 10% of the total biomass from the starting culture.

Dry weight measurements of each dilution and size fraction were measured to allow for the establishment of a biomass to Coulter counter volume distribution (Figure 7.5).

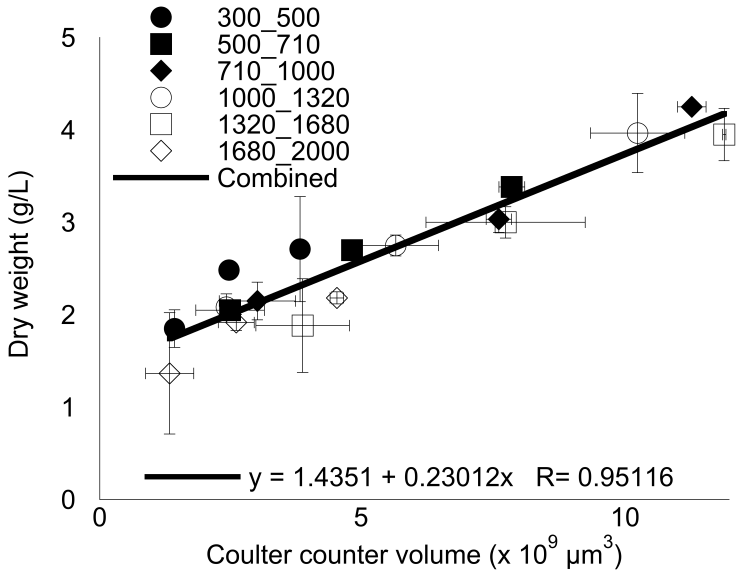

Figure 7.5. The Coulter counter to dry weight correlation determined by grouping all of the size fractions into a single data set. The R-value of 0.95 indicates a strong linear correlation. Data represent the average of four technical replicates for the Coulter counter and three technical replicates for the dry weight measurment.

There is a strong linear correlation across all size fractions (R = 0.951), allowing for the conversion of Coulter counter measurements to the more traditional dry weight measurement. Although the y-intercept was anticipated to be at 0, the correlation crosses the y-intercept at 1.44 g/L. This is likely due to the high concentration of sugars in the multiplication culture medium, which were not adequately washed from the filter prior to the dry weight measurement. Additionally, since the Coulter counter measures displaced volume, a broken suspensor cell would likely fall below the range of detection for the Coulter counter, but would still contribute to a dry weight measurement. To look at the individual contribution of each size fraction towards the dry weight, a linear correlation was established for each size fraction (Table 7.2).

Table 7.2. Parameters for the correlation between Coulter counter volume and dry weight for each size fraction.

	y-intercept (g/L)	Slope ($g/L*10^9$ μm^3)	R^2
Combined	1.4351	0.23	0.951
300_500	1.4479	0.35	0.942
500_710	1.4629	0.25	0.998
710_1000	1.3118	0.25	0.989
1000_1320	1.4566	0.24	0.998
1320_1680	0.9318	0.26	0.998
1680_2000	1.1267	0.25	0.951
Average	1.31	0.24	

There is a strong linear correlation between Coulter counter volume and dry weight for all of the size fractions, with R-values ranging from 0.942-0.998. The lowest size fraction (300-500 μm) had the largest slope, which was likely due to the drop off of the data at small particle sizes. Particles below the range of detection of the Coulter counter would still have a contribution to the dry weight measurement, resulting in a skewed correlation. The slope of the correlation for the remainder of the size bins ranges from 0.24-0.26 $g/L*10^9$ μm^3, indicating that the cell types and morphology have some effect on the correlation. That being said, the strength of the correlation for the grouped data set allows for a simplified conversion of the Coulter counter biomass to a biomass equivalent.

7.3.4. Long-term characterization of Loblolly Pine multiplication cultures

After a method to analyze the Loblolly pine SE multiplication cultures on the Coulter counter was developed, it was used to monitor the growth and aggregation of a culture (Genotype F) throughout a 7-week experiment. For this experiment, two replicate cultures of four treatments were maintained, for a total of eight cultures. Dry weight and Coulter counter data were collected at weeks 3, 5 and 7 of the experiment (Figure 7.6).

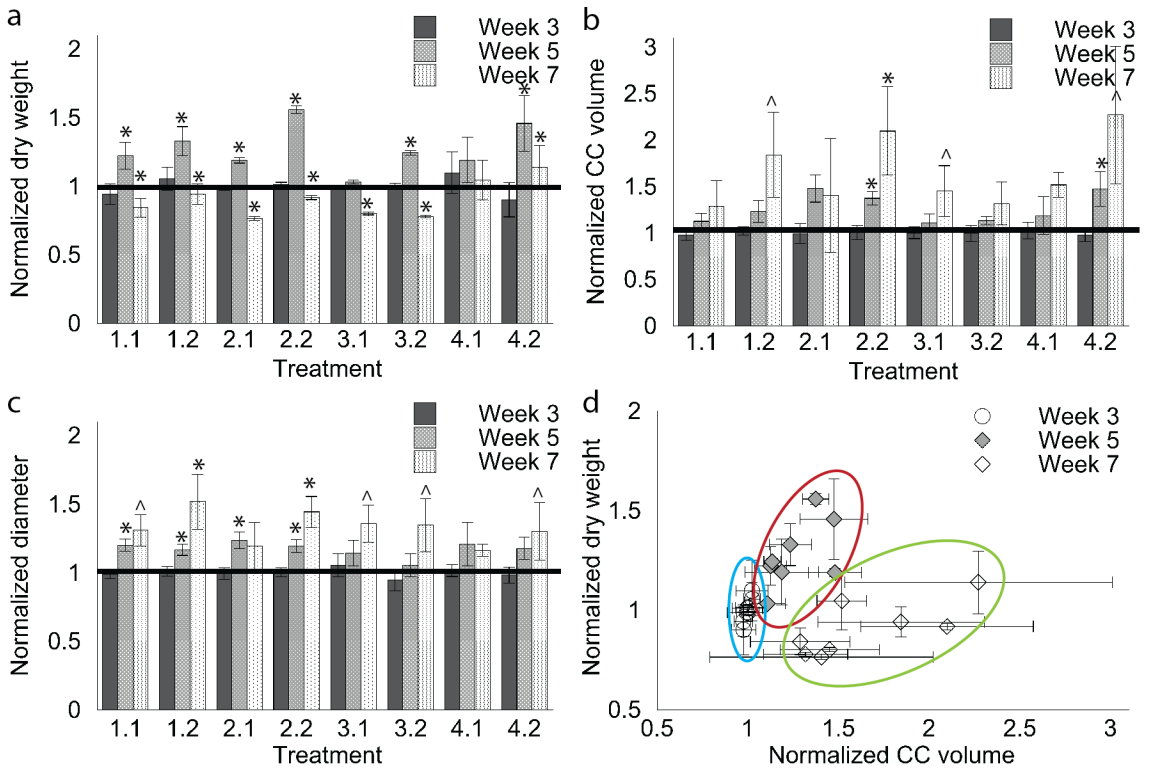

Figure 7.6. Normalized dry weight (a), Coulter counter volume (b) and Coulter counter diameter (c) from two replicate cultures of four experimental treatments (for a total of eight cultures). The treatment number corresponds to the treatment (1-4) and the replicate flask (1-2). Data were normalized to the average of the two treatment flasks at week 3. * indicates that the culture is statistically different from the previous time point. ^ indicates that the culture is statistically significant from the first time point. The relationship between the Coulter counter volume and dry weight is shown in (d). Groups of data are circled with week 3 in blue, week 5 in red and week 7 in green.

The dry weight for nearly every treatment increases between week 3 and week 5 of the study and then decreases again at week 7. This trend is different from what is seen in the Coulter counter volume data, which only shows an increase for treatment 2 between weeks 3 and 5. All other treatments show an increase in biomass at week 7. The relationship between the Coulter counter volume and dry weight (Figure 7.6d) is not

linear across all time-points and shows variability across the weeks of treatment. This result indicates that there is a more complicated relationship between the Coulter counter to dry weight correlation than was shown during the previous study of the Coulter counter to dry weight correlation at a single time point, as described further in the discussion. There is strong agreement across replicate cultures for all treatments and measurements. In fact, the Coulter counter indicates no statistical difference in the biomass and mean diameters of the two replicate bioreactors. The aggregate size distributions for the cultures can be seen in Figure 7.7.

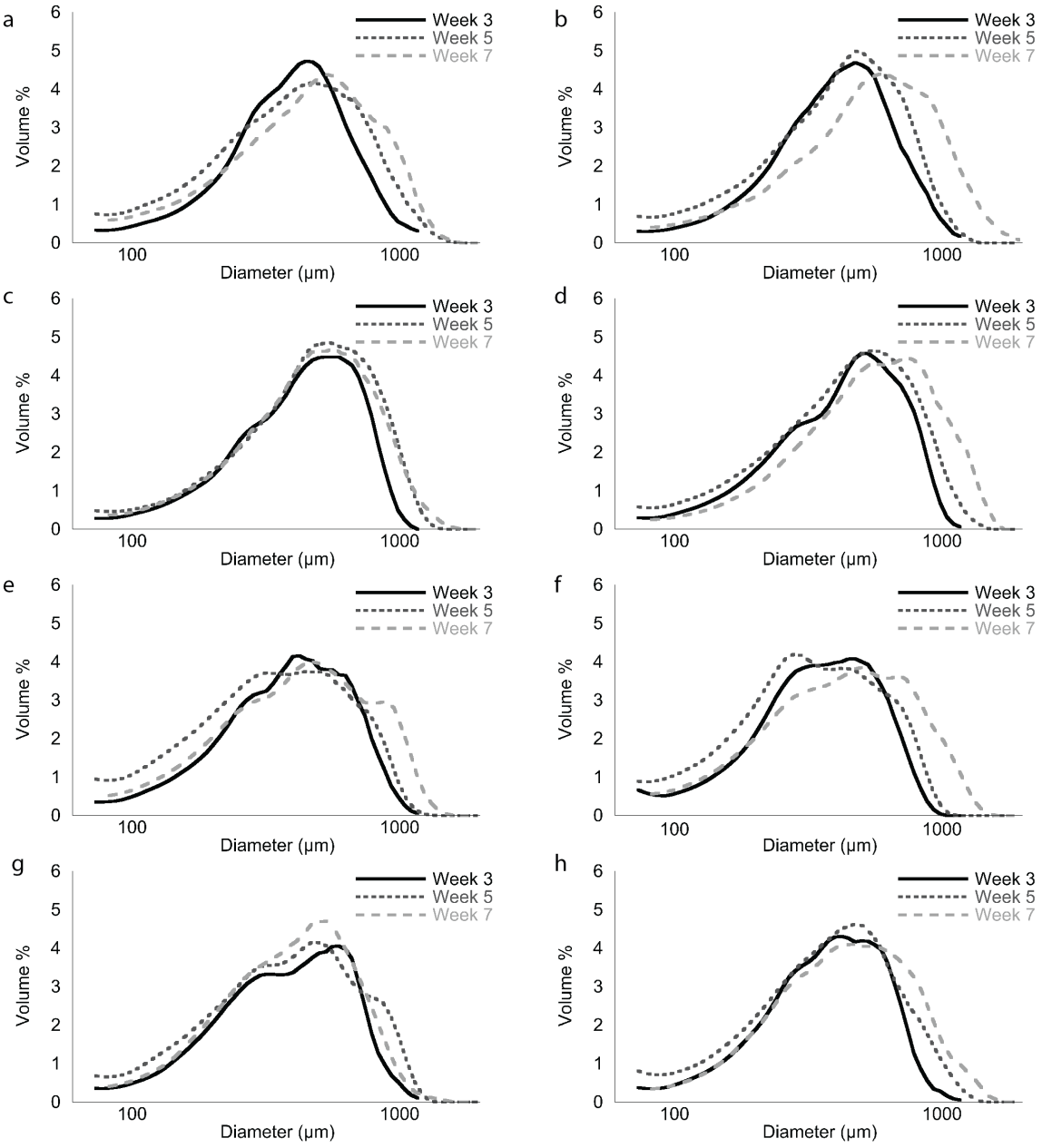

Figure 7.7. The aggregate size distributions for cultures (a) 1.1, (b) 1.2, (c) 2.1, (d) 2.2, (e) 3.1, (f) 3.2, (g) 4.1 and (h) 4.2 at weeks 3, 5 and 7 of an experiment.

Throughout the 7-weeks in culture, the aggregate size distribution of all cultures shifts towards larger particle sizes and the cultures become more heterogeneous (indicated by the broadness of the peak).

7.4. Discussion

The cellular morphology of somatic embryogenic cultures has been shown to directly affect embryo formation (Filonova et al., 2000). To allow for rapid characterization of cellular morphology and to determine the key morphological characteristics of multiplication cultures that lead to success through the embryo development and germination stages of SE, it is crucial to develop a rapid, reliable method to characterize tissue morphology. In this work, a method to characterize the size of tissue in multiplication cultures was developed through use of a Coulter counter. Due to the irregular morphology of ESM tissue, the Coulter counter makes an ideal tool for size characterization by measuring the displaced volume of each particle passing through the aperture. This method was successfully employed to analyze the cellular morphology of six distinct genotypes of loblolly pine somatic embryogenic cultures and could be further applied to characterize cellular morphology of somatic embryogenic cultures of other plant species.

7.4.1. Coulter counter effectively characterizes Lobolly Pine SE genotypes

Four genotypes of Loblolly Pine SE cultures were analyzed using a Coulter counter with 2,000, 1,000 and 560 μm apertures (Figure 7.2a-d). Results demonstrated that the 2,000 μm aperture is best able to characterize the genotypes, and only a small population of particles fall below the 70 μm cut-off of this aperture. In addition to the hypothesized growth cycle (Filonova et al., 2000), several papers have also shown that larger structures are more likely to develop into embryos (Fujimura, 2014). Hence, it is most important that size characterization of these genotypes is able to capture the morphology of these large tissues. Interestingly, size fractionation of several rose species

has shown that smaller PEM's (<540 μm) lead to a higher embryo yield (Kamo et al., 2004). Additionally, in carrot somatic embryogenic cultures, cluster of 3-10 cytoplasm-rich (not vacuolated) cells resulted in significantly higher embryo yields (Fujimura and Komamine, 1979). These results indicate that there is still a lack of knowledge about the ideal cellular morphology in SE maintenance cultures to promote embryo formation. That being said, the single suspensors that must be characterized using the smaller 560 μm aperture likely do not contribute to the embryogenic potential of the genotype (Fujimura, 2014; Fujimura and Komamine, 1979), further supporting the use of the 2,000 μm aperture in future analyses.

The hypothesized growth stages discussed in this paper were suggested from studies using cell types isolated in agarose gels (Filonova et al., 2000).Such experiments eliminate the complex cell-cell interactions and signaling found in a heterogeneous suspension cell culture and therefore may not accurately represent the culture phenotype. The ability to study the morphology of a heterogeneous cell culture using the Coulter counter provides an opportunity to study cell types without isolation of specific tissues. Additionally, cultures could be fractionated and specific size fractions could be followed through both maintenance and development stages. Results from such experiments would provide important information on how specific cell types cycle within the maintenance culture, as well as which specific cell types result in high embryo yields in the development phase.

7.4.2. Coulter counter volume to dry weight ratio could provide additional information about culture morphology

While a linear correlation between the Coulter counter volume and dry weight of the culture was found at a single time-point (Figure 7.5), contradicting trends between the dry weight and Coulter counter data were found during the long-term study (Figure 7.6a,b). This contradicting data is quite interesting and could provide additional information about the morphology of the culture that is not seen with the dry weight measurement alone (with the dry weight being the standard measurement of biomass levels in somatic embryogenic cultures). For instance, subjecting the cultures to varying treatments could result in a decrease in culture health and the cultures could take several weeks to recover. Whereas the dry weight measurement is unaffected by cell morphology, the Coulter counter is measuring the volume of electrolyte displaced by the cell, which would change for an intact vs. broken cell. Therefore, a broken cell will contribute significantly less to the measurement of the Coulter counter volume then it will to the dry weight measurement. Between weeks 3 and 5 in culture, there is an increase in the number of small aggregates within all of the bioreactors (Figure 7.7), as well as an increase in the dry weight measurement of all bioreactors. Between weeks 5 and 7, when the dry weight measurement decreases and the Coulter counter volume increases, there is a shift back towards larger particles in all of the cultures.

To learn more about how changes in a culture over time affect the Coulter counter data, a long-term study would have to be performed with microscopy to concurrently observe changes in cellular morphology. Additionally, determining the dry weight to Coulter counter volume correlation for cultures throughout this long-term study could

provide additional information about the cultures. For instance, a higher Coulter counter volume to dry weight ratio could indicate a higher proportion of healthy cells within a culture (because broken cells will not contribute as much to Coulter counter measurements). This long-term study could be paired with continuation of cultures through the development and germination stages to begin to understand more about how specific cell morphologies affect culture success.

A major limitation to the commercial success of somatic embryogenesis for clonal propagation is a lack of methods to predict culture success during the maintenance phase of culture. Currently, cultures must be followed for a minimum of eight weeks in development before early stages of embryo yield can be determined. Here we present a method to characterize the morphology of tissue within a multiplication culture, which has been shown to have a significant effect on culture embryogenesis. The Coulter counter is an effective method for characterizing biomass levels and the size distribution of cell types within a maintenance culture, as shown here with loblolly pine cultures. This method could easily be applied to the characterization of somatic embryogenic cultures from all plant species. Application of this method over a 7-week experiment demonstrated the utility of this method for the characterization of cell morphology and indicated that dry weight and Coulter counter measurements in tandem could provide additional information about the state of the culture. This method is an ideal platform for studying the cycling of cells within the multiplication culture and determining the cell morphologies that promote embryogenesis. This fundamental knowledge could allow for prediction of culture success during the maintenance phase, allowing for the propagation of only those cultures with ideal properties. Because the morphology of cell types in

somatic embryogenic cultures is identical across species, the knowledge gained from these fundamental studies could be applied to improve process development for somatic embryogenic cultures of any species.

7.5. Additional information

7.5.1. Method to disaggregate Loblolly pine cultures

To determine properties that are indicators for culture success, it is important to develop methods that allow for quantification of cellular masses in various stages of development. It is hypothesized that the presence of a high number of pre-embryogenic heads in the multiplication phase will lead to increased embryo yields during development. In addition, counts of developing embryos during development can be used as an indicator for overall culture success as high yields are necessary for commercialization. Currently, the only existing method for quantification of pre-embryogenic heads and early embryos is through the physical isolation of these objects from surrounding ESM using forceps under a microscope. This process is time consuming and impractical at a mid-large scale. Therefore, a high-throughput method must be developed to isolate well-defined heads and embryos from ESM in phase 1 and 2 cultures through the use enzymatic digestion. With the development of this method, the ability of these two properties to predict culture success could be evaluated by correlating the head and embryo yield in multiplication and development to the germination competent embryo yield.

Using enzymatic digestion, it is hypothesized that more vacuolated suspensor cells could be selectively digested over the more dense cells that make up the pre-embryogenic head. Therefore, a preliminary digestion was performed by placing one

gram of cells (Genotype B used in previous studies) in an enzyme solution consisting of 0.5% pectolyase and 0.04% cellulase in a 0.5 M mannitol solution. This enzyme concentration has been successfully utilized to isolate single cells from *Taxus* suspension cultures (Naill and Roberts, 2004). Cells were placed in an incubator at 25 °C and 125 rpm and microscope images were taken after one and two hours of incubation (Figure 7.8).

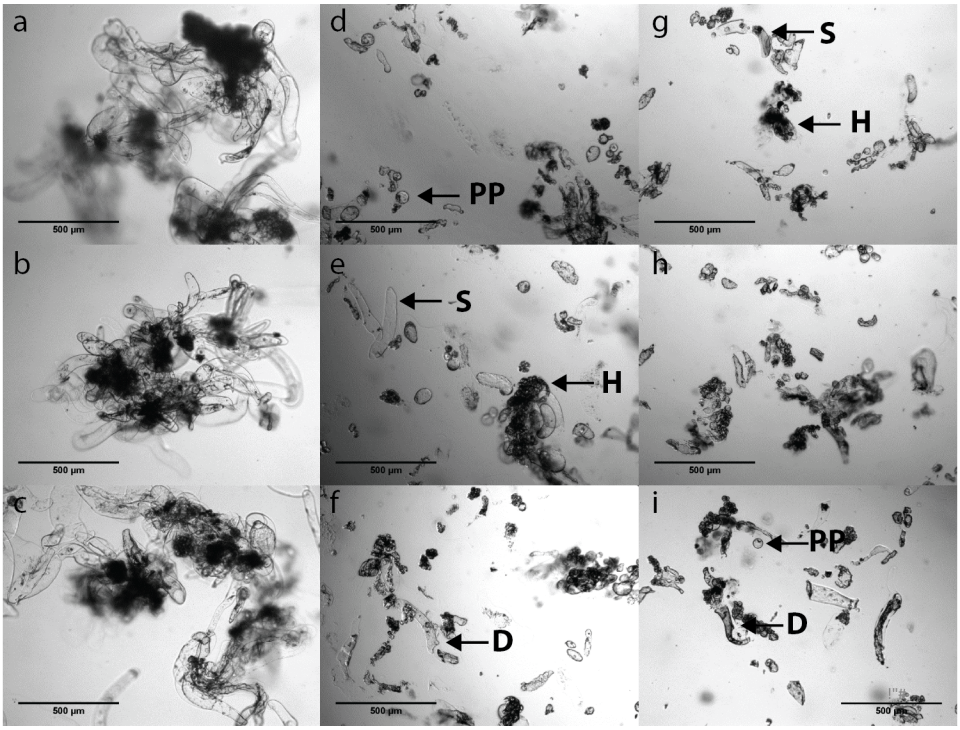

Figure 7.8. Microscope images of Loblolly Pine SE cultures that have been digested in a 0.5% pectolyase and 0.04% cellulose solution for zero (a,b,c), one (d,e,f) and two hours (g,h,i). Examples protoplasts (PP), suspensors (S), pre-embryogenic heads (H) and cellular debris within the samples have been identified with arrows.

After just one hour of incubation in enzyme solution, cellular aggregates are significantly digested and the presence of single suspensors, protoplasts and isolated pre-embryogenic heads begin to emerge. The presence of protoplasts is due to the digestion

of the cell wall, leading to the release of the cell into the osmoticum solution. Although an isolated pre-embryogenic head can be seen in Figure 7.8e, there is also the presence of debris. Additionally, after two hours, aggregates are further digested and most of the pre-embryogenic tissue appears digested or broken, indicating over digestion of the sample. Therefore, a lower enzyme concentration or a shorter incubation period should be utilized to successfully isolate pre-embryogenic heads from the suspensor tissue. Combining enzymatic digestion with mechanical shear could further assist in the separation of suspensor tissue from more developed pre-embryogenic heads.

When multiplication culture is transferred to solid medium for development, the ESM tissue continues to proliferate and embryos begin to emerge. Currently, characterization of cell types within the development stage occurs by sacrificing an entire plate to allow for manual isolation of embryos using forceps under a dissecting microscope. The isolated embryos are then qualitatively scored based on phenotype to indicate stage in the embryo development pathway. This process is time-intensive and it is difficult to distinguish embryos that are in the early stages of development from the surrounding ESM tissue. To allow for isolation of embryos of all stages from the ESM during development, it is hypothesized that a combination of enzymatic digestion with density centrifugation could be used. For this process, ESM tissue would be fully digested using cellulose and pectolyase. Because both the pre-embryogenic heads and the suspensors in ESM tissue are less complex than the embryo shown in Figure 7.1, it is anticipated that enzymatic digestion can be optimized to allow for isolation of both early and late-stage embryos. Fully digested samples can then be filtered through nylon mesh to allow for isolation of the embryos. Density centrifugation could then be used to

separate early stage embryos (less dense due to less complexity) from late stage embryos (as seen in Figure 7.1). The change in complexity of developing embryos that will be exploited has been clearly documented in *Picea abies* somatic embryos during the proliferation, early embryo, late embryo and maturation stages (Businge et al., 2012). The tissue isolated through density centrifugation could then be analyzed using either dry weight or manual counting methods. Developing methods to characterize the tissue types in both multiplication and development cultures will allow for the identification of key characteristics in the multiplication culture that lead to successful cultures in the development and germination stages.

CHAPTER 8.

IMPACT AND FUTURE RECOMMENDATIONS

Future efforts in plant cell culture engineering must consider simultaneous optimization of intracellular, intercellular and extracellular parameters. To date, most approaches focus on optimizing synthesis of a specific metabolite of interest using a single enhancement method. One key example is the intracellular pathway engineering to promote production of a specific specialized metabolite (e.g., paclitaxel in *Taxus* suspension cultures or vinblastine and vincristine in *Catharanthus roseus*). Because plant cell culture transformation efforts take months to assess results of genetic manipulations, particular care needs to be placed upstream of genetic engineering studies to better ensure success. Therefore, this thesis aimed to use a multi-scale engineering approach to both characterize and engineer plant cell culture systems. This strategy not only resulted in an increased understanding of the plant cell culture system, but also allowed for the development of engineering strategies to increase culture success. Here, I summarize the key results from this thesis, as well as provide recommendations for future work to improve the understanding and performance of plant cell culture systems.

8.1. Extracellular

On an extracellular level, methods were developed to control the aggregate size in *Taxus* suspension culture through the modulation of applied mechanical shear using a population balance equation model (Chapter 2). Although aggregate size has been shown to affect specialized metabolite accumulation in plant cell cultures (Kolewe et al., 2011a; Patil et al., 2012; Patil et al., 2013), no methods have been developed to control variability in aggregate size distributions. The developed model allowed for control of

aggregation dynamics within a single generation of culture, but aggregate breakage became more complex during application of the model over multiple generations of cell growth. Adding additional complexity to the model by accounting for the effect of changing aggregate strength on breakage could improve control, as well as provide important information how changes in aggregate composition affect specialized metabolite production.

From this study, it became evident that aggregation dynamics within isolated cell populations are connected either through culture pre-programming or environmental effects. To further investigate the cause of changes in aggregate properties of a culture, more controlled studies need to be performed. Many bioreactor systems have been designed specifically for plant cell culture systems, allowing for higher levels of control on properties such as pH, sugar concentration, humidity, dissolved oxygen and shear rate (Eibl and Eibl, 2008; Eibl et al., 2009; Lehmann et al., 2014). By studying changes in aggregation in this controlled environment, a better understanding about the cause of aggregation dynamics could be developed. Whereas pre-programming of aggregation properties would be difficult to overcome, identifying key environmental triggers for changes in aggregation could allow for better control of culture properties and decreased culture heterogeneity.

One of the biggest limitations to commercial somatic embryogenesis is a lack of understanding about how specific multiplication culture properties affect embryo yields. As a result, months of resources are devoted to cultures that in the end have very low product yields. In somatic embryogenic multiplication cultures, the morphology of cellular aggregates is hypothesized to greatly affect the embryogenic capacity of a

culture. Therefore, methods were developed to characterize the biomass levels and morphology of loblolly pine multiplication cultures (Chapter 7). Application of this method to multiplication cultures will provide increased detail about culture properties, allowing for the identification of ideal multiplication culture morphologies for high embryo yield.

The application of size fractionation to multiplication cultures could allow for characterization of the multiplication cell cycle, as well as identification of the key cellular morphologies that lead to high embryo yields throughout development. To study the multiplication cell cycle, a multiplication culture could be size segregated into populations of specific cell morphologies (like those identified in Figure 7.1). Reculturing these size fractions and characterization of morphology changes over time using both the Coulter counter and microscopy could provide insight into the multiplication cycle. Additionally, plating of these cells onto development medium would allow for determination of the ideal cellular morphologies that yield to high embryo yields. As more data is collected on the transition of specific cell types through a hypothesized growth cycle, as well as which cell types lead to the highest embryo yields, a predictive model could be developed to forecast changes in culture composition over time. A model has been developed to predict the effect of processing parameters on somatic embryo conversion in oil palm (Konan et al., 2006), but this model focuses on somatic embryo in the development stage. Modeling of cultures within the multiplication phase would allow for prediction of ideal plating times by determining when a culture will have the highest proportion of cell types that lead to high embryo yields.

8.2. Intercellular

Single cells within *Taxus* cultures have been shown to accumulate variable levels of paclitaxel (Naill and Roberts, 2005d), but there is no knowledge regarding why specific subpopulations within a culture develop. Therefore, a method to look at the spatial distribution of paclitaxel within a *Taxus* aggregate was developed (Chapter 3). With further optimization, this method will allow for investigation into the effect of aggregate size on the accumulation of paclitaxel and its precursors on single cells. Several hypotheses exist for why subpopulations exist in *Taxus* cultures. The first is that smaller aggregates accumulate higher levels of paclitaxel due to a decrease in diffusion limitations, as well as exposure to beneficial levels of shear within the culture (Kolewe et al., 2008). This hypothesis could be confirmed by showing that all cells within a smaller aggregate accumulate high product levels, whereas only exterior cells in a large aggregate have high accumulation levels. Strategies to reduce diffusion limitations or increase shear could be developed to improve culture performance, potentially through the application of the shearing model developed in Chapter 2 or cultivation in a controlled bioreactor. Another hypothesis is that changes in cellular metabolism lead to both changes in product accumulation, as well as changes in aggregate size. This could be confirmed by showing that all cells in smaller aggregates have high accumulation levels and all cells in larger aggregates have low accumulation levels. Using the transcriptome data for unelicited small and large aggregates (Lenka et al., Manuscript in progress.), key genes involved in the synthesis of cell wall compounds could be identified, which likely contribute to the changes in aggregate morphology. Down-regulation of these genes could allow for

development of a transgenic culture with inherently smaller aggregates, as well as higher product levels.

Regardless of the mechanism for heterogeneity of paclitaxel accumulation within single cells, a method to select for paclitaxel-accumulating subpopulations could allow for the development of cultures with superior performance. This has been successfully achieved using flow cytometry for the enrichment of high heterologous protein production (Kirchhoff et al., 2012). The biggest limitation to application of this technology in *Taxus* is the need to disaggregate cultures into single cells while maintaining cell viability. Through stable transformation of *Taxus* cultures with an inducible paclitaxel-binding caspase, caspase production could be initiated in paclitaxel accumulating cultures, leading to the selective apoptosis of the non-paclitaxel accumulating subpopulations (Chapter 4). The level of paclitaxel production required to prevent apoptosis could be gradually increased by increasing the concentration of inducer added to the culture medium, allowing for improved selection over time (Padidam, 2003). Additionally, the binding affinity of the caspase protein could be modified to increase or decrease the selection pressure.

One of the major limitations to transcriptomic studies of plant cell culture systems is the heterogeneity of cultures. Although high-producing cultures can be developed for transcriptomics through filtration into small and large aggregated populations (Lenka et al., Manuscript in progress.), differences in gene expression are muddled because these populations remain heterogeneous. Single cell transcriptomic techniques are being developed, which allow for more specific correlation between gene expression and cell phenotype, but collection of enough datasets (both in multiple single cells and over time)

can be difficult and costly (Tang et al., 2011). Through development of a more homogeneous, superior paclitaxel accumulating cell line using a selection mechanism such as the paclitaxel-binding caspase system, transcriptomic studies could more clearly identify the key genes involved in regulation of paclitaxel accumulation in culture.

8.3. Intracellular

One of the major limitations to the current technology is the lack of fully elucidated plant biosynthetic pathways. Although the 'omics' era has led to an enormous increase in the data available, correct annotation and functional characterization of enzymes is crucial to the successful implementation of these technologies. In addition, the complex interactions amongst biosynthetic pathways further complicate metabolic engineering strategies. For example, in *C. roseus* hairy root cultures, an increase in the expression of a single gene (1-deoxy-D-xylulose synthase, DXS) within the TIA biosynthetic pathway resulted in mixed results; however, co-overexpression of two genes (DXS with geraniol-10-hydroxylase or anthranilate synthase α subunit) within the pathway led to a significant increase in the accumulation of multiple TIA metabolites (Peebles et al., 2011). As a result, more complex engineering strategies that manipulate expression of multiple pathway genes and/or regulators is necessary to balance flux towards the product of interest (Morandini, 2013). Defining these strategies requires detailed systems knowledge and sophisticated metabolic models, which are presently lacking for plant systems. Therefore, to gain further understanding into the global metabolism of *Taxus* cultures, methods were developed to characterize active specialized metabolic pathways (Chapter 5). These methods were applied to both paclitaxel accumulating and non-paclitaxel accumulating cultures in both single generation and

long-term studies, allowing for a greater understanding of the metabolism of these cultures.

From these studies, targets for metabolic engineering strategies can be developed that are cell line specific. For instance, both paclitaxel accumulating and non-paclitaxel accumulating cultures produce lignin in response to methyl jasmonate elicitation. Silencing of genes involved in lignin biosynthesis (e.g., cinnamate 4-hydroxylase, p-coumarate 3-hydroxylase, ferulate 5-hydroxylase or phenylalanine ammonia-lyase (Vanholme et al., 2010)) could lead to an increase in carbon availability for the production of paclitaxel.

Cultures that were unable to produce paclitaxel showed increased basal levels of phenolics and flavonoids. Interestingly, increased basal levels of phenolics and flavonoids were also found in smaller aggregates of paclitaxel-accumulating cultures, which produce higher levels of paclitaxel than those cultures with smaller aggregates. Additionally, non-paclitaxel accumulating cultures exhibited no growth inhibition in the presence of methyl jasmonate, which could allow for increased culture productivity. Therefore, identifying the bottlenecks preventing the accumulation of paclitaxel in the non-paclitaxel accumulating cell lines could allow for redirection of cellular metabolism towards paclitaxel and potentially yield cultures with high production capability. By comparing the methyl jasmonate elicited transcriptomes of non-paclitaxel producing and paclitaxel producing cultures, the bottlenecks could be identified, allowing for the rescue of paclitaxel biosynthesis in these non-producing cultures.

To allow for creating of transgenic *Taxus* cell lines, a method was developed for the stable transformation of *Taxus* cultures using *Agrobacterium*-mediated

transformation. Although this step is crucial for gene upregulation and silencing studies, current stable transformation procedures are time consuming, making the development of high throughput transformation procedures desirable, especially as metabolic engineering schemes become more complex. Strategies have been developed for the high-throughput evaluation of genetic manipulations on the production of carotenoids in rice cell cultures due to the production of colored pigments in cultures with high levels of accumulation (Bai et al., 2014). That being said, strategies for the high-throughput evaluation of more complex systems such as *Taxus* have yet to be developed.

8.4. Synergistic application of engineering strategies for improved culture performance

Several plant cell culture systems have been used for the industrial production of secondary metabolites and heterologous proteins (Table 1.1), but a further understanding of plant cellular metabolism and development of new optimization strategies could dramatically affect the field and enable more wide-spread use of the technology. The work presented in this thesis, as well as the proposed future directions of this research, represent a multi-scale engineering approach to characterizing and engineering plant cell cultures. The synergistic application of these engineering strategies (as suggested in the future recommendations) could allow for redirection of cellular metabolism for improved culture performance.

BIBLIOGRAPHY

Abohatem, M., Zouine, J., El Hadrami, I., 2011. Low concentrations of BAP and high rate of subcultures improve the establishment and multiplication of somatic embryos in date palm suspension cultures by limiting oxidative browning associated with high levels of total phenols and peroxidase activities. Scientia Horticulturae. 130**,** 344-348.

Afendi, F. M., Okada, T., Yamazaki, M., Hirai-Morita, A., Nakamura, Y., Nakamura, K., Ikeda, S., Takahashi, H., Altaf-Ul-Amin, M., Darusman, L. K., Saito, K., Kanaya, S., 2012. KNApSAcK Family Databases: Integrated Metabolite-Plant Species Databases for Multifaceted Plant Research. Plant and Cell Physiology. 53**,** 12.

Aharoni, A., Galili, G., 2011. Metabolic engineering of the plant primary-secondary metabolism interface. Current Opinion in Biotechnology. 22**,** 239-244.

Ainsworth, E. A., Gillespie, K. M., 2007. Estimation of total phenolic content and other oxidation substrates in plant tissues using Folin–Ciocalteu reagent. Nature Protocols. 2**,** 875-877.

Akcay, U. C., Mahmoudian, M., Kamci, H., Yucel, M., Oktem, H. A., 2009. Agrobacterium tumefaciens-mediated genetic transformation of a recalcitrant grain legume, lentil (Lens culinaris Medik). Plant Cell Reports. 28**,** 407-417.

Amorim Madeira, P. J., Florencio, M. H., 2009. Flavonoid - matrix cluster ions in MALDI mass spectrometry. Journal of Mass Spectrometry. 44**,** 1105-1113.

Antony, F., Jordan, L., Schimleck, L. R., Clark, A., Souter, R. A., Daniels, R. F., 2011. Regional variation in wood modulus of elasticity (stiffness) and modulus of rupture (strength) of planted loblolly pine in the United States. Canadian Journal of Forest Research-Revue Canadienne De Recherche Forestiere. 41**,** 1522-1533.

Athey, S., Levin, J., Seira, E., 2011. Comparing open and sealed bid auctions: Evidence from timber auctions. Quarterly Journal of Economics. 126**,** 207-257.

Bai, C., Rivera, S. M., Medina, V., Alves, R., Vilaprinyo, E., Sorribas, A., Canela, R., Capell, T., Sandmann, G., Christou, P., Zhu, C., 2014. An in vitro system for the rapid functional characterization of genes involved in carotenoid biosynthesis and accumulation. Plant Journal. 77**,** 464-475.

Barampuram, S., Zhang, Z. J., 2011. Recent advances in plant transformation. Methods in molecular biology (Clifton, N.J.). 701**,** 1-35.

Belen Fernandez, M., Raul Daleo, G., Gabriela Guevara, M., 2015. Isolation and characterization of a Solanum tuberosum subtilisin-like protein with caspase-3 activity (StSBTc-3). Plant Physiology and Biochemistry. 86**,** 137-146.

Bjarnholt, N., Li, B., D'Alvise, J., Janfelt, C., 2014. Mass spectrometry imaging of plant metabolites – principles and possibilities. Natural Product Reports.

Bourgaud, F., Gravot, A., Milesi, S., Gontier, E., 2001. Production of plant secondary metabolites: a historical perspective. Plant Science. 161**,** 839-851.

Brentnall, M., Rodriguez-Menocal, L., De Guevara, R. L., Cepero, E., Boise, L. H., 2013. Caspase-9, caspase-3 and caspase-7 have distinct roles during intrinsic apoptosis. Bmc Cell Biology. 14.

Businge, E., Brackmann, K., Moritz, T., Egertsdotter, U., 2012. Metabolite profiling reveals clear metabolic changes during somatic embryo development of Norway spruce (Picea abies). Tree Physiology. 32**,** 232-244.

Busto, V. D., Calabro-Lopez, A., Rodriguez-Talou, J., Giulietti, A. M., Merchuk, J. C., 2013. Anthraquinones production in Rubia tinctorum cell suspension cultures: Down scale of shear effects. Biochemical Engineering Journal. 77**,** 119-128.

Capataz-Tafur, J., Trejo-Tapia, G., Rodriguez-Monroy, M., Sepulveda-Jimenez, G., 2011. Arabinogalactan proteins are involved in cell aggregation of cell suspension cultures of Beta vulgaris L. Plant Cell Tissue and Organ Culture. 106**,** 169-177.

Cenis, J. L., 1992. Rapid extraction of fungal DNA for PCR amplification. Nucleic Acids Research. 20**,** 2380-2380.

Chae, L., Kim, T., Nilo-Poyanco, R., Rhee, S. Y., 2014. Genomic Signatures of Specialized Metabolism in Plants. Science. 344**,** 510-513.

Chang, C. C., Yang, M. H., Wen, H. M., Chern, J. C., 2002. Estimation of total flavonoid content in propolis by two complementary colorimetric methods. Journal of Food and Drug Analysis. 10**,** 178-182.

Chang, M. C. Y., Keasling, J. D., 2006. Production of isoprenoid pharmaceuticals by engineered microbes. Nature Chemical Biology. 2**,** 674-681.

Chang, X. F., Chandra, R., Berleth, T., Beatson, R. P., 2008. Rapid, microscale, acetyl bromide-based method for high-throughput determination of lignin content in Arabidopsis thaliana. Journal of Agricultural and Food Chemistry. 56**,** 6825-6834.

Chattopadhyay, S., Srivastava, A. K., Bhojwani, S. S., Bisaria, V. S., 2002. Production of podophyllotoxin by plant cell cultures of Podophyllum hexandrum in bioreactor. Journal of Bioscience and Bioengineering. 93**,** 215-220.

Chau, M., Croteau, R., 2004. Molecular cloning and characterization of a cytochrome P450 taxoid 2 alpha-hydroxylase involved in Taxol biosynthesis. Archives of Biochemistry and Biophysics. 427**,** 48-57.

Chau, M., Jennewein, S., Walker, K., Croteau, R., 2004. Taxol biosynthesis: Molecular cloning and of a cytochrome p450 characterization taxoid 7 beta-hydroxylase. Chemistry & Biology. 11**,** 663-672.

Chin, M. S., Freniere, B. B., Fakhouri, S., Harris, J. E., Lalikos, J. F., Crosby, A. J., 2013. Cavitation Rheology as a Potential Method for In Vivo Assessment of Skin Biomechanics. Plastic and Reconstructive Surgery. 131**,** 303E-305E.

Cornett, D. S., Reyzer, M. L., Chaurand, P., Caprioli, R. M., 2007. MALDI imaging mass spectrometry: molecular snapshots of biochemical systems. Nature Methods. 4**,** 828-833.

Cragg, G. M., Boyd, M. R., Cardellina II, J. H., Grever, M. R., Schepartz, S., Snader, K. M., Suffness, M., 1993. The search for new pharmaceutical crops: Drug discovery and development at the National Cancer Institute. Wiley, New York.

Cragg, G. M., Newman, D. J., 2009. Nature: a vital source of leads for anticancer drug development. Phytochemistry Reviews. 8**,** 313-331.

Cragg, G. M., Simon, J. E., Jato, J. G., Snader, K. M., 1996. Drug discovery and development at the National Cancer Institute: Potential for new pharmaceutical crops. ASHS Press, Arlington, Va.

Cui, J., Lee, C. H., Delbos, A., McManus, J. J., Crosby, A. J., 2011. Cavitation rheology of the eye lens. Soft Matter. 7**,** 7827-7831.

Curtis, W. R., Emery, A. H., 1993. Plant-cell suspension culture rheology. Biotechnology and Bioengineering. 42**,** 520-526.

Cusido, R. M., Palazon, J., Bonfill, M., Exposito, O., Moyano, E., Pinol, M. T., 2007. Source of isopentenyl diphosphate for taxol and baccatin III biosynthesis in cell cultures of Taxus baccata. Biochemical Engineering Journal. 33**,** 159-167.

Day, C. D., Lee, E., Kobayashi, T., Holappa, L. D., Albert, H., Ow, D. W., 2000. Transgene integration into the same chromosome location can produce alleles that express at a predictable level, or alleles that are differentially silenced. Genes & Development. 14**,** 2869-2880.

De Luca, V., Salim, V., Atsumi, S. M., Yu, F., 2012. Mining the Biodiversity of Plants: A Revolution in the Making. Science. 336**,** 1658-1661.

Deal, R. B., Henikoff, S., 2011. The INTACT method for cell type-specific gene expression and chromatin profiling in Arabidopsis thaliana. Nature Protocols. 6**,** 56-68.

del Carmen Oliver-Salvador, M., Morales-Lopez, E., Duran-Paramo, E., Orozco-Alvarez, C., Garcia-Salas, S., 2013. Shear rate and microturbulence effects on the synthesis of proteases by Jacaratia mexicana cells cultured in a bubble column, airlift, and stirred tank bioreactors. Biotechnology and Bioprocess Engineering. 18**,** 808-818.

DellaPenna, D., O'Connor, S. E., 2012. Plant Gene Clusters and Opiates. Science. 336**,** 1648-1649.

Denis, J. N., Greene, A. E., Guenard, D., Guerittevoegelein, F., Mangatal, L., Potier, P., 1988. A highly efficient, practical approach to natural Taxol. Journal of the American Chemical Society. 110**,** 5917-5919.

Dixon, R. A., Strack, D., 2003. Phytochemistry meets genome analysis, and beyond. Phytochemistry. 62**,** 815-816.

Dong, Y., Duan, W., He, H., Su, P., Zhang, M., Song, G., Fu, C., Yu, L., 2015. Enhancing taxane biosynthesis in cell suspension culture of Taxus chinensis by overexpressing the neutral/alkaline invertase gene. Process Biochemistry. 50**,** 651-660.

Drud, A., 1994. CONOPT - a large-scale grg code. Journal of computing. 6**,** 207-216.

Edahiro, J., Seki, M., 2006. Phenylpropanoid metabolite supports cell aggregate formation in strawberry cell suspension culture. Journal of Bioscience and Bioengineering. 102**,** 8-13.

Eibl, R., Eibl, D., 2008. Design of bioreactors suitable for plant cell and tissue cultures. Phytochemistry Reviews. 7**,** 593-598-598.

Eibl, R., Werner, S., Eibl, D., 2009. Disposable bioreactors for plant liquid cultures at Litre-scale. Engineering in Life Sciences. 9**,** 156-164.

Enríquez-Obregón, G., Prieto-Samsónov, D., de la Riva, G., Pérez, M., Selman-Housein, G., Vázquez-Padrón, R., 1999. Agrobacterium-mediated Japonica rice transformation: a procedure assisted by an antinecrotic treatment. Plant Cell, Tissue and Organ Culture. 59**,** 159-168.

Exposito, O., Syklowska-Baranek, K., Moyano, E., Onrubia, M., Bonfill, M., Palazon, J., Cusido, R. M., 2010. Metabolic Responses of Taxus media Transformed Cell Cultures to the Addition of Methyl Jasmonate. Biotechnology Progress. 26**,** 1145-1153.

Feher, A., 2015. Somatic embryogenesis - Stress-induced remodeling of plant cell fate. Biochimica Et Biophysica Acta-Gene Regulatory Mechanisms. 1849**,** 385-402.

Feher, A., Pasternak, T. P., Dudits, D., 2003. Transition of somatic plant cells to an embryogenic state. Plant Cell Tissue and Organ Culture. 74**,** 201-228.

Fettneto, A. G., Zhang, W. Y., Dicosmo, F., 1994. Kinetics of Taxol production, growth and nutrient-uptake in cell suspension of *Taxus-cuspidata*. Biotechnology and Bioengineering. 44**,** 205-210.

Filonova, L. H., Bozhkov, P. V., von Arnold, S., 2000. Developmental pathway of somatic embryogenesis in Picea abies as revealed by time-lapse tracking. Journal of Experimental Botany. 51**,** 249-264.

Fomicheva, A. S., Tuzhikov, A. I., Beloshistov, R. E., Trusova, S. V., Galiullina, R. A., Mochalova, L. V., Chichkova, N. V., Vartapetian, A. B., 2012. Programmed cell death in plants. Biochemistry-Moscow. 77**,** 1452-1464.

Fourer, R., Gay, D. M., Kernighan, B. W., 1993. AMPL: A Modeling Language for Mathematical Programming. The Scientific Press, Redwood, Calif, USA.

Fu, C. X., Zhao, D. X., Huang, Y., Ma, F. S., 2005. Cellular aggregate size as the critical factor for flavonoid production by suspension cultures of Saussurea medusa. Biotechnology Letters. 27**,** 91-95.

Fujimura, T., 2014. Carrot somatic embryogenesis. A dream come true? Plant Biotechnology Reports. 8**,** 23-28.

Fujimura, T., Komamine, A., 1979. Synchronization of somatic embryogenesis in a carrot cell-suspension culture. Plant Physiology. 64**,** 162-164.

Garcia-Ochoa, F., Gomez, E., Alcon, A., Santos, V. E., 2013. The effect of hydrodynamic stress on the growth of Xanthomonas campestris cultures in a stirred and sparged tank bioreactor. Bioprocess and Biosystems Engineering. 36**,** 911-925.

Goodwin, R. J. A., 2012. Sample preparation for mass spectrometry imaging: Small mistakes can lead to big consequences. Journal of Proteomics. 75**,** 4893-4911.

Gorelick, J., Bernstein, N., 2014. Elicitation: An Underutilized Tool in the Development of Medicinal Plants as a Source of Therapeutic Secondary Metabolites. Advances in Agronomy, Vol 124. 124**,** 201-230.

Grosset, J., Marty, I., Chartier, Y., Meyer, Y., 1990. Messenger-RNAs newly synthesized by Tobacco mesophyll protoplasts are wound-inducible. Plant Molecular Biology. 15**,** 485-496.

Gupta, P., Hartle, J., 2015. Progress on Scale-up Somatic Embryogenesis and Manufacture Seed Technology of Conifer Species at Weyerhaeuser. In Vitro Cellular & Developmental Biology-Animal. 51**,** S13-S14.

Han, P.-p., Ye, T.-x., Qiao, B., Yuan, Y.-j., 2013. Taxoids profiling of suspension Taxus chinensis var. mairei cells in response to shear stress. Biochemical Engineering Journal. 77**,** 66-73.

Han, P.-P., Yuan, Y.-J., 2009. Metabolic Profiling as a Tool for Understanding Defense Response of Taxus Cuspidata Cells to Shear Stress. Biotechnology Progress. 25**,** 1244-1253.

Hao, D. C., Ge, G., Xiao, P., Zhang, Y., Yang, L., 2011. The First Insight into the Tissue Specific Taxus Transcriptome via Illumina Second Generation Sequencing. Plos One. 6.

Hefner, J., Rubenstein, S. M., Ketchum, R. E. B., Gibson, D. M., Williams, R. M., Croteau, R., 1996. Cytochrome P450-catalyzed hydroxylation of taxa-4(5),11(12)-diene to taxa-4(20),11(12)-dien-5 alpha-ol: The first oxygenation step in taxol biosynthesis. Chemistry & Biology. 3**,** 479-489.

Hemalatha, R. G., Pradeep, T., 2013. Understanding the Molecular Signatures in Leaves and Flowers by Desorption Electrospray Ionization Mass Spectrometry (DESI MS) Imaging. Journal of Agricultural and Food Chemistry. 61**,** 7477-7487.

Hill, P. J., Ng, K. M., 1996. Statistics of multiple particle breakage. Aiche Journal. 42**,** 1600-1611.

Hirasuna, T. J., Pestchanker, L. J., Srinivasan, V., Shuler, M. L., 1996. Taxol production in suspension cultures of Taxus baccata. Plant Cell Tissue and Organ Culture. 44**,** 95-102.

Holton, R. A., Method for preparation of taxol using an oxazinone. Vol. 5015744. Florida State University, Tallahassee, Fl., 1991.

Holton, R. A., Kim, H. B., Somoza, C., Liang, F., Biediger, R. J., Boatman, P. D., Shindo, M., Smith, C. C., Kim, S. C., Nadizadeh, H., Suzuki, Y., Tao, C. L., Vu, P., Tang, S. H., Zhang, P. S., Murthi, K. K., Gentile, L. N., Liu, J. H., 1994a. First total synthesis of Taxol. 2. Completion of the C-ring and D-ring. Journal of the American Chemical Society. 116**,** 1599-1600.

Holton, R. A., Somoza, C., Kim, H. B., Liang, F., Biediger, R. J., Boatman, P. D., Shindo, M., Smith, C. C., Kim, S. C., Nadizadeh, H., Suzuki, Y., Tao, C. L., Vu, P., Tang, S. H., Zhang, P. S., Murthi, K. K., Gentile, L. N., Liu, J. H., 1994b. First total synthesis of Taxol. 1. Functionalization of the B-ring. Journal of the American Chemical Society. 116**,** 1597-1598.

Howat, S., Park, B., Oh, I. S., Jin, Y.-W., Lee, E.-K., Loake, G. J., 2014. Paclitaxel: biosynthesis, production and future prospects. New Biotechnology. 31**,** 242-245.

Huang, T. K., McDonald, K. A., 2009. Bioreactor engineering for recombinant protein production in plant cell suspension cultures. Biochemical Engineering Journal. 45**,** 168-184.

Hulst, A. C., Meyer, M. M. T., Breteler, H., Tramper, J., 1989. Effect of aggregate size in cell-cultures of *Tagetes-patula* on thiopene production and cell-growth. Applied Microbiology and Biotechnology. 30**,** 18-25.

Ikeda-Iwai, M., Umehara, M., Satoh, S., Kamada, H., 2003. Stress-induced somatic embryogenesis in vegetative tissues of Arabidopsis thaliana. Plant Journal. 34**,** 107-114.

Jennewein, S., Rithner, C. D., Williams, R. M., Croteau, R., 2003. Taxoid metabolism: Taxoid 14 beta-hydroxylase is a cytochrome P450-dependent monooxygenase. Archives of Biochemistry and Biophysics. 413**,** 262-270.

Jennewein, S., Rithner, C. D., Williams, R. M., Croteau, R. B., 2001. Taxol biosynthesis: Taxane 13 alpha-hydroxylase is a cytochrome P450-dependent monooxygenase. Proceedings of the National Academy of Sciences of the United States of America. 98**,** 13595-13600.

Kamo, K., Jones, B., Castillon, J., Bolar, J., Smith, F., 2004. Dispersal and size fractionation of embryogenic callus increases the frequency of embryo maturation and conversion in hybrid tea roses. Plant Cell Reports. 22**,** 787-792.

Karkonen, A., Koutaniemi, S., 2010. Lignin Biosynthesis Studies in Plant Tissue Cultures. Journal of Integrative Plant Biology. 52**,** 176-185.

Keshari Lenka, S., 2011. Manuscript in preparation.

Kessler, M., ten Hoopen, H. J. G., Furusaki, S., 1999. The effect of the aggregate size on the production of ajmalicine and tryptamine in Catharanthus roseus suspension culture. Enzyme and Microbial Technology. 24**,** 308-315.

Ketchum, R. E. B., Wherland, L., Croteau, R. B., 2007. Stable transformation and long-term maintenance of transgenic Taxus cell suspension cultures. Plant Cell Reports. 26**,** 1025-1033.

Kim, B. J., Gibson, D. M., Shuler, M. L., 2005. Relationship of viability and apoptosis to taxol production in Taxus sp suspension cultures elicited with methyl jasmonate. Biotechnology Progress. 21**,** 700-707.

Kirchhoff, J., Raven, N., Boes, A., Roberts, J. L., Russell, S., Treffenfeldt, W., Fischer, R., Schinkel, H., Schiermeyer, A., Schillberg, S., 2012. Monoclonal tobacco cell lines with enhanced recombinant protein yields can be generated from heterogeneous cell suspension cultures by flow sorting. Plant Biotechnology Journal. 10**,** 936-944.

Koepp, A. E., Hezari, M., Zajicek, J., Vogel, B. S., Lafever, R. E., Lewis, N. G., Croteau, R., 1995. Cyclization of geranylgeranyl diphosphate to Taxa-4(5),11(12)-diene is the committed step of Taxol biosynthesis in Pacific Yew. Journal of Biological Chemistry. 270**,** 8686-8690.

Kolewe, M. E., Gaurav, V., Roberts, S. C., 2008. Pharmaceutically active natural product synthesis and supply via plant cell culture technology. Molecular Pharmaceutics. 5**,** 243-256.

Kolewe, M. E., Henson, M. A., Roberts, S. C., 2010. Characterization of aggregate size in Taxus suspension cell culture. Plant Cell Reports. 29**,** 485-494.

Kolewe, M. E., Henson, M. A., Roberts, S. C., 2011a. Analysis of Aggregate Size as a Process Variable Affecting Paclitaxel Accumulation in Taxus Suspension Cultures. Biotechnology Progress. 27**,** 1365-1372.

Kolewe, M. E., Henson, M. A., Roberts, S. C., 2011b. Analysis of Aggregate Size as a Process Variable Affecting Paclitaxel Accumulation in *Taxus* Suspension Cultures. Biotechnology Progress Journal. Submitted.

Kolewe, M. E., Roberts, S. C., Henson, M. A., 2012. A population balance equation model of aggregation dynamics in Taxus suspension cell cultures. Biotechnology and Bioengineering. 109**,** 472-482.

Konan, E. E., Durand-Gasselin, T., Kouadio, J. Y., Flori, A., Rival, A., 2006. A modeling approach of the in vitro conversion of oil palm (Elaeis guineensis) somatic embryos. Plant Cell Tissue and Organ Culture. 84**,** 99-112.

Kuboi, T., Yamada, Y., 1978. Changing cell aggregations and lignification in tobacco suspension cultures. Plant and Cell Physiology. 19**,** 437-443.

Kumar, S., Ramkrishna, D., 1996. On the solution of population balance equations by discretization .1. A fixed pivot technique. Chemical Engineering Science. 51**,** 1311-1332.

Kwon, J.-Y., Yang, Y.-S., Cheon, S.-H., Nam, H.-J., Jin, G.-H., Kim, D.-I., 2013. Bioreactor Engineering Using Disposable Technology for Enhanced Production of hCTLA4Ig in Transgenic Rice Cell Cultures. Biotechnology and Bioengineering. 110**,** 2412-2424.

Lehmann, N., Dittler, I., Lämsä, M., Ritala, A., Rischer, H., Eibl, D., Oksman-Caldentey, K.-M., Eibl, R., 2014. Disposable Bioreactors for Cultivation of Plant Cell Cultures. In: Paek, K.-Y., Murthy, H. N., Zhong, J.-J., Eds.), Production of Biomass and Bioactive Compounds Using Bioreactor Technology. Springer Netherlands, pp. 17-46.

Lelu-Walter, M.-A., Thompson, D., Harvengt, L., Sanchez, L., Toribio, M., Paques, L. E., 2013. Somatic embryogenesis in forestry with a focus on Europe: state-of-the-art, benefits, challenges and future direction. Tree Genetics & Genomes. 9**,** 883-899.

Lenka, S. K., Boutaoui, N., Paulose, B., Vongpaseuth, K., Normanly, J., Roberts, S. C., Walker, E. L., 2012. Identification and expression analysis of methyl jasmonate responsive ESTs in paclitaxel producing Taxus cuspidata suspension culture cells. Bmc Genomics. 13.

Lenka, S. K., Patil, R. A., Wilson, S. A., Normanly, J., Roberts, S. C., Walker, E. L., Manuscript in progress. Differential transcriptome analysis of *Taxus* cell cultures exhibiting metabolic and morphological heterogeneity provides molecular evidence for higher Taxol production in small aggregates.

Li, B., Knudsen, C., Hansen, N. K., Jorgensen, K., Kannangara, R., Bak, S., Takos, A., Rook, F., Hansen, S. H., Moller, B. L., Janfelt, C., Bjarnholt, N., 2013a. Visualizing metabolite distribution and enzymatic conversion in plant tissues by desorption electrospray ionization mass spectrometry imaging. Plant Journal. 74**,** 1059-1071.

Li, F.-L., Ma, X.-J., Hu, X.-L., Hoffman, A., Dai, J.-G., Qiu, D.-Y., 2011. Antisense-induced suppression of taxoid 14 beta-hydroxylase gene expression in transgenic Taxus x media cells. African Journal of Biotechnology. 10**,** 8720-8728.

Li, S., Zhang, P., Zhang, M., Fu, C., Yu, L., 2013b. Functional analysis of a WRKY transcription factor involved in transcriptional activation of the DBAT gene in Taxus chinensis. Plant Biology. 15**,** 19-26.

Li, S.-t., Fu, C.-h., Zhang, M., Zhang, Y., Xie, S., Yu, L.-j., 2012a. Enhancing Taxol Biosynthesis by Overexpressing a 9-Cis-Epoxycarotenoid Dioxygenase Gene in Transgenic Cell Lines of Taxus chinensis. Plant Molecular Biology Reporter. 30**,** 1125-1130.

Li, S.-t., Zhang, P., Zhang, M., Fu, C.-h., Zhao, C.-f., Dong, Y.-s., Guo, A.-y., Yu, L.-j., 2012b. Transcriptional profile of Taxus chinensis cells in response to methyl jasmonate. Bmc Genomics. 13.

Lin, P. J., Grimm, L. H., Wulkow, M., Hempel, D. C., Krull, R., 2008. Population balance modeling of the conidial aggregation of Aspergillus niger. Biotechnology and Bioengineering. 99**,** 341-350.

Liu, P., Liang, S., Yao, N., Wu, H., 2012. Programmed cell death of secretory cavity cells in fruits of Citrus grandis cv. Tomentosa is associated with activation of caspase 3-like protease. Trees-Structure and Function. 26**,** 1821-1835.

Lyons, E., Freeling, M., 2008. How to usefully compare homologous plant genes and chromosomes as DNA sequences. Plant Journal. 53**,** 661-673.

Madhusudhan, R., Ravishankar, G. A., 1996. Gradient of anthocyanin in cell aggregates of Daucus carota in suspension cultures. Biotechnology Letters. 18**,** 1253-1256.

Maindarkar, S. N., Henson, M. A., Achieving Target Emulsion Drop Size Distributions using Population Balance Equation Models of High Pressure Homogenization In: Systems, P. o. t. t. I. I. S. o. D. a. C. o. P., (Ed.), The International Federation of Automatic Control December 18-20, 2013, Mumbai, India 2013.

Maindarkar, S. N., Raikar, N. B., Bongers, P., Henson, M. A., 2012. Incorporating emulsion drop coalescence into population balance equation models of high pressure homogenization. Colloids and Surfaces a-Physicochemical and Engineering Aspects. 396**,** 63-73.

Martinez-Esteso, M. J., Selles-Marchart, S., Vera-Urbina, J. C., Pedreno, M. A., Bru-Martinez, R., 2011. DIGE analysis of proteome changes accompanying large resveratrol production by grapevine (Vitis vinifera cv. Gamay) cell cultures in response to methyl-beta-cyclodextrin and methyl jasmonate elicitors. Journal of Proteomics. 74**,** 1421-1436.

McCabe, P. F., Levine, A., Meijer, P. J., Tapon, N. A., Pennell, R. I., 1997. A programmed cell death pathway activated in carrot cells cultured at low cell density. Plant Journal. 12**,** 267-280.

Meyer, H.-P., Schmidhalter, D., 2014. Industrial Scale Suspension Culture of Living Cells.

Miao, G.-p., Zhu, C.-s., Feng, J.-t., Han, J., Song, X.-W., Zhang, X., 2013. Aggregate cell suspension cultures of Tripterygium wilfordii Hook. f. for triptolide, wilforgine, and wilforine production. Plant Cell Tissue and Organ Culture. 112**,** 109-116.

Misra, B. B., Assmann, S. M., Chen, S., 2014. Plant single-cell and single-cell-type metabolomics. Trends in Plant Science. 19.

Montalban, I. A., De Diego, N., Moncalean, P., 2010. Bottlenecks in Pinus radiata somatic embryogenesis: improving maturation and germination. Trees-Structure and Function. 24**,** 1061-1071.

Morandini, P., 2013. Control limits for accumulation of plant metabolites: brute force is no substitute for understanding. Plant biotechnology journal. 11**,** 253-267.

Morosi, L., Spinelli, P., Zucchetti, M., Pretto, F., Carra, A., D'Incalci, M., Giavazzi, R., Davoli, E., 2013. Determination of Paclitaxel Distribution in Solid Tumors by Nano-Particle Assisted Laser Desorption Ionization Mass Spectrometry Imaging. Plos One. 8.

Mountford, P. G., 2010. The Taxol® Story – Development of a Green Synthesis via Plant Cell Fermentation. Wiley-VCH Verlag GmbH & Co. KGaA.

Moussaieff, A., Rogachev, I., Brodsky, L., Malitsky, S., Toal, T. W., Belcher, H., Yativ, M., Brady, S. M., Benfey, P. N., Aharoni, A., 2013. High-resolution metabolic mapping of cell types in plant roots. Proceedings of the National Academy of Sciences of the United States of America. 110**,** E1232-E1241.

Naill, M. C., Roberts, S. C., 2004. Preparation of single cells from aggregated Taxus suspension cultures for population analysis. Biotechnology and Bioengineering. 86**,** 817-826.

Naill, M. C., Roberts, S. C., 2005a. Cell cycle analysis of Taxus suspension cultures at the single cell level as an indicator of culture heterogeneity. Biotechnology and Bioengineering. 90**,** 491-500.

Naill, M. C., Roberts, S. C., 2005b. Culture of isolated single cells from Taxus suspensions for the propagation of superior cell populations. Biotechnology Letters. 27**,** 1725-1730.

Naill, M. C., Roberts, S. C., 2005c. Flow cytometric analysis of protein content in Taxus protoplasts and single cells as compared to aggregated suspension cultures. Plant Cell Reports. 23**,** 528-533.

Naill, M. C., Roberts, S. C., 2005d. Flow cytometric identification of paclitaxel-accumulating subpopulations. Biotechnology Progress. 21**,** 978-983.

Newman, D. J., Cragg, G. M., 2012. Natural Products As Sources of New Drugs over the 30 Years from 1981 to 2010. Journal of Natural Products. 75**,** 311-335.

Nic-Can, G. I., Galaz-Avalos, R. M., De-la-Pena, C., Alcazar-Magana, A., Wrobel, K., Loyola-Vargas, V. M., 2015. Somatic Embryogenesis: Identified Factors that Lead to Embryogenic Repression. A Case of Species of the Same Genus. PloS one. 10**,** e0126414-e0126414.

Nicolaou, K. C., Yang, Z., Liu, J. J., Ueno, H., Nantermet, P. G., Guy, R. K., Claiborne, C. F., Renaud, J., Couladouros, E. A., Paulvannan, K., Sorensen, E. J., 1994. TOTAL SYNTHESIS OF TAXOL. Nature. 367**,** 630-634.

Nims, E., Dubois, C. P., Roberts, S. C., Walker, E. L., 2006. Expression profiling of genes involved in paclitaxel biosynthesis for targeted metabolic engineering. Metabolic Engineering. 8**,** 385-394.

Onrubia, M., Moyano, E., Bonfill, M., Ma Cusido, R., Goossens, A., Palazon, J., 2013. Coronatine, a more powerful elicitor for inducing taxane biosynthesis in Taxus media cell cultures than methyl jasmonate. Journal of Plant Physiology. 170**,** 211-219.

P.G.M., W., 1998. Semisynthesis of Taxol. Current Opinion in Drug Discovery and Development. 1**,** 329-337.

Padidam, M., 2003. Chemically regulated gene expression in plants. Current Opinion in Plant Biology. 6**,** 169-177.

Park, Y. S., 2002. Implementation of conifer somatic embryogenesis in clonal forestry: technical requirements and deployment considerations. Annals of Forest Science. 59**,** 651-656.

Pasternak, T. P., Prinsen, E., Ayaydin, F., Miskolczi, P., Potters, G., Asard, H., Van Onckelen, H. A., Dudits, D., Feher, A., 2002. The role of auxin, pH, and stress in the activation of embryogenic cell division in leaf protoplast-derived cells of alfalfa. Plant Physiology. 129**,** 1807-1819.

Patakas, A., 2012. Abiotic Stress-Induced Morphological and Anatomical Changes in Plants. Abiotic Stress Responses in Plants: Metabolism, Productivity and Sustainability. 21-39.

Patel, R. N., 1998. Tour de paclitaxel: Biocatalysis for semisynthesis. Annual Review of Microbiology. 52**,** 361-395.

Patil, R., Lenka, S., Normanly, J., Walker, E., Roberts, S., 2014a. Methyl jasmonate represses growth and affects cell cycle progression in cultured Taxus cells. Plant Cell Reports. 1-14.

Patil, R. A., Kolewe, M. E., Normanly, J., Walker, E. L., Roberts, S. C., 2012. Contribution of taxane biosynthetic pathway gene expression to observed variability in paclitaxel accumulation in Taxus suspension cultures. Biotechnology Journal. 7**,** 418-427.

Patil, R. A., Kolewe, M. E., Roberts, S. C., 2013. Cellular aggregation is a key parameter associated with long term variability in paclitaxel accumulation in Taxus suspension cultures. Plant Cell Tissue and Organ Culture. 112**,** 303-310.

Patil, R. A., Lenka, S. K., Normanly, J., Walker, E. L., Roberts, S. C., 2014b. Methyl jasmonate represses growth and affects cell cycle progression in cultured Taxus cells. Plant Cell Rep. 33**,** 1479-92.

Pauwels, L., Morreel, K., De Witte, E., Lammertyn, F., Van Montagu, M., Boerjan, W., Inzé, D., Goossens, A., 2008. Mapping methyl jasmonate-mediated transcriptional reprogramming of metabolism and cell cycle progression in cultured Arabidopsis cells. Proceedings of the National Academy of Sciences. 105**,** 1380-1385.

Peebles, C. A. M., Sander, G. W., Hughes, E. H., Peacock, R., Shanks, J. V., San, K.-Y., 2011. The expression of 1-deoxy-D-xylulose synthase and geraniol-10-hydroxylase or anthranilate synthase increases terpenoid indole alkaloid accumulation in Catharanthus roseus hairy roots. Metabolic Engineering. 13**,** 234-240.

Pepin, M. F., Smith, M. A. L., Reid, J. F., 1999. Application of imaging tools to plant cell culture: Relationship between plant cell aggregation and flavonoid production. In Vitro Cellular & Developmental Biology-Plant. 35**,** 290-295.

Pichersky, E., Lewinsohn, E., 2011. Convergent Evolution in Plant Specialized Metabolism. Annual Review of Plant Biology, Vol 62. 62**,** 549-566.

Pullman, G. S., Zeng, X. Y., Copeland-Kamp, B., Crockett, J., Lucrezi, J., May, S. W., Bucalo, K., 2015. Conifer somatic embryogenesis: improvements by supplementation of medium with oxidation-reduction agents. Tree Physiology. 35**,** 209-224.

Raikar, N. B., Bhatia, S. R., Malone, M. F., Henson, M. A., 2009. Experimental studies and population balance equation models for breakage prediction of emulsion drop size distributions. Chemical Engineering Science. 64**,** 2433-2447.

Ramkrishna, D., Mahoney, A. W., 2002. Population balance modeling. Promise for the future. Chemical Engineering Science. 57**,** 595-606.

Saito, K., Mizukami, H., 2002. Plant cell cultures as producers of secondary compounds. Plant Biotechnology and Transgenic Plants. 77-109.

Schoendorf, A., Rithner, C. D., Williams, R. M., Croteau, R. B., 2001. Molecular cloning of a cytochrome P450 taxane 10 beta-hydroxylase cDNA from Taxus and functional expression in yeast. Proceedings of the National Academy of Sciences of the United States of America. 98**,** 1501-1506.

Schwachtje, J., Baldwin, I. T., 2008. Why does herbivore attack reconfigure primary metabolism? Plant Physiology. 146**,** 845-851.

Sharma, S., Shahzad, A., da Silva, J. A. T., 2013. Synseed technology-A complete synthesis. Biotechnology Advances. 31**,** 186-207.

Shekhawat, U. K. S., Ganapathi, T. R., Srinivas, L., Bapat, V. A., Rathore, T. S., 2008. Agrobacterium-mediated genetic transformation of embryogenic cell suspension cultures of Santalum album L. Plant Cell Tissue and Organ Culture. 92**,** 261-271.

Song, G. Q., Sink, K. C., 2004. Agrobacterium tumefaciens-mediated transformation of blueberry (Vaccinium corymbosum L.). Plant Cell Reports. 23**,** 475-484.

Stancheva, N., Weber, J., Schulze, J., Alipieva, K., Ludwig-Mueller, J., Haas, C., Georgiev, V., Bley, T., Georgiev, M., 2011. Phytochemical and flow cytometric analyses of Devil's claw cell cultures. Plant Cell Tissue and Organ Culture. 105**,** 79-84.

Sumner, L. W., Amberg, A., Barrett, D., Beale, M. H., Beger, R., Daykin, C. A., Fan, T. W. M., Fiehn, O., Goodacre, R., Griffin, J. L., Hankemeier, T., Hardy, N., Harnly, J., Higashi, R., Kopka, J., Lane, A. N., Lindon, J. C., Marriott, P., Nicholls, A. W., Reily, M. D., Thaden, J. J., Viant, M. R., 2007. Proposed minimum reporting standards for chemical analysis. Metabolomics. 3**,** 211-221.

Sun, G., Yang, Y., Xie, F., Wen, J.-F., Wu, J., Wilson, I. W., Tang, Q., Liu, H., Qiu, D., 2013. Deep Sequencing Reveals Transcriptome Re-Programming of Taxus x media Cells to the Elicitation with Methyl Jasmonate. Plos One. 8.

Takahashi, K., Kozuka, T., Anegawa, A., Nagatani, A., Mimura, T., 2015. Development and application of high resolution imaging mass spectroscope for the study of plant tissues. Plant and Cell Physiology.

Tang, F., Lao, K., Surani, M. A., 2011. Development and applications of single-cell transcriptome analysis. Nature Methods. 8**,** S6-S11.

Vanholme, R., Demedts, B., Morreel, K., Ralph, J., Boerjan, W., 2010. Lignin Biosynthesis and Structure. Plant Physiology. 153**,** 895-905.

Vaucheret, H., Beclin, C., Elmayan, T., Feuerbach, F., Godon, C., Morel, J. B., Mourrain, P., Palauqui, J. C., Vernhettes, S., 1998. Transgene-induced gene silencing in plants. Plant Journal. 16**,** 651-659.

Vongpaseuth, K., Nims, E., Amand, M. S., Walker, E. L., Roberts, S. C., 2007. Development of a particle bombardment-mediated transient transformation system for Taxus spp. cells in culture. Biotechnology Progress. 23**,** 1180-1185.

Vongpaseuth, K., Roberts, S. C., 2007. Advancements in the understanding of paclitaxel metabolism in tissue culture. Current Pharmaceutical Biotechnology. 8**,** 219-236.

Vrána, J., Cápal, P., Bednářová, M., Doležel, J., 2014. Flow Cytometry in Plant Research: A Success Story. In: Nick, P., Opatrny, Z., Eds.), Applied Plant Cell Biology. vol. 22. Springer Berlin Heidelberg, pp. 395-430.

Walker, K., Croteau, R., 2000a. Molecular cloning of a 10-deacetylbaccatin III-10-O-acetyl transferase cDNA from Taxus and functional expression in Escherichia coli. Proceedings of the National Academy of Sciences of the United States of America. 97**,** 583-587.

Walker, K., Croteau, R., 2000b. Taxol biosynthesis: Molecular cloning of a benzoyl-CoA : taxane 2 alpha-O-benzoyltransferase cDNA from Taxus and functional expression in Escherichia coli. Proceedings of the National Academy of Sciences of the United States of America. 97**,** 13591-13596.

Walker, K., Fujisaki, S., Long, R., Croteau, R., 2002a. Molecular cloning and heterologous expression of the C-13 phenylpropanoid side chain-CoA acyltransferase that functions in Taxol biosynthesis. Proceedings of the National Academy of Sciences of the United States of America. 99**,** 12715-12720.

Walker, K., Ketchum, R. E. B., Hezari, M., Gatfield, D., Goleniowski, M., Barthol, A., Croteau, R., 1999. Partial purification and characterization of acetyl coenzyme A: Taxa-4(20),11(12)-dien-5 alpha-ol O-acetyl transferase that catalyzes the first acylation step of Taxol biosynthesis. Archives of Biochemistry and Biophysics. 364**,** 273-279.

Walker, K., Long, R., Croteau, R., 2002b. The final acylation step in Taxol biosynthesis: Cloning of the taxoid C13-side-chain N-benzoyltransferase from Taxus. Proceedings of the National Academy of Sciences of the United States of America. 99**,** 9166-9171.

Walker, K. D., Klettke, K., Akiyama, T., Croteau, R., 2004. Cloning, heterologous expression, and characterization of a phenylalanine aminomutase involved in Taxol biosynthesis. Journal of Biological Chemistry. 279**,** 53947-53954.

Wender, P. A., Badham, N. F., Conway, S. P., Floreancig, P. E., Glass, T. E., Granicher, C., Houze, J. B., Janichen, J., Lee, D. S., Marquess, D. G., McGrane, P. L., Meng, W., Mucciaro, T. P., Muhlebach, M., Natchus, M. G., Paulsen, H., Rawlins, D. B., Satkofsky, J., Shuker, A. J., Sutton, J. C., Taylor, R. E., Tomooka, K., 1997a. The pinene path to taxanes .5. Stereocontrolled synthesis of a versatile taxane precursor. Journal of the American Chemical Society. 119**,** 2755-2756.

Wender, P. A., Badham, N. F., Conway, S. P., Floreancig, P. E., Glass, T. E., Houze, J. B., Krauss, N. E., Lee, D. S., Marquess, D. G., McGrane, P. L., Meng, W., Natchus, M. G., Shuker, A. J., Sutton, J. C., Taylor, R. E., 1997b. The pinene path to taxanes .6. A concise stereocontrolled synthesis of taxol. Journal of the American Chemical Society. 119**,** 2757-2758.

Wildung, M. R., Croteau, R., 1996. A cDNA clone for taxadiene synthase, the diterpene cyclase that catalyzes the committed step of taxol biosynthesis. Journal of Biological Chemistry. 271**,** 9201-9204.

Wilson, S. A., Cummings, E. M., Roberts, S. C., 2014a. Multi-scale engineering of plant cell cultures for promotion of specialized metabolism. Current Opinion in Biotechnology. 29**,** 163-170.

Wilson, S. A., Roberts, S. C., 2012. Recent advances towards development and commercialization of plant cell culture processes for the synthesis of biomolecules. Plant Biotechnology Journal. 10**,** 249-268.

Wilson, S. A., Roberts, S. C., 2014. Metabolic engineering approaches for production of biochemicals in food and medicinal plants. Current Opinion in Biotechnology. 26**,** 174-182.

Wilson, S. A., Vilkhovoy, M. V., Bevacqua, S. P., Roberts, S. C., Mechanical shearing Taxus plant suspension cultures reduces aggregation without affecting cell health Proceedings of the 40th Annual Northeast Bioengineering Conference. Institute of Electrical and Electronics Engineers, Boston, Ma, 2014b.

Wu, Q. O., Sun, C., Luo, H. M., Li, Y., Niu, Y. Y., Sun, Y. Z., Lu, A. P., Chen, S. L., 2011. Transcriptome Analysis of Taxus cuspidata Needles Based on 454 Pyrosequencing. Planta Medica. 77**,** 394-400.

Yang, D.-L., Yao, J., Mei, C.-S., Tong, X.-H., Zeng, L.-J., Li, Q., Xiao, L.-T., Sun, T.-p., Li, J., Deng, X.-W., Lee, C. M., Thomashow, M. F., Yang, Y., He, Z., He, S. Y., 2012. Plant hormone jasmonate prioritizes defense over growth by interfering with gibberellin signaling cascade. Proceedings of the National Academy of Sciences of the United States of America. 109**,** E1192-E1200.

Yang, X., Zhang, X., 2010. Regulation of Somatic Embryogenesis in Higher Plants. Critical Reviews in Plant Sciences. 29**,** 36-57.

Yang, Z., Nakabayashi, R., Okazaki, Y., Mori, T., Takamatsu, S., Kitanaka, S., Kikuchi, J., Saito, K., 2013. Toward better annotation in plant metabolomics: isolation and structure elucidation of 36 specialized metabolites from Oryza sativa (rice) by using MS/MS and NMR analyses. Metabolomics. 1-13.

Ye, H., Gemperline, E., Venkateshwaran, M., Chen, R., Delaux, P.-M., Howes-Podoll, M., Ane, J.-M., Li, L., 2013. MALDI mass spectrometry-assisted molecular imaging of metabolites during nitrogen fixation in the Medicago truncatula-Sinorhizobium meliloti symbiosis. Plant Journal. 75**,** 130-145.

Zhang, D., Yang, R., Wang, S., Dong, Z., 2014. Paclitaxel: new uses for an old drug. Drug Design Development and Therapy. 8**,** 279-284.

Zhang, P., Li, S. T., Liu, T. T., Fu, C. H., Zhou, P. P., Zhao, C. F., Yu, L. J., 2011. Overexpression of a 10-deacetylbaccatin III-10 beta-O-acetyltransferase gene leads to increased taxol yield in cells of Taxus chinensis. Plant Cell Tissue and Organ Culture. 106**,** 63-70.

Zhao, D., Huang, Y., Jin, Z., Qu, W., Lu, D., 2003. Effect of aggregate size in cell cultures of Saussurea medusa on cell growth and jaceosidin production. Plant Cell Reports. 21**,** 1129-1133.

Zimberlin, J. A., McManus, J. J., Crosby, A. J., 2010. Cavitation rheology of the vitreous: mechanical properties of biological tissue. Soft Matter. 6**,** 3632-3635.